DEVELOPMENT AND VALIDATION OF A FINITE ELEMENT MODEL OF THE Q3 ANTHROPOMORPHIC TESTING DEVICE

by

Christoph A. Maurath

Vordiplom Maschinenwesen, September 1999, Universität Stuttgart
M.S. in Civil and Environmental Engineering, January 2002, The George Washington University

A Dissertation submitted to

The Faculty of

The Department of Civil and Environmental Engineering
of The School of Engineering and Applied Science
of The George Washington University in partial satisfaction
of the requirements for the degree of Doctor of Science

November 05, 2007

Dissertation directed by
Dr. Kennerly H. Digges
Research Professor of Engineering and Applied Science

Academic Advisor
Dr. Vahid Motevalli
Associate Professor of Engineering and Applied Science

ABSTRACT

This paper describes the development of a finite element model of the Q3 three year old anthropomorphic test device (ATD) in LS-DYNA. The model, which consists of about 50,000 elements, includes all materials and structural details of the Q3 dummy. It was developed by means of non-destructive reverse engineering which included digitizing, x-rays and a CAT-scan of the whole dummy. The materials were calibrated with component level tests and through an optimization analysis. The component tests include head drop, lateral and frontal neck pendulum, lateral and frontal lumbar spine pendulum, ribcage compression, and abdomen compression tests. The optimization process has yielded satisfactory component responses within the range of the specific materials and the functionality of the finite element analysis software. Assembly level tests were used for validation. Satisfactory results were achieved for the validation. The Q3 model was run in a child restraint system in a simulated 48 km/h frontal crash on a test bench. The response of the Q3 was compared to the simpler Madymo Q3 model and the Hybrid III 3-year old dummy. Finally, the spine box was modified to improve the biofidelity of the dummy model.

TABLE OF CONTENTS

LIST OF FIGURES

LIST OF TABLES

CHAPTER 1 - INTRODUCTION

Despite constant improvement in occupant safety child protection in automotive crashes is still not optimal. According to Arbogast et al. [3] the rate of injury for children is about 2.7 per 1000 crashes for frontal and 4.5 per 1000 crashes for side impact. This is already a relatively low rate. Still, through development of better child safety systems, through enhancement of the safety of the environment of child safety systems in cars, and through improvement of the compatibility of child restraints with cars the rate of injury for children can be further reduced.

These developments are time consuming and expensive if everything ahs to be tested. To reduce costs and time manufacturers and researchers nowadays rely on finite element analysis. At the time this research was undertaken only one detailed finite element model representing a three-year-old child dummy was available, the Hybrid III three-year-old. A new dummy, the Q3, with improved biofidelity over the Hybrid III was developed by TNO automotive.

The purpose of this research is to create a finite element model of the Q3 anthropomorphic testing device (ATD) as a tool for safety research for children and to find out if the rigid spine in current child dummies causes the number of neck injuries to be higher than for real children with a flexible spine.

The research presented contributes in four ways to the body of science:

1. A new validated tool for safety research for children was created. The finite element model of the Q3 anthropomorphic testing device can be used to evaluate the safety for children in injury threatening situations in a relatively cost effective and fast way.
2. A way to obtain previously unknown, relatively accurate material properties in simulations through optimization is presented.
3. A possible modification to the Q3 to improve its biofidelity is shown.
4. An objective rating criteria was used to rate the accuracy of the model.

The challenges faced with this research were the complete lack of material properties for the dummy, the lack of complete dummy tests beyond the pendulum tests, and the fact that the dummy has gone through further development since the model was created.

The approach can be summarized as follows: The actual dummy was digitized and a finite element mesh representing the dummy was created. The material properties for the major components were determined through optimization with component tests. Then the major components and their material properties were validated with additional component tests. Impact tests with the complete dummy were utilized for validation of the complete dummy. The complete dummy was compared to other dummy models and a sled test with a comparable dummy. Finally the spine of the dummy was modified and the results of the modification were analyzed.

The following is an outline of the remaining chapters of this dissertation:

Chapter 2 - is an overview of the relevant literature, like dummy history, head and neck injuries in adults and children, child dummy development, finite element and optimization theory, the theory behind the material models used, and objective rating criteria for simulation results.

Chapter 3 - describes the methodology used to create the finite element model of the Q3 dummy and the modifications that have been done to the Q3 model.

Chapter 4 - contains the results and findings of the component level simulations, the complete dummy simulations, the comparison of the finite element model to two MADYMO models, and the comparison of the original Q3 model to the modified Q3 model.

Chapter 5 - sums up the conclusions from this research.

Chapter 6 - is a list of all references used for this study.

CHAPTER 2 - LITERATURE REVIEW

2.1 Crash Test Dummies

Crash test dummies, in technical terms usually called Anthropomorphic Test Devices (ATD), are life-size mannequins that measure forces, moments, and accelerations that can be interpreted to the extend of injuries humans would experience in impact conditions or other injury threatening conditions. Therefore they should ideally be built and behave like real human beings. They are equipped with numerous sensors to measure for example forces, moments, accelerations, deformations, and so on. Since humans come in different sizes and shapes there is a large variety of crash test dummies available.

The first purposefully built crash test dummies were developed in 1949 mainly for aviation research. They were equipped with very few sensors and were not very humanlike. This started the history of anthropomorphic testing devices [1][17][46][47]. Anderson and Grumman developed the first dummy that was used in aviation and automobile testing in the early 1950s. In 1966 Anderson research labs designed the VIP-50 dummies that were sold to Ford and General Motors. This was the first dedicated automotive dummy. It had biofidelic features and was, among other sensors, equipped with the first load cells in the femur. Sierra engineering developed the Sierra Stan in

1967. This was also a dedicated dummy for automotive testing. It was equipped with the first chest deflection sensor. In 1970 Sierra engineering designed the first child dummies, Sierra Sammy, representing a six-year-old, and Sierra Toddler, representing a three-year-old. General Motors designed the Hybrid I in 1971 and the Hybrid II in 1972. The Hybrid II dummy was the first regulated dummy and it had improved biofidelity. In 1976 General Motors released the Hybrid III dummy that was later put into regulation by the National Highway Traffic Safety Agency (NHTSA). It had improved biofidelity, correct center of gravity and mass of all body parts and it is repeatable and reproducible. The Hybrid III 50^{th}%tile dummy is still the most used crash test dummy in the world. Since then many other dummies have been developed for special purposes.

Overview of some of the current crash test dummies:

- Hybrid III family: Different versions of the Hybrid III, representing the large male, average male, small female, ten-year-old child, six-year-old child, and three-year-old child population
- US-SID: the standard US side impact dummy
- Euro-SID: the standard European side impact dummy
- BioRID: a rear impact dummy with fully articulated spine
- THOR: an advanced frontal impact dummy
- CRABI series: representing 6, 12, and 18 month old children
- P-series: representing newborn, and children ¾, 1.5, 3, 6, and 10 years old
- Q-series: child dummies that can be used in frontal and side impact situations.

2.2 Current Knowledge

2.2.1 Neck and Spine Research in Adult Population

For the adult population the research on neck and spine injury in based on a large number of cadaver tests and volunteer tests. Volunteer tests are often preferred, but can only be conducted at relatively low levels to not harm the participants of the tests.

By testing 96 adult volunteers, grouped in three age groups, regarding their static neck section while standing and in a simulated automotive seating position Lawrence W. Schneider et al. [55] found that the range of motion decreased by between 20 to 45 percent between the youngest and oldest study group. Volunteers were also exposed to low-level acceleration and head and neck response was measured. Since the study focus was on whiplash injury the shoulders of the volunteers where kept against a brace to prevent torso movement.

M.Seemann et al. [57] compared the dynamic response of the head and neck of a 50th percentile hybrid III dummy with that of adult human volunteers. While the head trajectories of the lateral and oblique sled tests matches relatively closely, the Hybrid III neck and head did not represent the trajectory of the head of the human volunteers well. It is concluded, that the neck of the Hybrid III is to stiff to represent those tests. In fact, the angle of the head during frontal impact seems to match, but the position of the head in the human volunteers is much lower and further extended than in the dummy tests.

J. Wismans et al. [67] conducted a series of frontal sled tests with post-mortem human subjects (PMHS) in the same manner as M.Seemann [57] did with the human volunteers. Some tests were performed at a similar acceleration level as the human volunteer tests and some at a higher acceleration level. The results were comparable to the results from the study by Seemann, with the exception of a somewhat higher rotation of the head in the cadaver tests during the later stages of each test. The higher rotation was thought to be due to the lack of muscle response in the cadavers.

Later, J. Wismans et al. [68] reevaluated the human volunteer testing performed at the Naval Biodynamics Laboratory and again came to the conclusion that the Hybrid III neck is too stiff to represent human necks. J. Thunnissen et al. [60] confirmed these findings later, especially for the frontal direction.

In low acceleration volunteer testing conducted by T. Matsushita et al. [39], the kinematic responses were, amongst other measurements, captured with high speed x-ray film. Therefore the cervical and thoracic vertebrae could be traced throughout the test. A comparison test with a test dummy showed significant differences between the initial position of the dummy and the human volunteers. Further, the initial curvature of the spine of the human volunteers greatly impacted the results of the tests. During the frontal loading, a not insignificant part of the bending and rotation seem to stem from the thoracic spine, whereas the global head angle remains fairly constant.

M.Behr et al. [8] developed a human model comparable to a 50th percentile European male in Radioss to investigate injury mechanisms. The model is detailed enough that the spine was modeled with individual bones and cartilage discs. Material models were derived from component tests, literature and optimization methods in the Radioss software. A simulation of a frontal crash with the human model restrained by a three point seatbelt indicates a not insignificant bending of the thoracic spine during impact.

All of the above mentioned studies seem to indicate that the spine and neck of the Hybrid III could be made more biofidelic by making it less stiff.

2.2.2 Child Crash Test Dummies and Head and Neck Injuries in Children

The physiology of children is significantly different from the physiology of adults. The greatest difference is the head, which, for a newborn attributes to 30% of the body weight as compared to 6% for adults. Also, humans are born with the skull bones not fused which makes the head more flexible. The bones fuse at the age of roughly 18 months. The spine is also more flexible than in adults [11][22].

Mechanical tests of the femur bones and cranial bones of children and adults revealed that in general the bones of children have a lower modulus of elasticity and lower ultimate strength, but higher ultimate elongation than the bones of adults [69][14][30][32].

Unlike for the adult population there are only a very small number of cadaver tests available for children. Therefore the development of child crash test dummies and injury criteria is largely done by scaling adult size crash test dummies and adult injury criteria. In a study performed by the University of Heidelberg, four child cadavers between the age of 2.5 and 11 year-old were tested on a sled test [34][16]. The results were compared with tests performed with two different child dummies. The cadavers showed a greater flexibility especially in the thoracic spine. It also showed a greater head extension.

In another study from the Highway Safety Research Institute of University of Michigan one child cadaver test was compared to two tests with different dummies [66]. The Hybrid III three-year old matched the cadaver tests in the measured acceleration better, but the TNO P3 dummy matched the motion of the cadaver more precise.

Brun Cassan et al. [10] later summarized the data from the cadaver tests and also compared them to crash test dummy tests with the TNO P3 and the CRABI three-year-old. In this case the head trajectories matched the cadaver data reasonably well.

The aforementioned cadaver tests were only equipped with a small number of sensors and the sample size is very limited.

According to studies that look at automotive crashes recorded in the National Automotive Sampling System (NASS) database only a relatively small number of crashes involve children with severe injuries [35]. According to this study, head and face injuries and injuries to the lower extremities are common, whereas neck and thorax injuries and injuries to the lower extremities are relatively infrequent.

A later study based on data from Partners for Child Passenger Safety (PCPS) program largely confirms those finding with the exception that here upper extremities see a similar rate of injury as lower extremities [3].

A study from Australia finds that neck injuries of properly restrained children in car crashes can almost always be contributed to head contact with the interior of the vehicle and not to sole loading through deceleration [50].

Contrary to this the neck injury criteria measured with child dummies in frontal New Car Assessment Program (NCAP) tests is very high in many cases and would suggest frequent neck injury [51]. Since this is not observed in the field data current child dummies are largely over-predicting neck injuries in children.

The scaling of adult size dummies to child sizes is the only feasible possibility to develop child dummies. The process of scaling is usually done in a two step process. In the first step a large step of anthropometry data of the target population is gathered and compared with the data from the population that an adult dummy represents.

An adult dummy is scaled according to the differences found in the anthropometry data in the second step.

The Hybrid III child dummies and the CRABI dummies [41], the TNO P series child dummies [59], and the TNO Q series child dummies [54] were developed using scaling techniques. The process of scaling is also used to represent other than standard adult size populations [1][27][42][29].

With the dummies the injury parameters have to be scaled as well [18][38][43][45].

This set of scaled crash test dummies and scaled injury parameters results in a reasonable good representation of child physiology in many impact situations. However, since there is so little data available for the design of child dummies, the biofidelity of the child dummies is not as good as the biofidelity of some of the adult dummies. Studies that involve detailed neck and spine models of children and comparisons to the existing cadaver tests reveal that especially the representation of the spine in current child dummies seems to be an issue in some cases [58][70][21]. The study by Zang et al. [70] compared a finite element model of a child [48] with the finite element model of the Hybrid III child dummy. The human finite element dummy shows a larger neck bending and extension and has lower head injury numbers.

2.3 Theoretical Discussion

2.3.1 Introduction to Finite Element Analysis and Finite Element Method

Finite element analysis (FEA) is the use of finite element method (FEM) to simulate a real world problem. Finite element method is a numerical method to find approximate solutions for partial differential equations with boundary conditions. It is very commonly used in modern engineering. This section is based on several publications [7][13][36][37][53][56].

In the finite element method the area that is to be solved is split up into a large but finite number of elements of a small, but finite size. For each of these elements a basis function will be defined. The basis functions in conjunction with the partial differential equation and the boundary conditions form a large system of equations. The solution of this system of equations yields the results of the problem.

The general procedure is that first the problem area P will be split into smaller parts, called elements:

$$P = \sum_{e=1}^{m} P_e \tag{2.1}$$

Within the finite element n basis functions will be defined which equal zero for most elements. A linear combination of these n basis functions within the element defines the possible solutions y of the numerical approximation.

$$y\Big|P_e \approx \sum_{i=1}^{n} c_{e,i}\Psi_{e,i} \tag{2.2}$$

The differential equations and boundary conditions are multiplied with test functions ψ and integrated over the problem area. The integral is then replaced by the sum of the individual integrals of the elements. Usually the integration is done by an approximate numerical integration. Since the basis function has a value not equal to zero for very few elements the resulting system of equations is only lightly populated.

In case of a linear partial differential equation and if the number of element is not to large, the in this case linear system of equations can be solved directly through Gauss elimination. To solve linear systems with more elements iterative methods are used.

In case the partial differential equation is non-linear, the resulting system of equations is non-linear. This can usually only be solved through numerical approximation methods. Nowadays there is a large number of commercial software available that works with the finite element method.

In finite element analysis for structural analysis, as applied in this research, the basic principle is the principle of virtual displacement. It states, that a small virtual displacement applied to a body in the equilibrium, for this body to remain in the equilibrium, the internal virtual work has to be equal the external virtual work:

$$\int_V \bar{\varepsilon}\, \tau \, dV = \int_V \overline{U}^T f^B dV + \int_S \overline{U}^{S^T} f^S dS + \sum_i \overline{U}^{i^T} F^i \tag{2.3}$$

The internal virtual work on the left side is the work of the stresses τ along the strains ε. The external virtual work on the right side is virtual displacements U with the volume forces f^B, the surface forces f^S, and the individual forces F^i.

In a model with N nodes the displacement interpolation matrix $H^{(m)}$ is derived through:

$$u^{(m)}(x,y,z) = H^{(m)}(x,y,z) \tag{2.4}$$

Where $\hat{U}$ is a vector that lists all individual displacements of all nodes N.

The individual element strains can be calculated via:

$$\varepsilon^{(m)}(x,y,z) = B^{(m)}(x,y,z)\hat{U} \tag{2.5}$$

Where $B^{(m)}$ is the strain displacement matrix, that can be derived from the matrix $H^{(m)}$. In a finite element the stresses $\tau^{(m)}$ are connected with the strains $\varepsilon^{(m)}$ through the material condition:

$$\tau^{(m)} = C^{(m)}\varepsilon^{(m)} \tag{2.6}$$

Where $C^{(m)}$ contains the material parameters of the element. With the use of equation (2.4) thru (2.6), equation (2.3) can be rewritten as follows:

$$\bar{\hat{U}}^T \left[\sum_m \int_{V^{(m)}} B^{(m)^T} C^{(m)} B^{(m)} dV^{(m)} \right] \hat{U} =$$
$$\bar{\hat{U}}^T \left\{ \sum_m \int_{V^{(m)}} H^{(m)^T} f^{B(m)} dV^{(m)} + \sum_m \int_{S^{(m)}} H^{S(m)^T} f^{S(m)} dS^{(m)} + F \right\} \tag{2.7}$$

To find the unknown node displacements $\bar{\hat{U}}^T$ is then replaced by the unit displacement vector *I* and the equation can be expressed as:

$$KU = R_B + R_S + R_E \tag{2.8}$$

Where K is the stiffness matrix of the group of elements, R_B are the volume forces, R_S are the surface forces, and R_E are the individual forces. So far this is a static problem. For a dynamic problem inertia and damping have to be considered. In that case the volume forces are as follow:

$$R_B = \sum_m \int_{V^{(m)}} H^{(m)^T} \left[f^{B(m)} - \rho^{(m)} H^{(m)} \ddot{U} - \kappa^{(m)} H^{(m)} \dot{U} \right] dV^{(m)} \tag{2.9}$$

Where $\rho^{(m)}$ is the density $\kappa^{(m)}$ is the damping coefficient of element m. Equation (2.8) can then be expressed as:

$$M\ddot{U}(t) + D\dot{U}(t) + KU(t) = R(t) \tag{2.10}$$

Where M is the mass matrix for the model and D is the damping matrix. To solve this equation LS-DYNA employs the explicit central difference method. To advance from time step r to time step r+1 the following is used:

$$\ddot{U}(t_r) = M^{-1}\left[R(t_r) - D\dot{U}(t_r) - KU(t_r)\right] \tag{2.11}$$

$$\dot{U}(t_{r+\frac{1}{2}}) = \dot{U}(t_{r-\frac{1}{2}}) + \ddot{U}(t_r)\Delta t_r \tag{2.12}$$

$$U(t_{r+1}) = U(t_r) + \dot{U}(t_{r+\frac{1}{2}})\Delta t_{r+\frac{1}{2}} \tag{2.13}$$

Where:

$$\Delta t_{r+\frac{1}{2}} = \left(\Delta t_r + \Delta t_{r+1}\right)/2 \tag{2.14}$$

Since this is an approximation, it is important that the time step is very small to receive accurate results.

2.3.2 Introduction to Optimization

The field of optimization in applied mathematics and engineering deals with the search of optimal parameters of a usually complex system. Optimal in this case means that the objective function will be minimized or maximized. Optimization problems are also called mathematical programming problems. Optimization is used in all scientific fields that work with unknown parameters [2][5][19][49][71].

The simplest optimization problem is to find the minimum or maximum of an analytical one-dimensional function *f(x)*, which is usually done by finding the root of the first differentiation.

Assuming an optimization to search for a minimum, for example a distance between two points, what is supposed to be minimized is called the *objective function* or *cost function*. What is going to be changed during the optimization are called *parameters* or *variables* of the target function. In a two-dimensional problem, that has two independent variables, the objective function can in most cases be imagined as values on the z axis that form a usually non-planar surface, if the two parameters are the x and y axis. The z value of this surface is then the value of the objective function for a specific pair of variables X and Y. The lowest point on this surface would then be the optimal result of this problem.

In most cases there would be several low and high points on the surface. The absolute lowest point is defined as the *global minimum* and the absolute highest point the *global maximum*. Optimization for these points is called *global optimization*.

A low point, which is surrounded in any direction only by higher points, but is not the absolute lowest point is called a *local minimum*. Similarly a high point that is surrounded only by lower points, but is not the absolute highest point is called a *local maximum*. Finding a local minimum or local maximum from a given point is called *local optimization*.

The more complex the objective function and the more variables it contains, the more difficult it is to use global optimization.

Optimization problems are either scalar optimization problems or vector optimization problems. Scalar optimization problems satisfy a single objective function *f* and can mathematically be defined as "min/max(f(x)) $f : M \rightarrow R$ from some set M to real numbers with the boundary conditions of $x \in X$ and $M \subseteq R$". Vector optimization problems use several objective functions. A single solution for these vector optimization problems is usually not existent. To select a single solution out of the set of solutions the individual objective functions have to be weight against each other.

Major categories of scalar optimization problems are:

- Linear optimization, where *f* is a linear function

- Quadratic optimization, where *f* is a quadratic function
- Discrete or Integer optimization, where x can only be part of a discrete subset of real numbers or an integer number
- Nonlinear optimization, where *f* is a nonlinear function
- Stochastic optimization, where parts of *f* are unknown, but the random distribution of *f* is known

Some techniques of local nonlinear optimization are:

- Line search: This method only works for one-dimensional problems
- Simplex method: No calculation of a gradient is needed. Many iteration steps are necessary, but the optimization technique is relatively robust against "problems" in the objective function.
- Gradient descent or steepest descent/ascent: Requires the first gradient of the objective function. With the gradient the steepest ascent/descent is followed for the next step. This method often requires many optimization steps.
- Quasi-Newton method: This method requires the first gradient. It is similarly robust as methods that do not require the first gradient, but it requires fewer steps than those.
- Newton method: In this case the first and second gradient are required. It is very fast, but very unstable against "problems" in the objective function.
- Method of feasible direction: This method is a simple method in optimization problems where the variables have to meet certain boundary conditions. It basically moves from one feasible point to the next along a feasible direction. The distance is determined by a line search algorithm.

- Sequential response surface method: this method starts with a small number of samples that generate a local response surface around the starting point via a regression analysis. Then it uses the gradient descent method to get closer to the minimum of the objective function. Finally around the minimum it uses samples to generate a multivariate polynomial that represents the area around the minimum. It uses the results of the previous steps in the current step and is therefore relatively fast.

2.3.3 Material Models in LS-DYNA

The following material models [25] were used in this research. The reasons for choosing these particular material models are discussed in *3.2.3 Material Models Used.*

2.3.3.1 Material Type 1: Elastic

In the elastic material model the co-rotational rate of the deviatoric Cauchy stress tensor is defined as:

$$\overset{\nabla}{\sigma}_{ij}^{\,n+1/2} = 2G\dot{\varepsilon}'^{\,n+1/2}_{ij} \tag{2.15}$$

And the pressure is defined as:

$$p^{n+1} = -K \ln V^{n+1} \tag{2.16}$$

Where G is the elastic shear modulus, K is the bulk modulus and V is the ratio of the current volume to the initial volume.

2.3.3.2 Material Type 6: Viscoelastic

The viscoelasitc material model is based on the deviatory part of the stress tensor $\overset{\nabla}{\sigma}_{ij}$ in a Jaumann rate formulation:

$$\overset{\nabla}{\sigma}'_{ij} = 2\int_0^t G(t-\tau)\frac{\partial \varepsilon'_{ij}(\tau)}{\partial \tau}\,d\tau \tag{2.17}$$

The shear relaxation behavior is defined according to Hermann and Peterson [28]:

$$G(t) = G_\infty + (G_0 - G_\infty)e^{-\beta t} \tag{2.18}$$

2.3.3.3 Material Type 62: Viscous Foam

This material model was originally added to LS_DYNA to model the energy absorbing foam found on the ribs of some crash test dummies.

The model is made of a viscous damper *D* in parallel with a non-linear spring E_1. For model stability reasons another spring was added in-line with the damper. The equations for the damper and the main spring are as follows:

$$E_1^t = E_1(V^{-n_1}) \tag{2.19}$$

$$D^t = D(abs(1-V))^{n_2} \tag{2.20}$$

Where V is ratio of the current to the initial volume and n_1 and n_2 are material parameters that have to be chosen for each case.

2.3.4 Coupling between MADYMO and LS_DYNA

Coupling between MADYMO [62][63] and LS-DYNA is a practice to use MADYMO models and LS-DYNA models in one simulation. MADYMO is well known for its geometrically detailed, accurate and well validated multibody, facet, and finite element dummy models. There are two common methods for coupling these two codes. In the traditional coupling method between LS-DYNA and MADYMO only linear contact stiffness of ellipsoids based on the Penalty Based Contact Method could be applied. This limited the usability of the MADYMO dummy models in LS-DYNA coupled simulations, since the non-linear material and therefore contact properties of the dummies were implemented. With the extended coupling method, described by Happee et al. [26] and commonly taught in Introductions to MADYMO, the contact forces are not calculated by the LS-DYNA solver, but by the MADYMO solver. LS-DYNA provides the contact surface position to MADYMO and MADYMO provides the contact forces to LS-DYNA. Therefore the full range of MADYMO dummies can now be used in LS-DYNA with all their contact properties.

2.3.5 Objective Rating of Simulation Results

To validate a model of any kind it has to be based on known properties or performances. In finite element modeling the simulation is usually based on tested material properties and then later its results are compared to a real world test outcome. Traditionally it is up to the experience and knowledge of the engineer to rate if and how valid a certain simulation result is. Since this is a highly subjective method and a more objective rating is desired, several rating systems have been discussed.

Some of these rating systems are based on predefined and user defined correlation criteria [15], some are based on experience and statistics [52], and others are developed specifically for automotive crash application [33].

Most of the rating systems use some form of comparing two curves according to one or several of the criteria of the peak value, the timing of the peak value, the shape of the curves, and how well a curve stays within a certain boundary.

Further the rating systems usually allow for user input, mostly through weighting factors. The weighting factors in combination with the criteria result in a final rating score.

The rating system that is used by TNO to rate the validation of their dummy models uses the following three criteria to compare two curves [31][64]:

- The value of peak absolute amplitude of the curves
- The timing of the peak absolute amplitude relative to the start of the time history
- The overall correlation of the curves

The criterion for the peak value comparison uses the following formula:

$$crit_1 = \frac{\max(0, f(t) \cdot g(t))}{\max(f(t)^2, g(t)^2)} \tag{2.21}$$

The criterion for the timing of the peak goes as follows:

$$crit_2 = \frac{\max(0, t(\max(f(t))) \cdot t(\max(g(t))))}{\max(t(\max(f(t)))^2, t(\max(g(t)))^2)} \tag{2.22}$$

The overall correlation between two curves is defined by the following criterion:

$$crit_3 = 1 - \sqrt{\frac{\int_T \max(|f(t)|, |g(t)|) \cdot \left(1 - \frac{\max(0, f(t) \cdot g(t))}{\max(\delta, f(t)^2, g(t)^2)}\right)^2 dt}{\int_T \max(|f(t)|, |g(t)|) dt}} \tag{2.23}$$

The overall rating is a combination of the three individual criteria according to:

$$comb = 1 - \sqrt{\frac{\sum_{i=1}^{3} (W_i \cdot (1 - crit_i)^2)}{\sum_{i=1}^{3} W_i}} \tag{2.24}$$

Where W_i is the weighting the user assigns to each criteria. All of the rating criteria and the combined rating return a scalar between 0 and 1. 1 would be a perfect match between the two curves.

2.4 Why a model of the Q3 dummy?

There have been many studies of the spines and necks of adults in regards to:

- The behavior during front, side, rear, and oblique crash situation and during rollover
- The structure of the neck and spine

- Direct impact of the body
- Airbag loading and much more

There are also many models of the adult spine and neck available. This ranges from relatively simple mass-spring-damper models and other abstract models over a large variety of adult size crash test dummies with varying detail of the spine and neck to very detailed finite element models of the spine and neck often derived from computer tomography and magnetic resonance imaging scans with extremely complicated material models of the hard and soft tissue to achieve the best results possible.

The reasons why the child population is much less well represented in automotive safety research than the adult population are:

- There is always at least one adult in each automobile on the roads, but much fewer children
- A model for a specific height and weight of adult covers a much larger number of individual of several different ages, whereas a child model only represents a children of a relatively narrow age gap
- Volunteer testing is only done on adults
- Cadaver tests, a good resource for research data to support models, are almost non-existent for children. Only a handful of tests are known, but none are recent. But adult cadaver testing is a common practice.
- Scaling techniques to scale models, data, and injury criteria from adult to child size are available, but have to be used with caution.
- Less injury data is available for children.
- Children tend to sit in the rear of a vehicle which is generally the safer seat

- Children properly restrained in child seat restraints have a lower likelihood of injury than properly restrained adults in a similar situation [24].

But since children are still growing and since even smaller injuries in childhood can have a greater impact then for adults and affect the child its whole life it is important to research possibilities to keep children safer. Child dummies are a great way to test safety features for children, but no child dummy represents correctly. Improved methods to evaluate injury threatening situations in laboratory environments have been called for, especially for side impact [4].In terms of biofidelity, the Q3 is , according to First Technology Safety Systems (FTSS), the best child dummy to date [23]. It is also currently the only child dummy representing three-year-olds that is designed to be used in side impacts. A finite element model of this dummy can help advance safety research for children.

CHAPTER 3 - METHODOLOGY

3.1 Model Creation

This chapter describes what process was used to create the finite element model of the Q3 anthropomorphic testing device.

3.1.1 Digitizing

Digitizing is a process in which three-dimensional surface geometry is captured by a point probe. In case of the Q3 finite element model development a FARO bronze arm was used. First the complete dummy was affixed to a very rigid steel table. Then three point-indicating stickers (yellow round stickers on upper arm of dummy in Figure 3.1) were placed on least deformable parts of every mayor component, like the head, chest, spine, pelvis, upper and lower arm, and upper and lower leg. Those three points generate a coordinate system for each specific component. The three points of all components were captured with the Faro arm and placed into a single file. The collection of coordinate systems in reference to each other makes it possible to generate the geometry of a component while it is not attached to the rest of the dummy and later position this geometry in the right position relative to the rest of the parts.

After that the mayor parts were unattached from the dummy for easier access with the point probe. Before points and spline lines of the geometry were captured, the three points for the coordinate system of the part were recaptured into a new file for the part. Initially the traditional approach, where a grid of masking tape is laid over the part and then the intersection point are digitized, was attempted (see arm of the dummy in Figure 3.1). But, since the Q3 dummy is relatively small and the surface contains many small radius curvatures, a new approach led to better result. In the new approach many free-hand spline lines of the surface were generated. The result was a close scatter of lines that many points and successive surfaces could be generated from (see Figure 3.2). Each edge, connection, and joint on every component was digitized with special care.

Figure 3.1: Digitizing Process

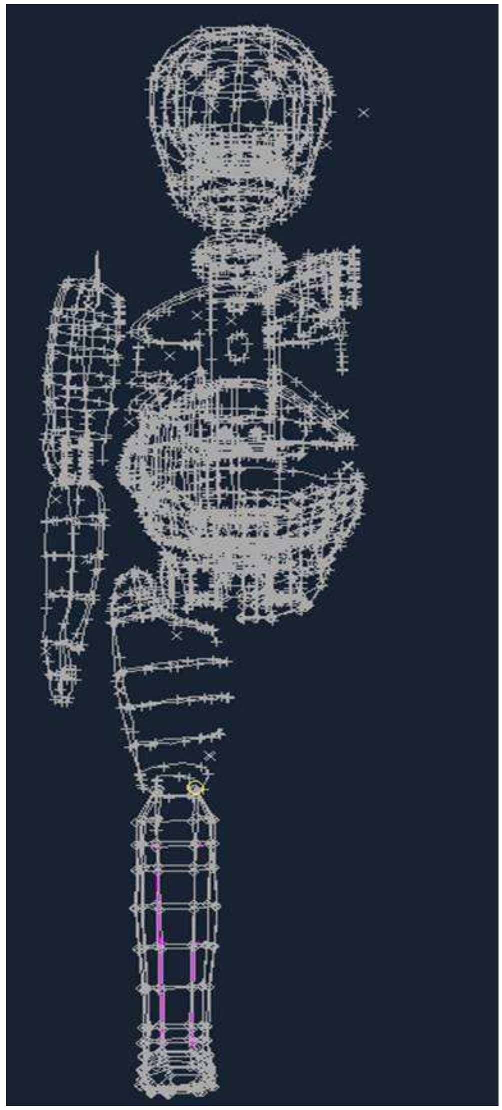

Figure 3.2: Point and Line Data of the Dummy

3.1.2 Other Methods for Surface Generation

Some of the components of the Q3 dummy are permanently glued or otherwise fused together and cannot be disassembled for digitization without destroying the dummy. Since the dummy was only a loaned model and no budget to buy parts was available other methods to capture hidden and inaccessible surfaces had to be employed.

Initially, the head, neck, upper and lower arm, lumbar spine, and upper and lower leg were x-rayed from the front and the side at Lancaster Community Hospital in Pennsylvania. The x-rays revealed the shape and thickness of the bone representing structures in the extremities, the thickness of the skin and flesh representing layer on the head, and the inside structure of the neck and lumbar spine. This information was used during the meshing process described in *3.1.3 Meshing*.

After the meshing process was nearly complete another opportunity for generating the inaccessible surfaces was presented. The research staff at Children's Hospital of Philadelphia (CHOP) offered to perform a Computed Tomography (CT-scan) of the whole dummy (see

Figure 3.3). The data from the CT-scan can be viewed in special software and surfaces can be generated. In this case, since the meshing was nearly complete, the CT-scans were used for verification of the surfaces generated through digitization and the x-ray pictures.

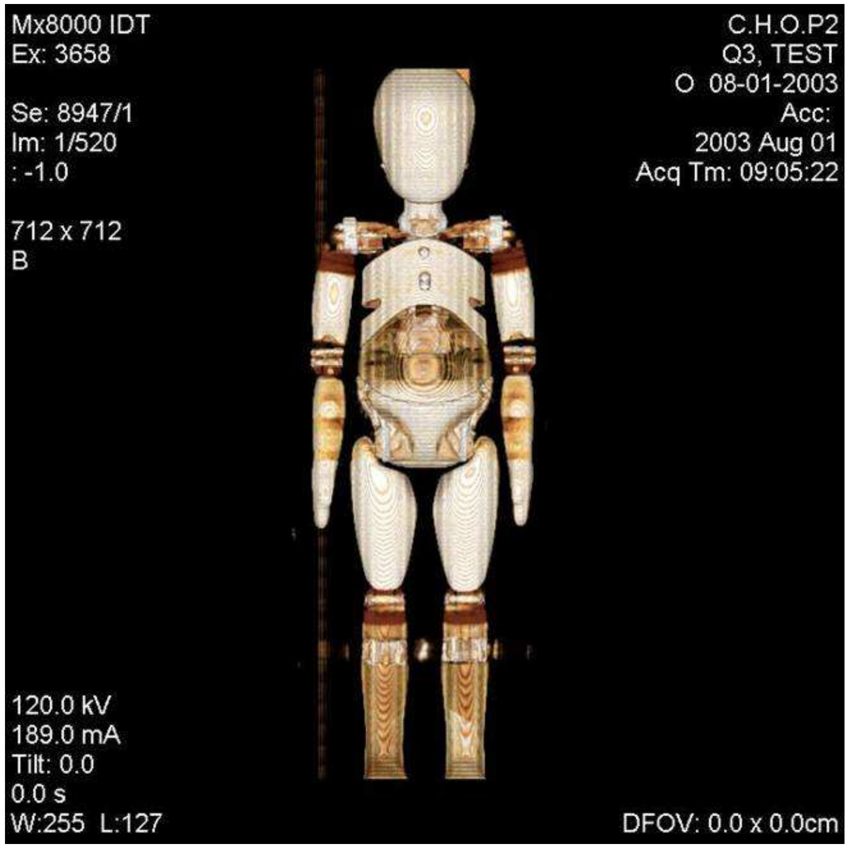

Figure 3.3: CT-scan of The Q3 Dummy

3.1.3 Meshing

General mesh parameters were chosen according to standards used for NCAC's finite element vehicle models and other similar models. For compatibility of the FEM models it is important that the mesh size and the critical edge length of elements do not vary too much. Non-uniform mesh size can cause contact problems. Non-uniform critical edge lengths can cause significant run-time increase or significant added mass, both of which are not desirable for fast run-times and accurate results. The meshing process was done in the Altair Hypermesh 7.0 meshing software. First the geometry files generated in the digitizing process were imported into the meshing software. Then the edge lines were identified. After that points were created on the spline lines. For parts with larger smooth surfaces, a careful selection of points was used to create lines approximately parallel to the edge lines. A sum of those parallel lines was used to create a surface including these lines. In some cases, like for example the head, those surfaces where then projected along the surface normal to create inner layers.

Initially all solid components were meshed using hexahedron also called “brick” elements. In prism-like structures, like neck, lumbar spine, and spine the elements were created by extrusion from a single meshed surface or by extrapolating between two surfaces. In case of the extremities the solid elements were created by creating multiple meshed surfaces and then using this mesh to create solid elements. More complex components were created by a combination of techniques. The abdomen as the most complex part had to be remeshed several times.

During the component level simulations it turned out that the foam parts that were modeled with hexahedron elements were unstable under large deformations. Therefore, all foam parts (upper and lower arms, upper and lower legs, and the abdomen) were remeshed out of tetrahedron elements, see Figure 3.4. Tetrahedron elements result in a stiffer response than they are supposed to, but in case of modeling foam materials the effect is minimal and the resulting mesh is much more stable than a mesh out of hexahedron elements [20].

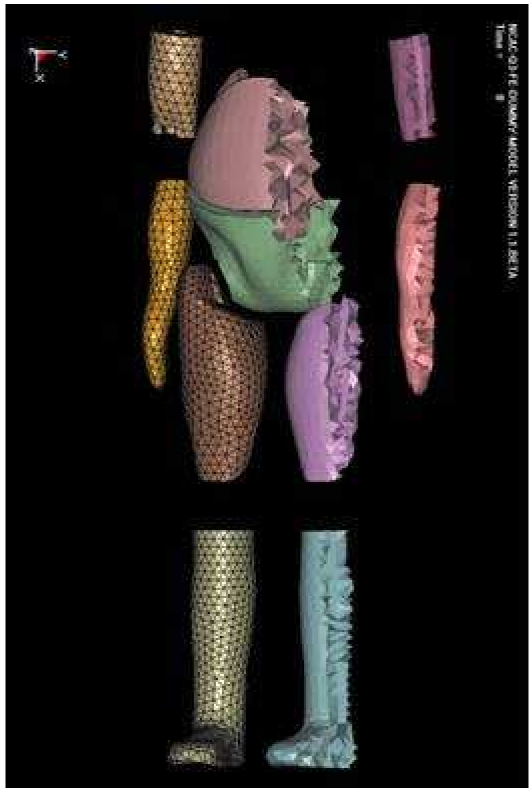

Figure 3.4: Foam Parts Modeled with Tetrahedron Elements

3.1.4 Model description

The finite element model of the Q3 consists of little fewer than 50,000 elements in 133 parts. More than 3/2 of the elements are solid elements. The rest are shell elements with the exception of 45 beam elements in the joints and in the cable of the lumbar spine, three discrete elements in the load cells, and three seatbelt accelerometer elements to represent the accelerometers in the dummy. The model incorporates 17 joints most of which represent actual joints in the Q3 dummy. Figure 3.5 shows a frontal and a side view of the finite element model of the Q3 Dummy.

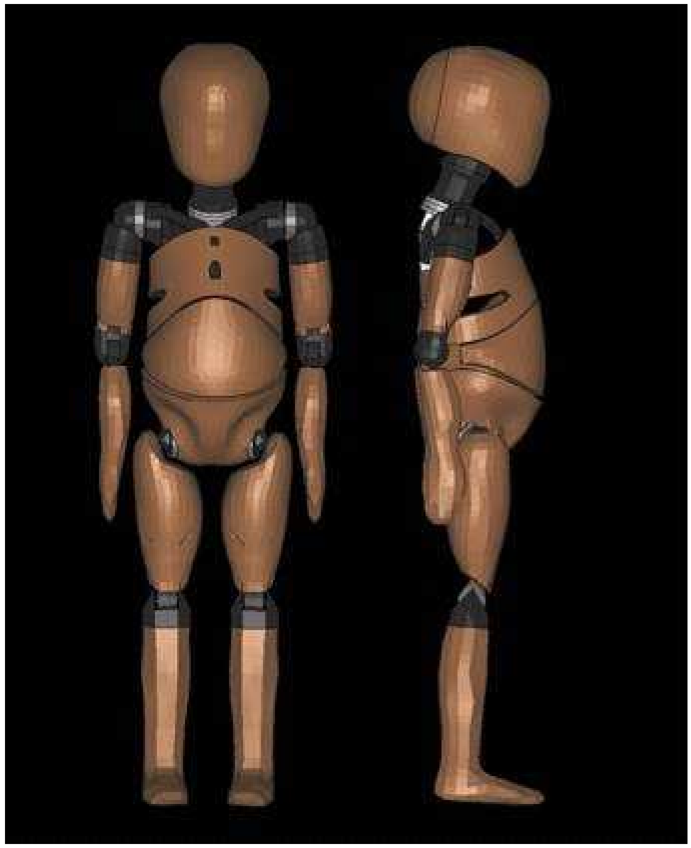

Figure 3.5: Finite Element Model of the Q3Dummy

3.1.5 Assembly and Early Tests

After completing the meshing part, the individual components were composed into one file. Then they were positioned with help of their local coordinate system and the corresponding coordinate system that was recorded when the dummy was fully assembled.

Parts that on the physical dummy are glued together were merged on glued surfaces if they are both represented by deformable material cards in LS-DYNA 3D. For deformable to rigid connections, constrained extra nodes were utilized. In case of fixed rigid body to rigid body connections, the rigid bodies were merged.

Bolts in the physical dummy are represented as nodal constraints in the finite element model. All movable joints in the dummy were also implemented in the finite element model.

Simple simulation runs were used to check if all components are properly connected. Further, those simulations also were used to determine if the mesh was stable enough for impacts that cause large elastic deformations on the dummy model.

3.1.6 Weighing and Photography

Since the physical Q3 anthropomorphic test device was loaned from the Japanese Automotive Research Institute (JARI) and was going to be given back within a relatively short time, every component was photographed from different angles with a scale next to it; as example, see Figure 3.6. Therefore those pictures could be used in an eventual need for remeasuring. Every component was weighted on a digital scale. The complete set of photos and a list of the components including their weight can be found in the appendix.

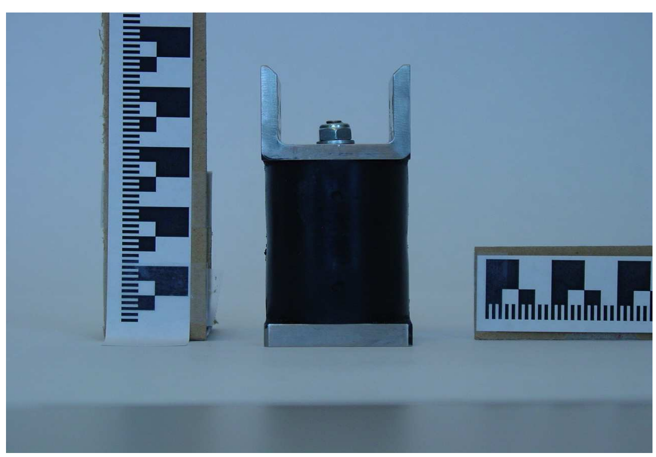

Figure 3.6: Example of Photographic Documentation, Lumbar Spine

3.2 Material optimization and Model validation

Validation is the most important part of a finite element analysis process. The results generated using finite element models that are not validated or of which the degree of correlation to the real world is unknown are practically worthless.

Ideally the materials used in a part that is modeled and their characteristics are known. Then the appropriate material characteristics can usually be relatively well represented in a finite element analysis.

Unfortunately in this case the manufacturer was not willing to share the material characteristics or even the type of material used in the dummy. Therefore other means of gathering and approximating the material characteristics were necessary.

3.2.1 Joint calibration

All movable joints on the dummy are revolute joints with exception of the hip joints and the shoulder joints. The hip and shoulder joints are ball joints. The shoulder also incorporates a revolute joint. This revolute joint is the only joint without a stop angle. All other joints are restricted in their range of motion.

All joints were measured for their internal friction and their range of motion. The data was implemented into the joint definition of the finite element model of the Q3 dummy.

3.2.2 Approximate Material Properties

The density of most of the materials used could be extracted from the weight of the components and the volume displaced when submerged, since most materials are used repeatedly throughout the dummy. However, the density of the rubber and foam used in the extremities had to be approximated.

To gather more approximate material properties, that are needed as a starting point for the optimization process the materials had to be further analyzed. The analysis consisted of mass spectrometer analysis of the metals performed by the Chemistry Department at the George Washington University and compression tests of the abdomen, ribcage, neck, lumbar spine, and the shoulder compound. Since these compression tests are not standardized and had to be performed without damaging the components, only a rough estimated stress strain relationship could be determined. It was however determined that all tested components experience a strong hysteresis in the stress strain relationship. The tests in and Figure 3.8 were performed at the Japan Automobile Research Institute (JARI). The tests pictured in Figure 3.9, Figure 3.10, and Figure 3.11 were performed at the School of Engineering and Applied Science Material Testing Lab of The George Washington University.

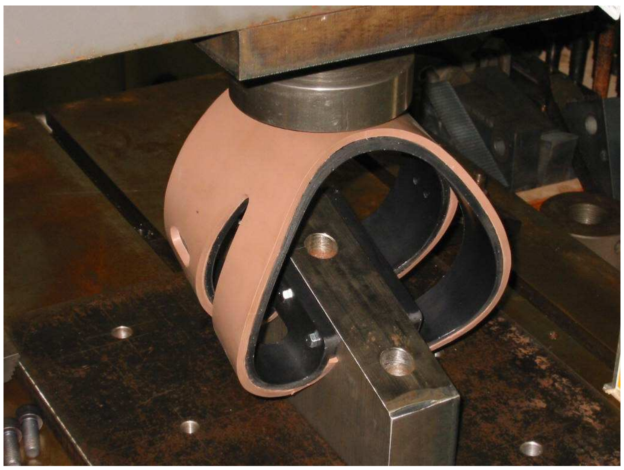

Figure 3.7: Rib Compression Test for Approximating Material Properties

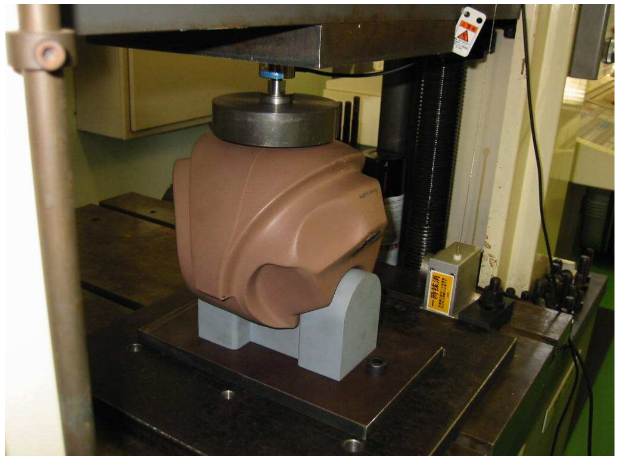

Figure 3.8: Abdomen Compression Test for Approximating Material Properties

Figure 3.9: Neck Compression Test for Approximating Material properties

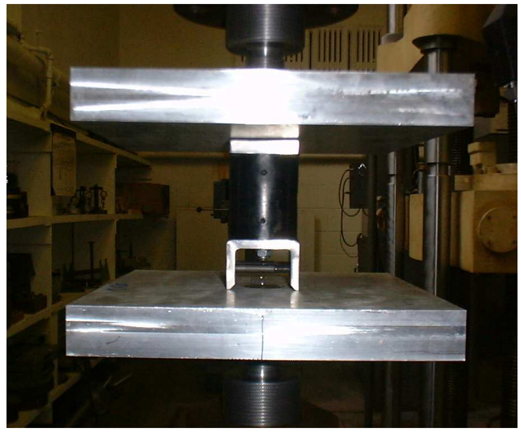

Figure 3.10: Lumbar Spine Compression Test for Approximation Material Properties

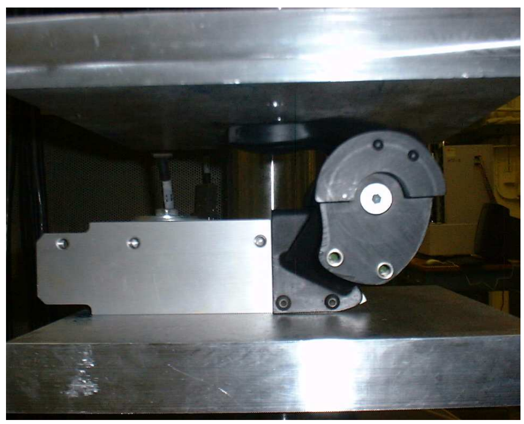

Figure 3.11: Shoulder Compound Compression Test for Approximation Material Properties

The data was compared to several available material databases [6][9][65] and the best matches were assumed as starting point for the optimization process.

3.2.3 Material Models Used

LS-DYNA offers the user a large variety of material models. They range from very simple models with only basic material parameters to very complex models that require the input of many different material parameters. The complex models are usually for a very specific material and sometimes only for a certain loading condition. Often they are sensitive in terms of mesh quality, amount of deformation, direction of loading and others conditions.

The material models used to model the Q3 dummy are relatively simple material models. In the early stages of the optimization process several models were tried out for each material used in the dummy. Some material models could not be modified to make the component tests match even remotely, even though they could have been an option according to the material model description. Other material models required many input parameters. Since practically none of the material parameters were known this would have complicated the optimization drastically. The last decision was made according to how stable the material model would behave during large and non-uniform deformations of the individual component.

The chosen materials were:

- Material type 1 for the thin skin of the dummy, for the black plastic part that basically represent the skeleton of the dummy and for the white plastic that is used as the main part of the head.
- Material type 6 for the thick skin on the head and on the ribs, for the rubber of the neck and for the rubber of the lumbar spine.
- Material type 20 for all metal parts of the dummy, like the spine box and the pelvis.
- Material type 62 for the foam in the abdomen, arms and legs.

3.2.4 Optimization Process

The optimization process is split up into two parts. The first part was the design of experiment and the second part the actual optimization. Both parts were performed with the help of the program Altair Hyperstudy 7.0. For each of the components that were tested in the component level tests a design of experiment and an optimization was performed.

The design of experiment is basically a more or less random check for the outcome of an equation or in this case a simulation within a certain predefined range of each unknown variable to find a good starting point for the optimization.

In this case the material parameters were the unknowns and the equation was a finite element analysis simulation of a component level test. The desired outcome is to match the test results of the individual component test. To compare the simulation outcome with the actual test outcome the basis equation was formulated that defines how good of a match each set of variables produced. This equation took into account the integral of the square of difference of the test results and the simulation results. In case of the neck and lumbar spine it also took into account the timing of the peak of the bending angles.

To start the design of experiment the approximate material parameters were utilized. First a rough design of experiment was performed with a relatively low number of simulations here called samples (20 to 50), but in a wider range of 10% to 1000% of the approximate material parameters. Unfortunately such a wide range was necessary to cover the wide range in materials in plastics and foams that could have possibly been used in the dummy.

A second design of experiment with a smaller range (50% to 200%) and a higher number of samples (around 100) was performed around the best matching material parameters. The best matching material parameters from the second design of experiment were used as a starting point for the optimization.

The samples within the range of the variables were drawn by the method of Latin Hypercube Sampling [40]. This generates a relatively good distribution of parameter values from a multidimensional distribution.

The optimization was run so that the earlier mentioned equation converges to a minimum. Ideally it would converge to zero, but that was not the case for any of the components. Instead it converged towards one of many local minima.

For the optimization process the Sequential Response Surface Method [12] was used.

After the main optimization procedure a stochastic analysis was performed around the found optimal material parameters to confirm their robustness.

3.2.5 Component Tests Used for Optimization and Validation

The component level tests that were used for optimizing the material properties and also for validating the components were all performed at Japan Automobile Research Institute (JARI).

3.2.5.1 Head Drop Test

The head drop tests have been performed according to the TNO Q3 dummy user documentation [61]. The tests were carried out from two different heights, 130mm and 200mm. For each height the test was repeated three times. The configuration for the test can be seen in Figure 3.12 and Figure 3.13 shows the actual test. During the test, the acceleration of the head was measured by the three-axial accelerometer mounted roughly in the center of gravity of the head form. For the optimization the X and Z direction of the acceleration of the lower head drop test were used. For the validation the X and Z direction of the higher drop were used. Since the accelerations of the three tests at each height were almost identical, only the acceleration curve that was closest to the average of the three acceleration curves was used.

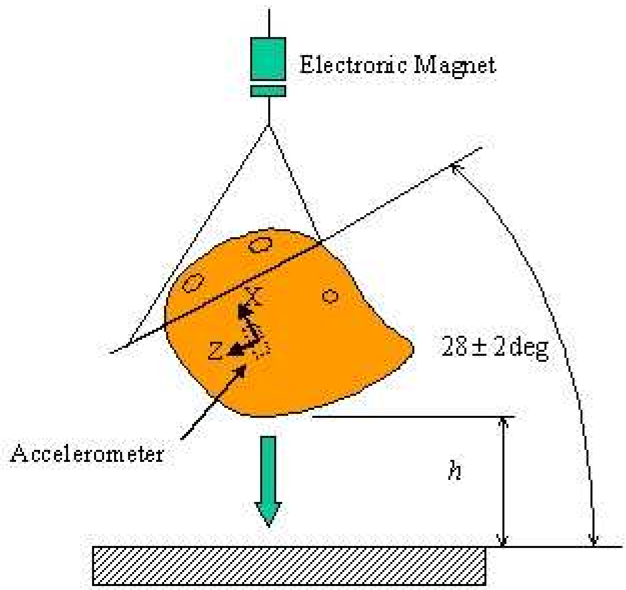

Figure 3.12: Head Drop Test Configuration

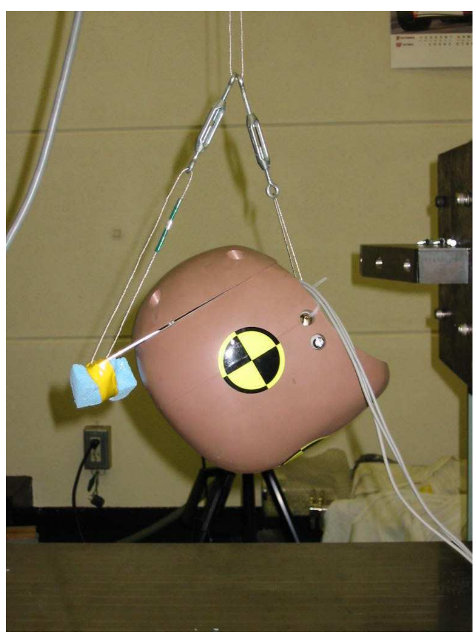

Figure 3.13: Head Drop Test

3.2.5.2 Neck Pendulum Tests

The frontal and lateral neck pendulum tests have been performed according to the TNO Q3 Dummy user documentation [61]. The pendulum used for the neck and the lumbar spine tests is shown in Figure 3.14. For the test the neck is mounted lateral or frontal, depending on the test configuration, upside-down at the end of the pendulum and a weight representing the head form is mounted at the end. The test configuration for the frontal test is shown in Figure 3.15 and for the lateral test in Figure 3.16. For the test the pendulum arm is lifted to a certain angle and then released. When the pendulum passes it's vertical position it impacts an aluminum honeycomb block that decelerates the pendulum. The acceleration of the pendulum is measured with an accelerometer that is mounted on the pendulum arm itself. The impact speed of the pendulum is measured by a speed sensor. Further the neck bending angle is measured via two rotational potentiometers, one mounted on the pendulum arm and one mounted on the head form. The neck load cell that is between the top of the neck and the head form measures the forces and moments in three directions. The tests were performed at two different angles, resulting in two different impact speeds. Each test condition was repeated three times.

For the optimization process the lower impact speed was utilized. The result of the higher impact speed was used for the validation of the neck.

Figure 3.14: Pendulum for Neck and Lumbar Spine Tests

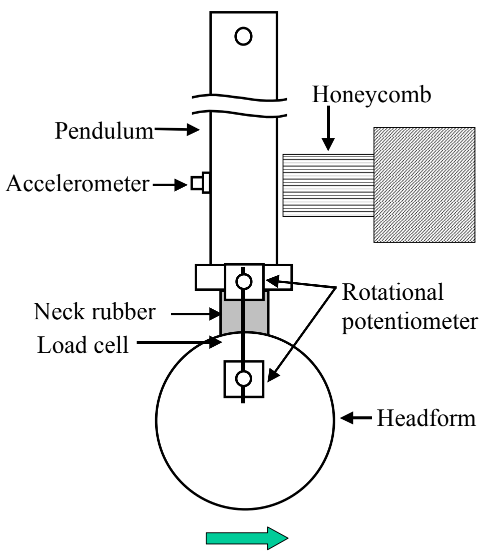

Figure 3.15: Frontal Neck Pendulum Test Setup

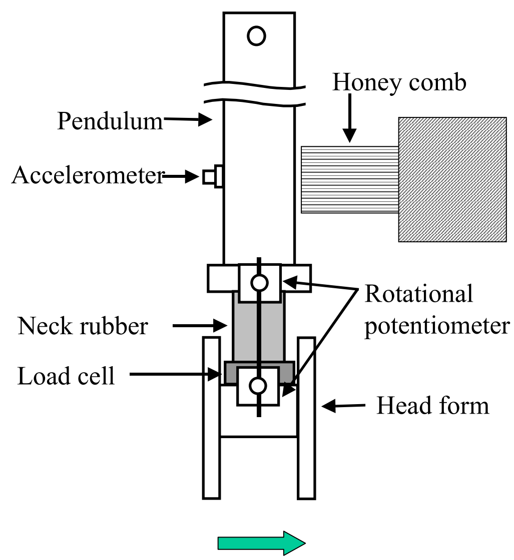

Figure 3.16: Lateral Neck Pendulum Test Setup

3.2.5.3 Lumbar Spine Pendulum Tests

The lumbar spine pendulum tests were also performed according to the TNO Q3 dummy user manual [61]. For the tests the lumbar spine is mounted lateral or frontal upside-down at the end of the pendulum. On the other end of the pendulum is the head form mounted. The setup of the frontal and lateral lumbar spine pendulum test can be seen in Figure 3.17 and Figure 3.18. As in the neck pendulum tests, the pendulum is released from two different angles and each test condition is repeated three times. The acceleration and the impact speed of the pendulum are measured. The bending angle of the lumbar spine and the forces and moments at the base of the lumbar spine are recorded.

The data from the lower impact speed was used for the optimization process and the data from the higher impact speed was used for validation of the lumbar spine.

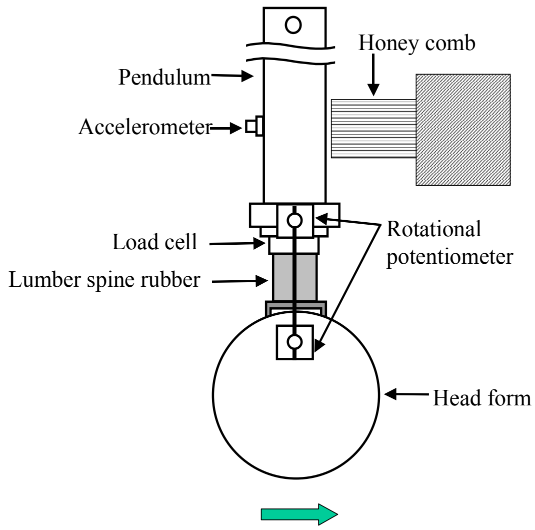

Figure 3.17: Frontal Lumbar Spine Pendulum Test Setup

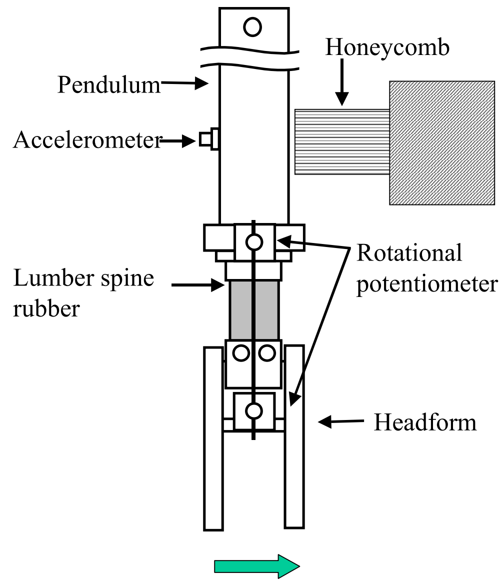

Figure 3.18: Lateral Lumbar Spine Pendulum Test Setup

3.2.5.4 Ribcage Impact Tests

In these tests, the ribcage was impacted with a piston that is propelled with compressed air and then glides almost frictionless until it impacts the ribcage. The ribcage is bolted to a special fixture so that the piston head hits the front center of the ribcage at a zero degree angle as can be seen in Figure 3.19 and Figure 3.20. The piston has a mass of 4kg and its head has a diameter of 100mm. The data of the accelerometer on the piston and the speed of the piston before impact are recorded. The tests were performed at three different impact speeds and were repeated three times.

The low and medium impact speed tests were used for the optimization process whereas the high impact speed test was used for the validation of the ribcage.

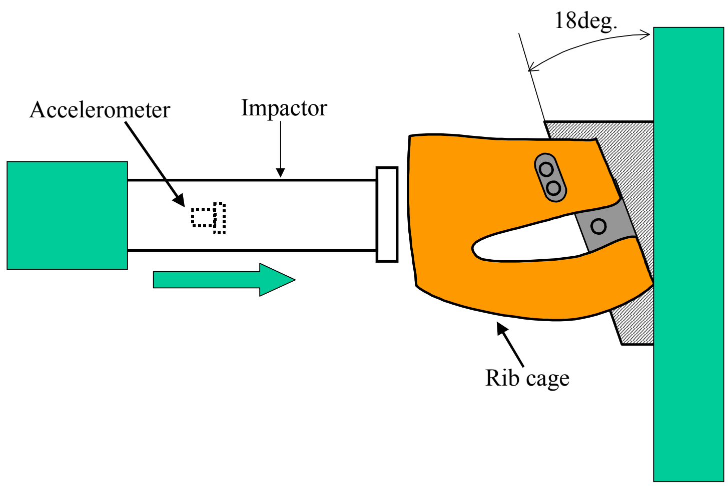

Figure 3.19: Ribcage Impact Test Setup

Figure 3.20: Ribcage Impact Test

3.2.5.5 Abdomen Impact Tests

The abdomen impact test is performed with the same piston as described in the ribcage impact test above. The abdomen is only held in place by a formfitting mount and short strips of tape. The setup of this test can be seen in Figure 3.21 and Figure 3.22. The impact speed of the piston and the acceleration of the piston are recorded. The tests were performed at three different impact speeds of the piston and were repeated three times each.

The low and high speed tests were used for optimizing the abdomen. For its validation the medium speed tests were used.

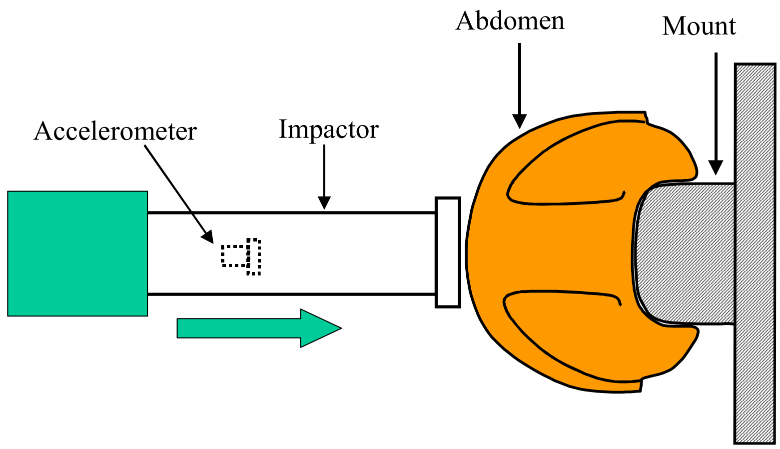

Figure 3.21: Abdomen Impact Test Setup

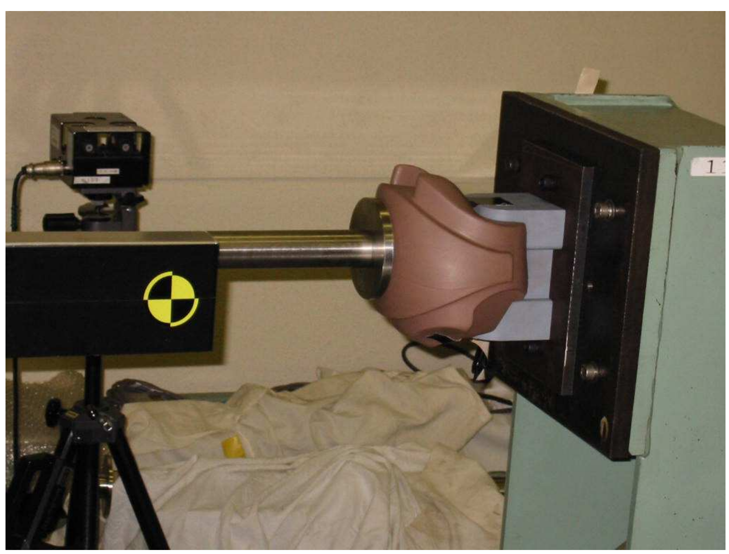

Figure 3.22: Abdomen Impact Test

3.2.6 Complete Dummy Tests Used for Validation

Two types of tests were performed with the complete dummy. Both have the Q3 dummy sitting on two Teflon sheets on top of each other to minimize friction with the ground and being impacted by a piston setup similar to the ribcage or abdomen tests described above. The piston in the complete dummy tests has a mass of 3.8kg and the face of the piston is 82mm in diameter.

In both cases the dummy is fully equipped with sensors and the acceleration and impact speed of the piston are recorded. The measurements on the dummy are as described in Figure 3.23. The accelerations are measured by three linear accelerometers that are mounted on an accelerometer mounting block. The moments and forces are measured by load cells that record moments and loads in three directions. The chest deflection is measured by a string potentiometer that is mounted in the spine box of the dummy with the other end of the string being connected to the inside of the center of the ribcage.

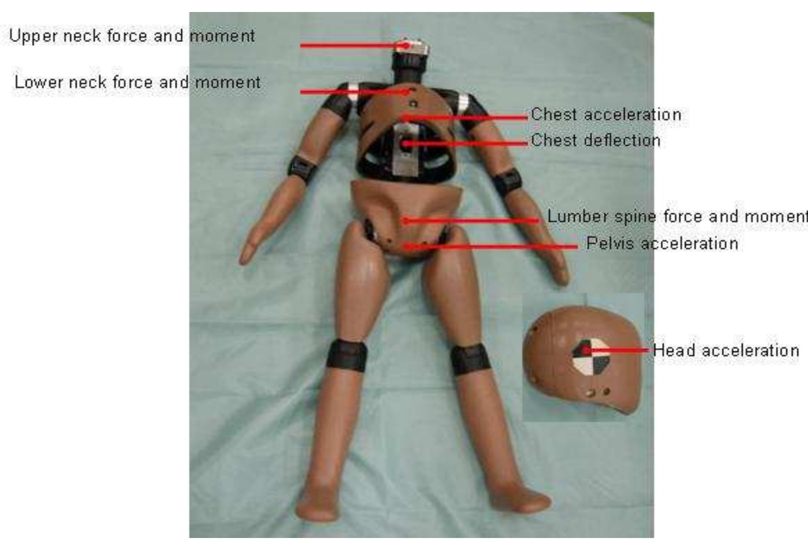

Figure 3.23: Q3 Dummy Instrumentation

3.2.6.1 Complete Dummy Frontal Impact Test

In the frontal impact test of the complete Q3 dummy, the piston impacts the center of the ribcage. The setup of the frontal impact test can be seen in Figure 3.24 and Figure 3.25. The tests were run at a lower and a higher impact speed of the piston and were repeated three times.

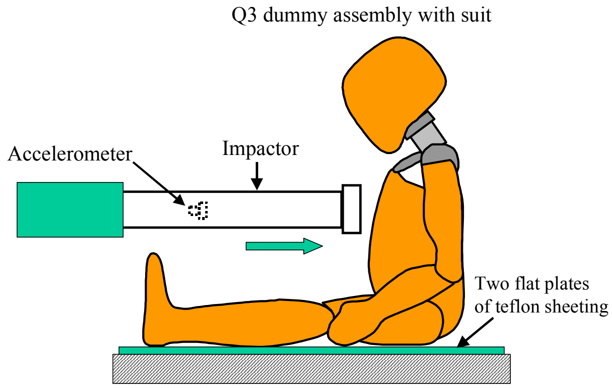

Figure 3.24: Frontal Impact Test Setup

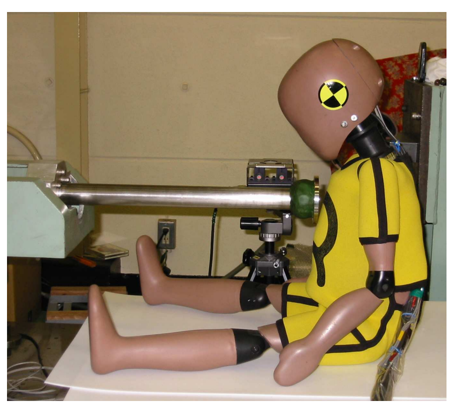

Figure 3.25: Frontal Impact Test

3.2.6.2 Complete Dummy Lateral Impact Test

In the lateral impact test of the sitting dummy, the right arm is removed so that the piston hits the center of the ribcage directly as pictured in Figure 3.26 and Figure 3.28. In this test the dummy is initially supported by a heavy metal cylinder that is placed behind the dummy. The cylinder is placed, so that its centerline is 50mm further towards the piston than the centerline of the dummy, see Figure 3.27. The tests were run at two different impact speeds and repeated three times each.

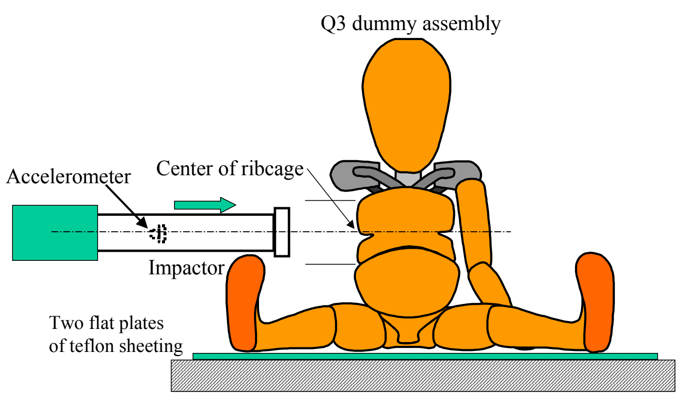

Figure 3.26: Lateral Impact Test Setup

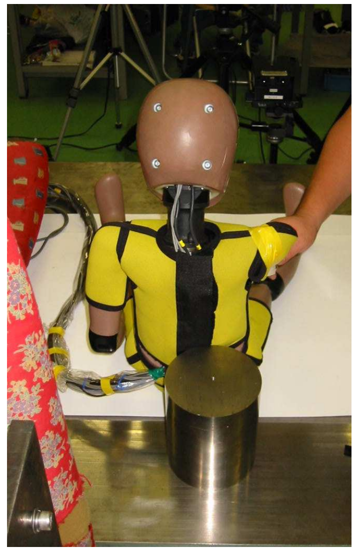

Figure 3.27: Lateral Impact Test Setup, Back View

Figure 3.28: Lateral Impact Test

3.3 Comparison with MADYMO Models

There is no available full scale test run with the version of Q3 dummy that was modeled for this research. MADYMO, the company that developed the Q3, provides an ellipsoid model of the Q3 in their modeling software. According to TNO, this model was validated. A comparison of the MADYMO Q3 ellipsoid model and the FE model of the

Q3 developed for this research may make the results of the FE model more acceptable in the research community.

A New Car Assessment Program (NCAP) test that is available through the National Highway Traffic Safety Administration (NHTSA) and that was run with a Hybrid III three-year-old anthropomorphic test device was simulated using a finite element model of the rear seat bench of the Hyundai Santa Fee, a finite element model of a child seat, and the ellipsoid model of the Hybrid III dummy. This method required that coupling of MADYMO and LS-DYNA was used.

The MADYMO Hybrid III ellipsoid model was then replaced with the MADYMO Q3 ellipsoid model. The results from that were compared to a simulation run with the finite element model of the Q3 dummy developed in this research.

The setup of the sled for the simulations is as shown in Figure 3.29. The pulse for the simulations was generated using the right rear cross-member deceleration of the NCAP test. This represents the deceleration that the rear seat bench experiences. The pulse was then filtered to ensure it does not cause instabilities in the simulations and inverted as is typically done with sled test pulses. The pulse used for the simulations is pictured in Figure 3.30.

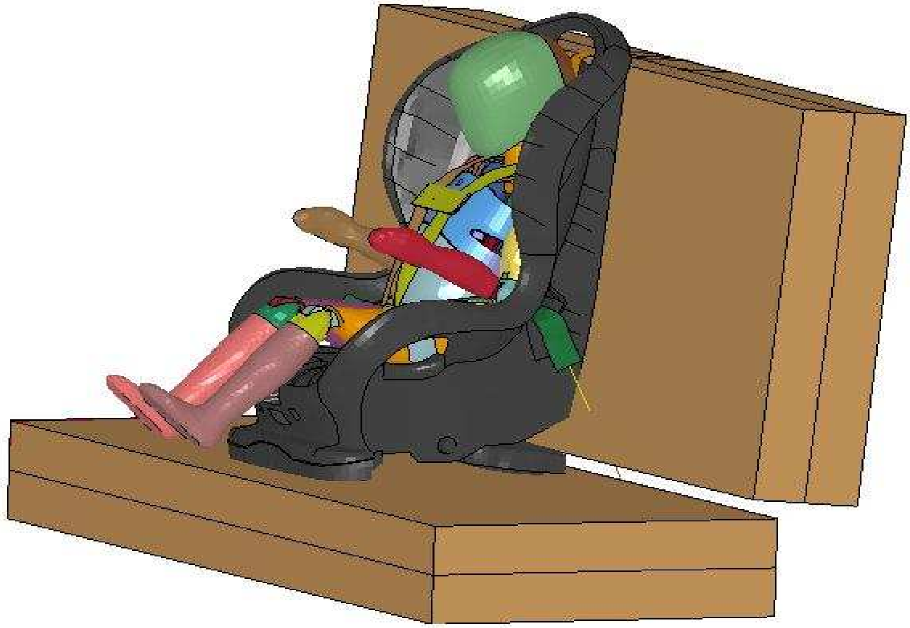

Figure 3.29: Sled Setup for Simulations

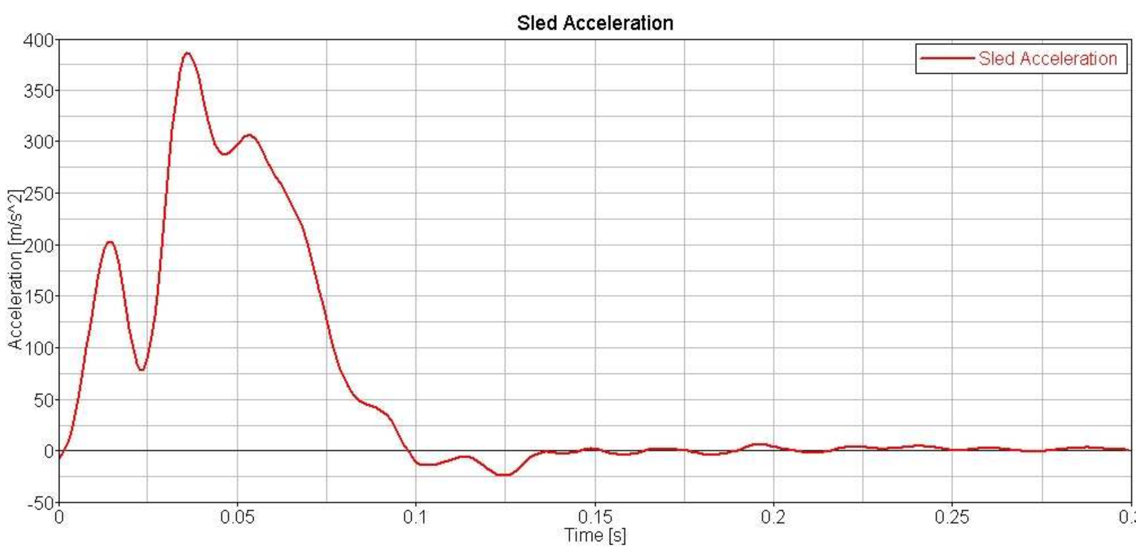

Figure 3.30: Sled Acceleration Pulse

3.4 Alteration of the Spine of the Q3

As previous research has shown [58][70], the solid spine box used in current production child crash test dummies may be not as biofidelic as it could be. Simple changes to the spine box change the injury response of child dummies in crash tests and may make the dummy more realistic. Therefore the rigid aluminum spine was modified in several stages. Combinations and variations of the green section and the two light red sections in the spine pictured on the right of Figure 3.31 were replaced with flexible rubber material from the dummy's neck.

The dummy was then run in the same simulation environment as in *Comparison with MADYMO Models* described above with the sled setup shown in Figure 3.29 and the pulse shown in Figure 3.30. The only stable simulation was achieved with only the green section replaced by rubber material.

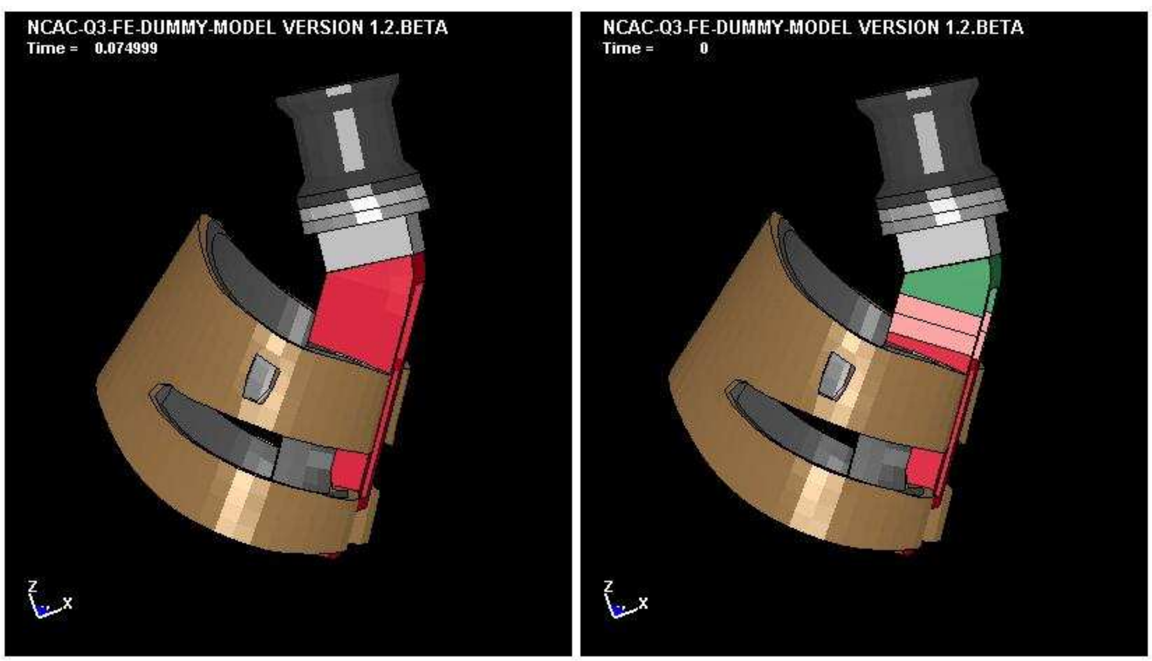

Figure 3.31: Comparison Between Original Spine and Modified Spine

CHAPTER 4 - RESULTS AND FINDINGS

4.1 Component level

In the following five sections are the results from the component level simulation compared to the results from the component level tests. Some of the figures show results from optimization runs, others show results from validation runs. The red doted line is always from the test; the green solid line is from the corresponding optimization or validation simulation.

4.1.1 Head Drop Test

Of the two drop test performed by JARI, the lower one was utilized for the optimization and the higher one was used for validation. The measurement was taken from the standard head accelerometer that is mounted roughly in the center of gravity of the head.

4.1.1.1 Head optimization

Figure 4.1 and Figure 4.2 show the results of the optimization of the head drop test. The peak acceleration in X and Z direction are less than 10% higher in the simulation than the test. The timing of the peak acceleration is very close to the test, the peak of the Z acceleration matches the test better than the peak of the X acceleration.

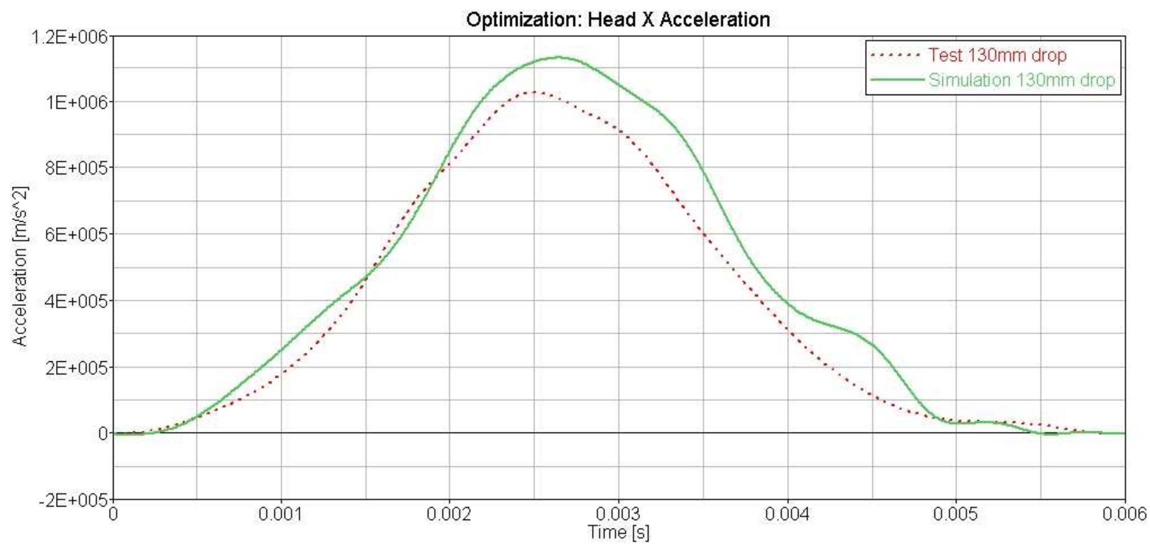

Figure 4.1: Optimization: Head Drop Test X Acceleration Low

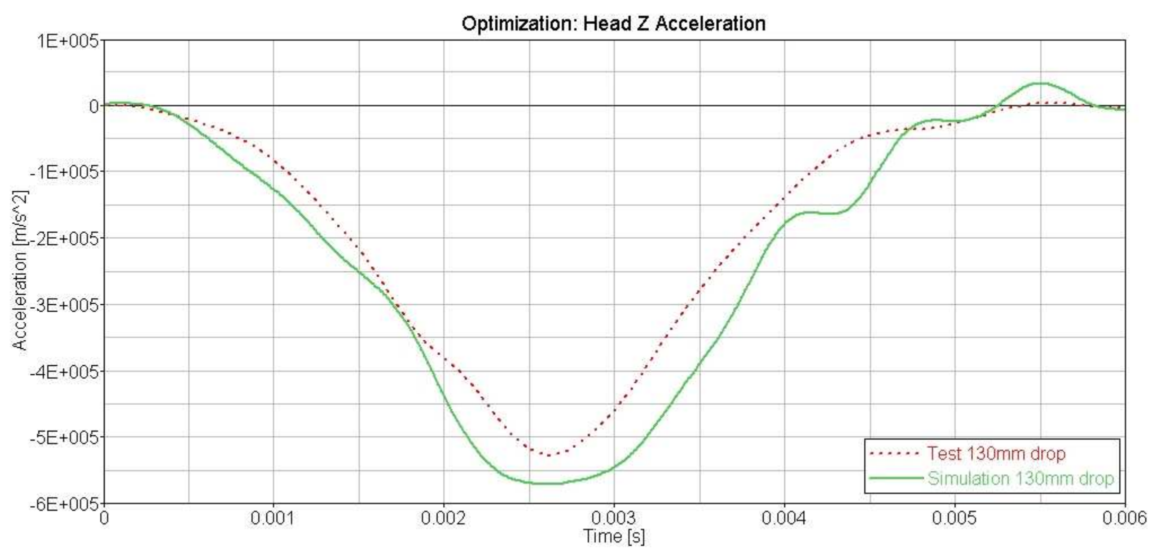

Figure 4.2: Optimization: Head Z Acceleration Low

4.1.1.2 Head Validation

Figure 4.3 and Figure 4.4 show the results of the validation simulation compared to the higher head drop test from a height of 200mm. In the validation, the timing of the peak accelerations resembles the test closely. The value of the peak acceleration in X direction is around 10% higher in the simulation than the test, for the Z direction it is less. The accelerometer in the model experiences a vibration that is not observed in the test.

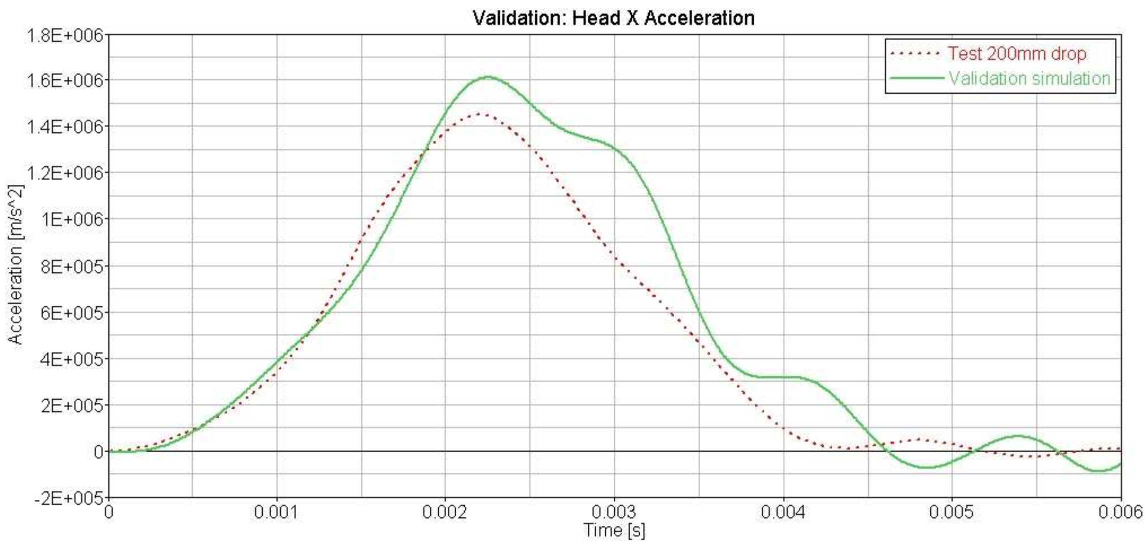

Figure 4.3: Validation: Head X Acceleration High

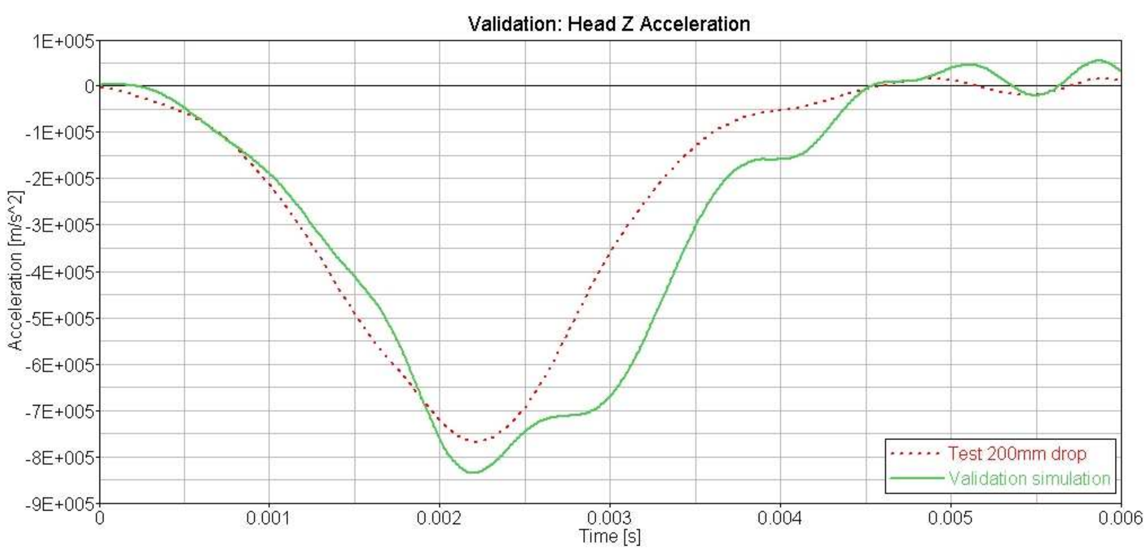

Figure 4.4: Validation: Head Z Acceleration High

Table 4.1 shows the objective ratings of the head drop test results. With an average match of 87% between the tests and the simulations, the head drop test can be considered successfully validated.

Table 4.1: Objective Rating of the Head Drop Test Results

	crit 1: Peak Value	crit 2: Timing of Peak Value	crit 3: Overall Correlation	comb: Combined Objective Rating
Optimization X Direction	0.902158	0.94371	0.847787	0.8905919
Optimization Z Direction	0.923059	0.983821	0.812891	0.8828228
Validation X Direction	0.898168	0.982128	0.784448	0.8619761
Validation Z Direction	0.919417	0.994863	0.731679	0.8382222

4.1.2 Neck Pendulum Test

The neck component test was the only component test that involved a joint within the component test. The nodding joint is between the neck and the head form. It allows the head form to rotate 28 degrees to either side from its neutral position and is dampened at the end of the rotation by a relatively soft rubber stopper. Even though the neck joint was tested and therefore predefined in the simulation, it added another degree of complexity into the optimization.

4.1.2.1 Neck Optimization

The neck flexion angles in the frontal test, Figure 4.5, show that the neck in the simulation flexes a little to fast. However, in the lateral test, Figure 4.6, the flexion angle of the simulation and the test are very close. Since the nodding joint does not influence the lateral bending angle, this indicates that the fast bending is actually a function of the nodding joint. The peak flexion angles in the frontal and lateral optimization were about 15-20 percent to high for the simulation.

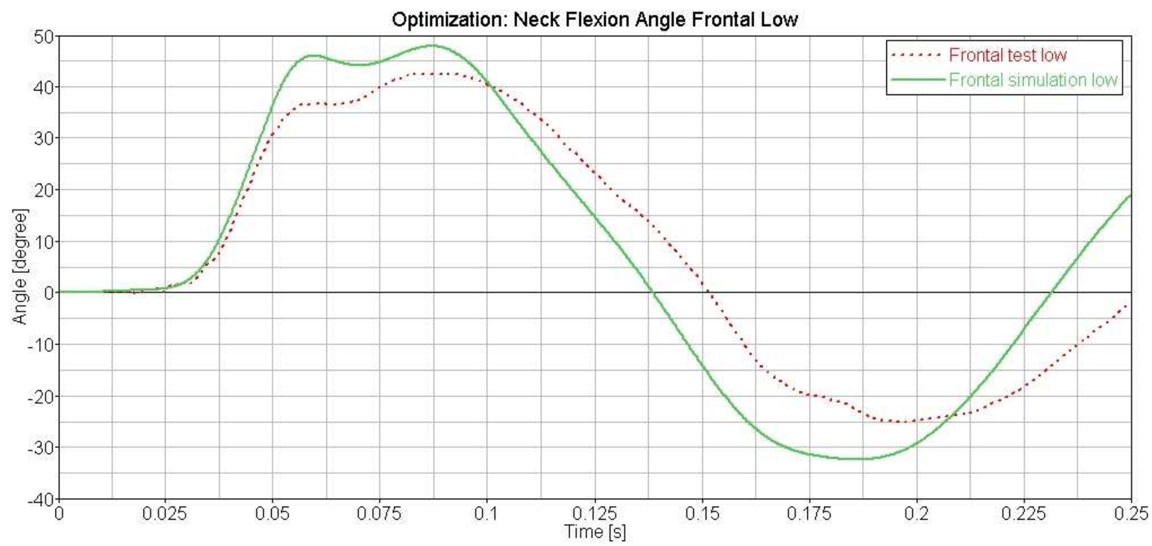

Figure 4.5: Optimization: Neck Flexion Angle Frontal Low

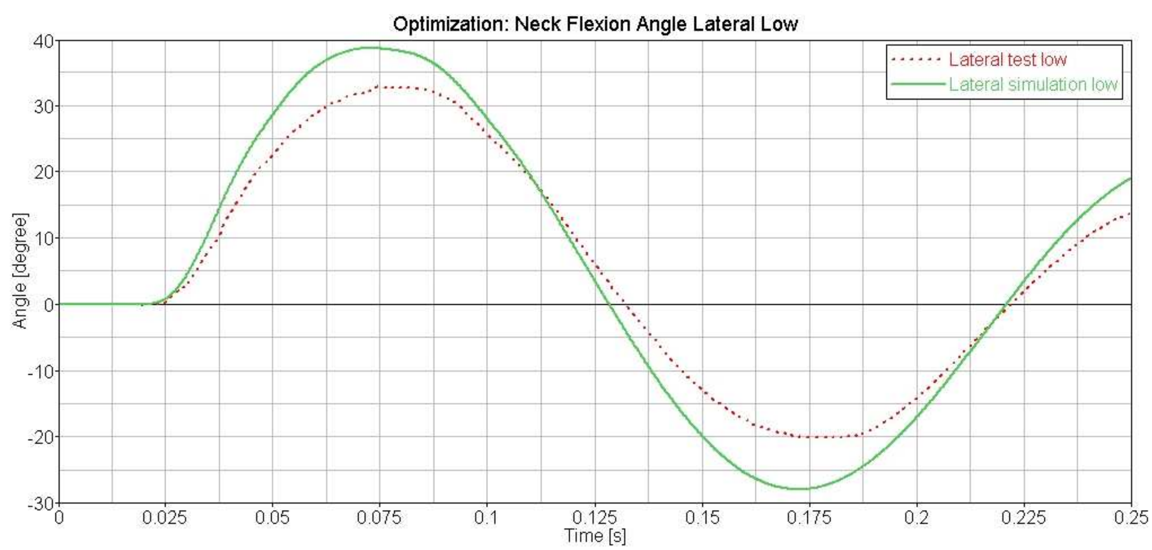

Figure 4.6: Optimization: Neck Flexion Angle Lateral Low

The peak moments at the neck load cell and their timing were very similar for the optimization simulations and the tests, Figure 4.7 and Figure 4.8.

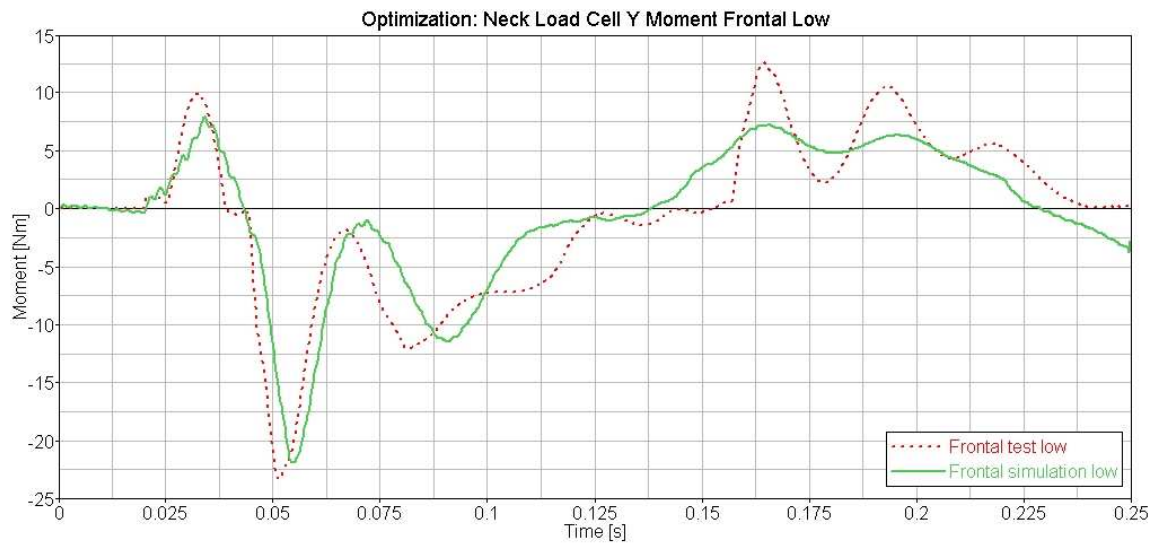

Figure 4.7: Optimization: Neck Load Cell Y Moment Frontal Low

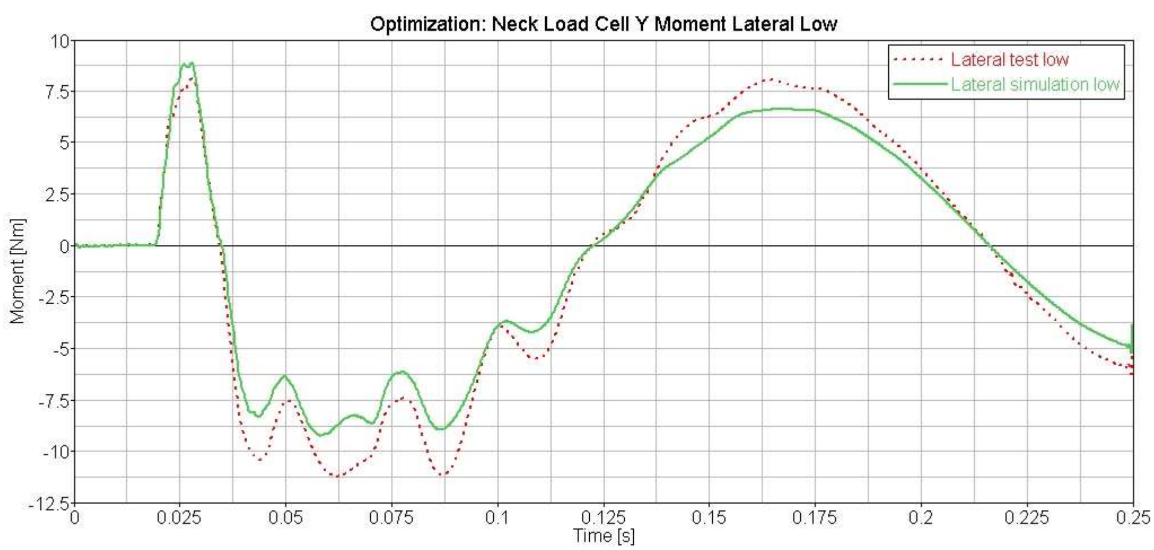

Figure 4.8: Optimization: Neck Load Cell Y Moment Lateral Low

The peak force in X direction in the frontal optimization simulation, Figure 4.9, is less than 10% higher than the test data. The peaks in the simulation are also a little later than in the test. The spike on the rebound in the test is possibly a second contact of the pendulum with the honeycomb structure that stops the pendulum and it is not as pronounced in the simulation.

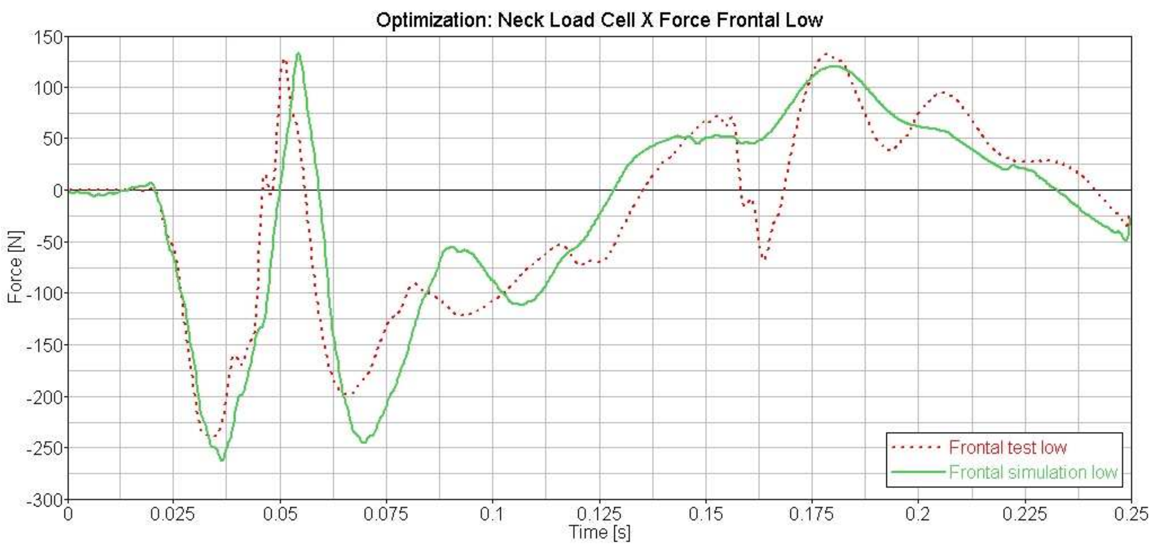

Figure 4.9: Optimization: Neck Load Cell X Force Frontal Low

In the lateral optimization of the neck, the force in X direction is almost a 100% match of the forces in the test, Figure 4.10.

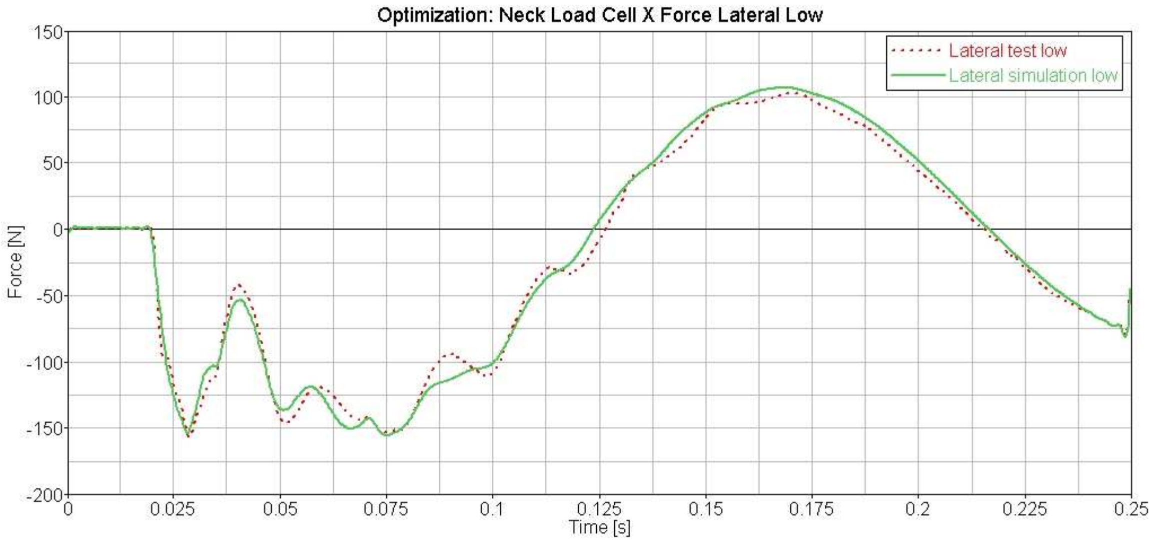

Figure 4.10: Optimization: Neck Load Cell X Force Lateral High

A similar picture for the forces in Z direction, the forces in the frontal case, Figure 4.11, the peaks in the simulation lag in timing the peak in the test and the peak values are off by several percent. But in the lateral case, the timing is almost perfect and the peak values also match better, Figure 4.12.

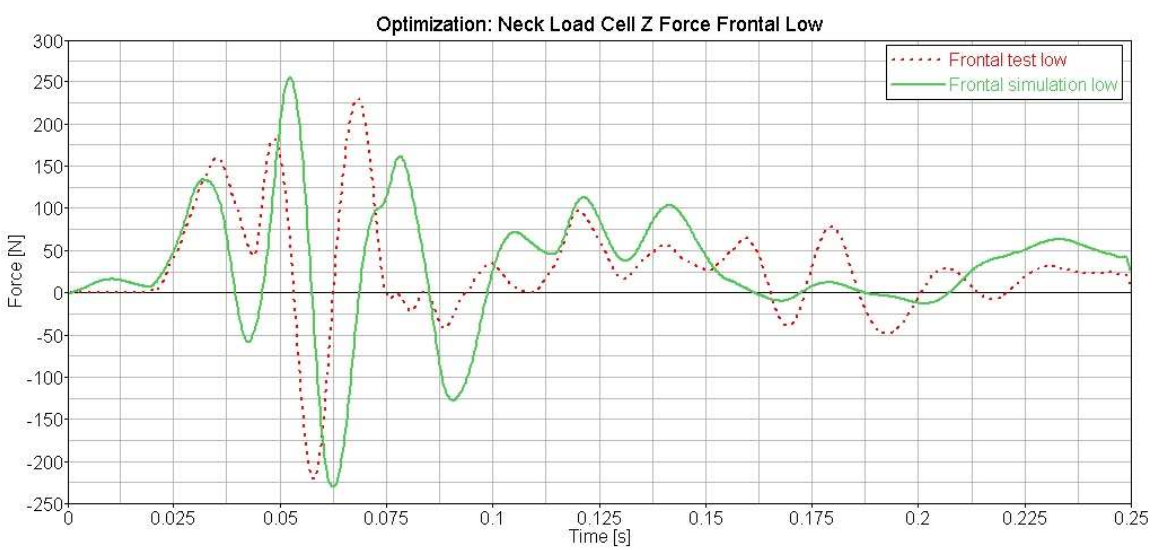

Figure 4.11: Optimization Neck Load Cell Z Force Frontal Low

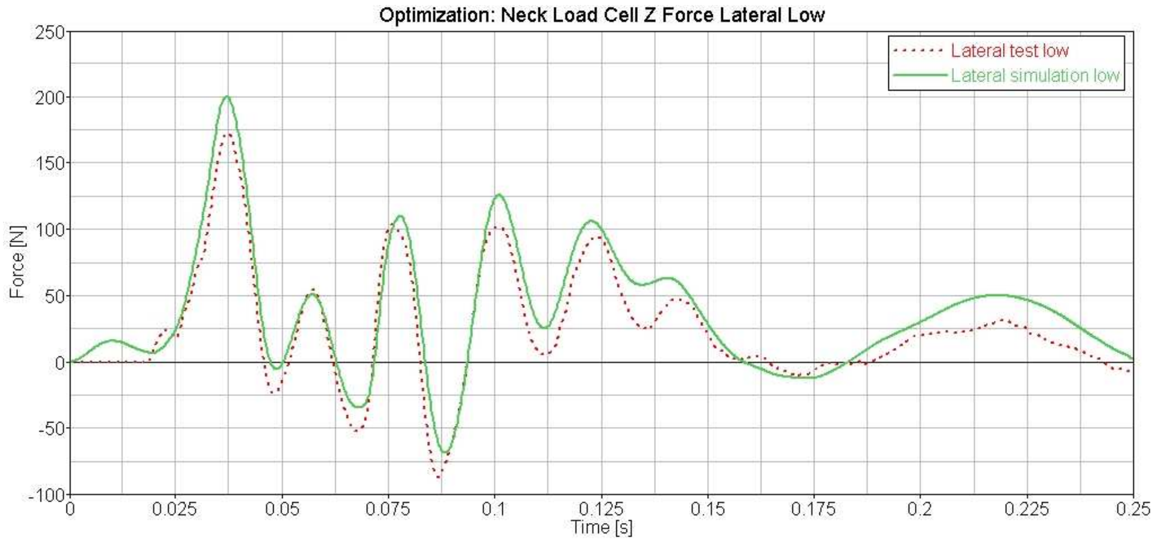

Figure 4.12: Optimization Neck Load Cell Z Force Lateral Low

4.1.2.2 Neck Validation

For the validation, the frontal and lateral pendulum test with a higher closing velocity were chosen. Similar to the optimization results, the timing of the frontal flexion angle is faster in the simulation than the test, Figure 4.13. In the lateral case, the timing is much better, Figure 4.14. In both cases, the finite element neck bends about 15% further than the neck in the test.

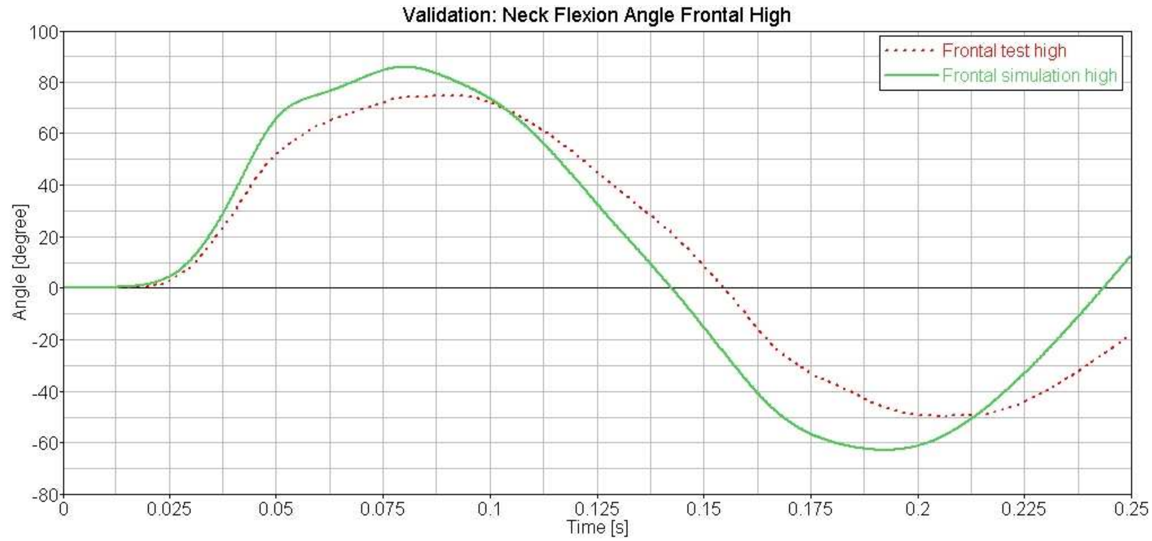

Figure 4.13: Validation: Neck Flexion Angle Frontal High

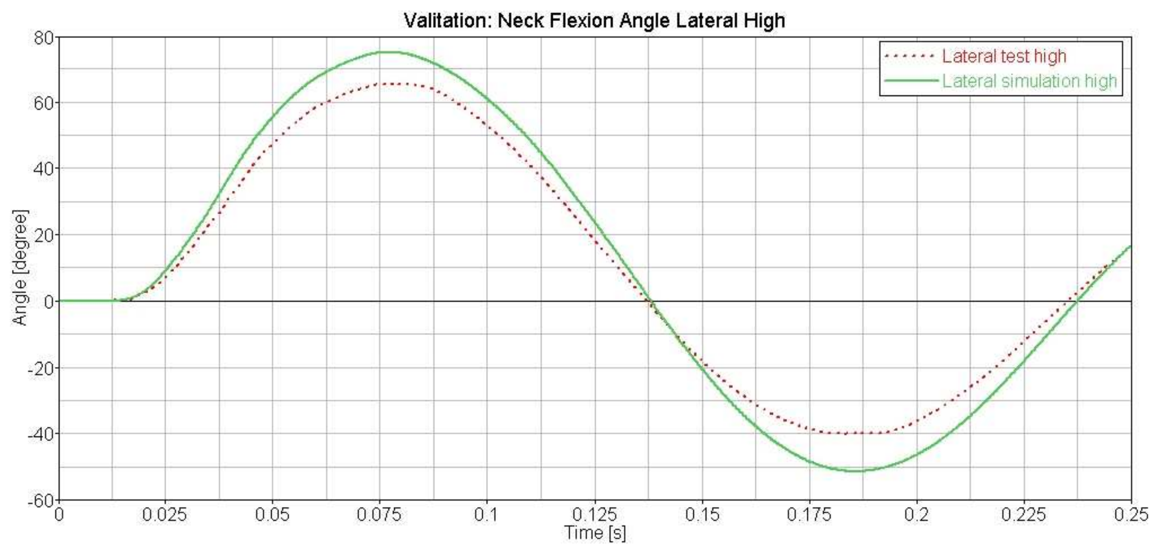

Figure 4.14: Validation: Neck Flexion Angle Lateral High

The timing of the moment in the validation simulations match the test very well, but in the frontal case, Figure 4.15, the peak moment for the simulation is about 20% higher and in the lateral case, Figure 4.16, it is around 25% lower than the test

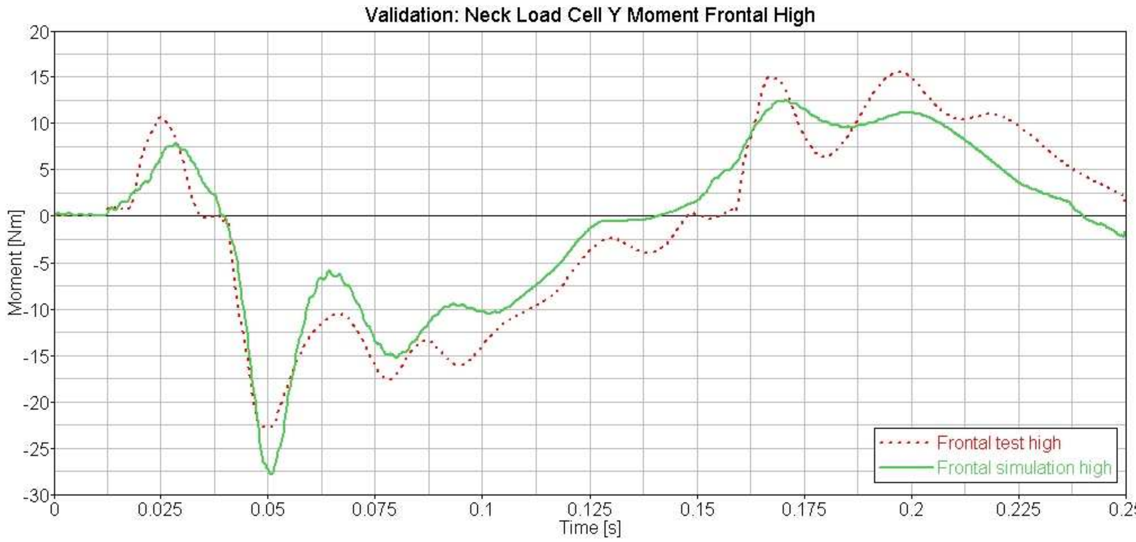

Figure 4.15: Validation: Neck Load Cell Y Moment Frontal High

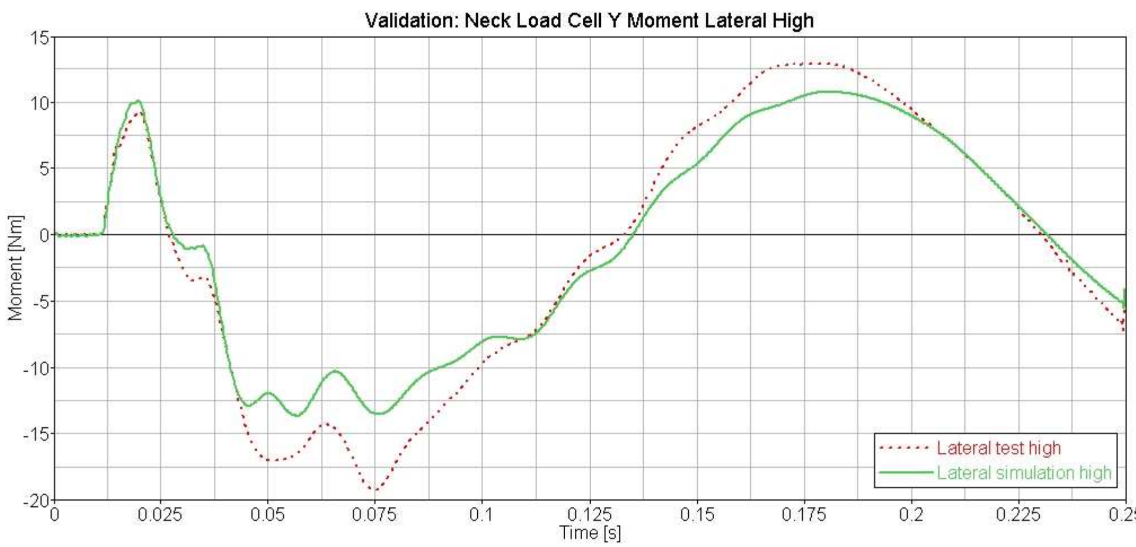

Figure 4.16: Validation: Neck Load Cell Y Moment Lateral High

The test data in Figure 4.17 also shows the spike on the rebound. In this case the simulation follows this spike a little better than in the optimization. The timing of the peaks in general is relatively good, but the peak values are about 20% to high in the simulation.

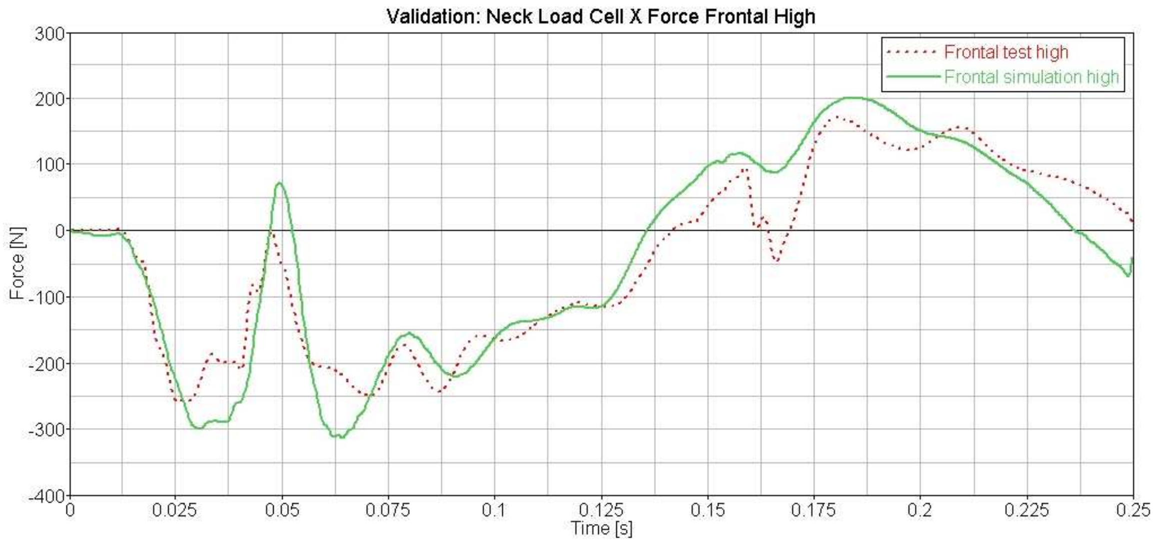

Figure 4.17: Validation Neck Load Cell X Force Frontal High

In the lateral case, Figure 4.18, the match of the forces in X direction of the simulation to the test is very good and the force of the simulation is only around 10% lower than the force in the test.

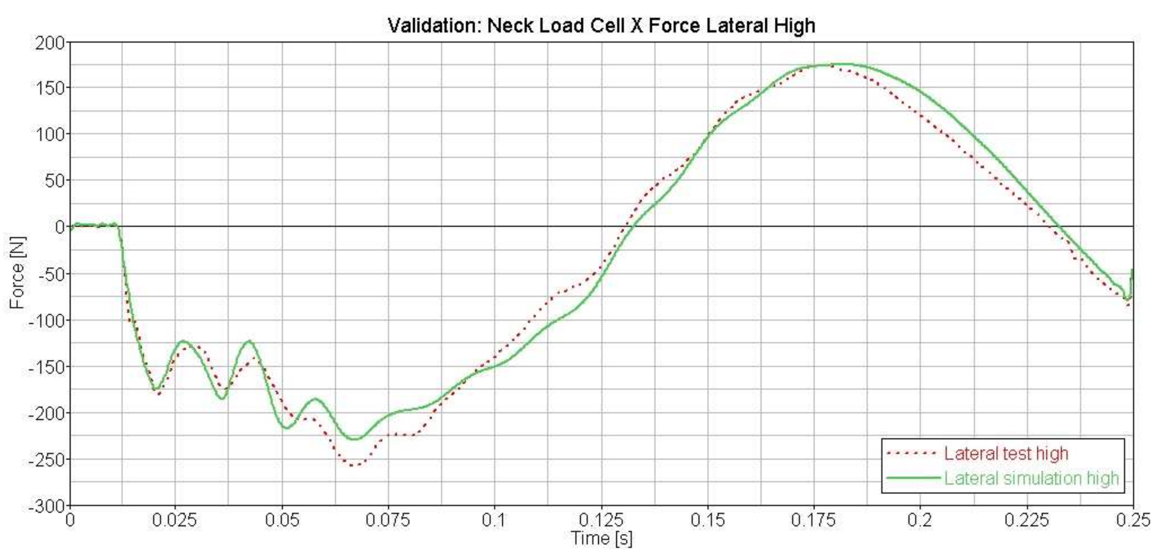

Figure 4.18: Validation: Neck Load Cell X Force Lateral High

In both, the frontal (Figure 4.19) and the lateral (Figure 4.20) case the shape of the force curve in Z direction is very good. The peak forces are about 20% to high in the frontal case and about 15% to high in the lateral case.

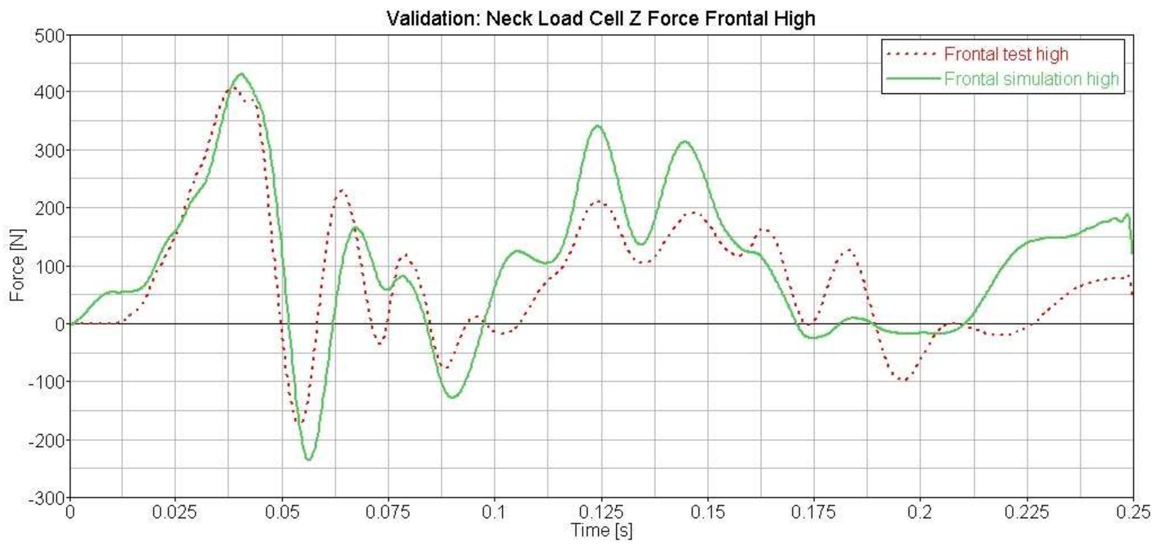

Figure 4.19: Validation Neck Load Cell Z Force Frontal High

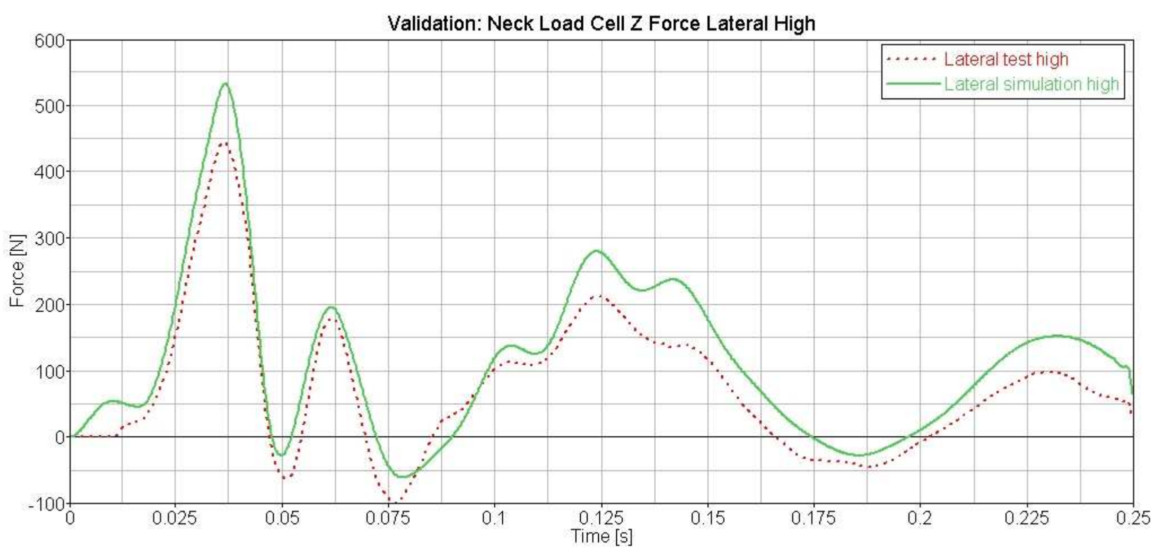

Figure 4.20: Validation: Neck Load Cell Z Force Lateral High

According to the combined objective rating criterion the neck simulations match the tests to an average of 80%, see Table 4.2. All three individual criteria were weighted equally for the combined criterion.

Table 4.2: Objective Rating of Neck Pendulum Test Results

	crit 1: Peak Value	crit 2: Timing of Peak Value	crit 3: Overall Correlation	comb: Combined Objective Rating
Optimization Frontal Low Angle	0.88805	0.971075	0.705926	0.8175637
Optimization Lateral Low Angle	0.847272	0.924412	0.78874	0.8432941
Optimization Frontal Low Moment Y	0.848842	0.945047	0.603745	0.7530948
Optimization Lateral Low Moment Y	0.802001	0.938697	0.82575	0.843662
Optimization Frontal Low Force X	0.873196	0.950552	0.647471	0.781825
Optimization Lateral Low Force X	0.974232	0.995283	0.919693	0.9512303
Optimization Frontal Low Force Z	0.516071	0.767821	0.253758	0.4692862
Optimization Lateral Low Force Z	0.863186	0.999127	0.725367	0.822854
Validation Frontal Low Angle	0.864151	0.875704	0.731839	0.8121927
Validation Lateral Low Angle	0.874218	0.992957	0.836231	0.880709
Validation Frontal Low Moment Y	0.816437	0.99213	0.701978	0.797866
Validation Lateral Low Moment Y	0.703064	0.982329	0.772807	0.7838982
Validation Frontal Low Force X	0.764639	0.979348	0.713706	0.7856906
Validation Lateral Low Force X	0.891787	0.969225	0.886407	0.9076952
Validation Frontal Low Force Z	0.927519	0.955027	0.561825	0.7422706
Validation Lateral Low Force Z	0.835504	0.993531	0.72063	0.812785

4.1.3 Lumbar Spine Pendulum Test

The lumbar spine is composed of two metal pieces that squeeze a rubber cylinder via a steel cable that goes through the center of the cylinder and connects the two metal end pieces. Besides this compression force, the cylinder is not glued or otherwise connected to the other pieces. During the pendulum test the side that is not in compression lifts off from the steel end piece. On top of that the rubber experiences a hysteresis curve that is depending on the compression speed. Thus the lumbar spine was the most difficult part to model of the Q3 dummy.

Fortunately, the lumbar spine of the Q3 dummy is relatively stiff in comparison with other parts of the dummy and therefore the rather large bending in the component test does usually not happen in a full scale dummy test. So the influence of the lumbar spine on the overall performance of the dummy is not as significant as other parts.

During the initial neck pendulum test simulations the model was very unstable. The rubber part in the simulation would partially slip over either one of the metal end pieces. In most cases this caused the simulation to crash. Since the diameter of the rubber and the edge length of the metal end pieces of the neck are almost identical this would continue to happen frequently. To prevent the simulation from crashing the contact surface of the end pieces was extended beyond the actual metal piece, see Figure 4.21. This is only for the contact between the rubber of the lumbar spine and its metal end pieces. The influences of the extension on the behavior of the component will be minimal, but the component now runs very stable.

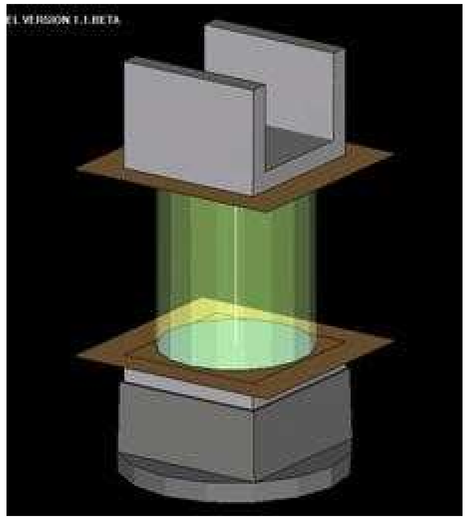

Figure 4.21: Lumbar Spine with Extended Contact Surfaces

Further, the cable that connects the two end pieces and holds the neck together was initially modeled with a string of beam elements where only the first and the last connect to the end pieces. For small bending angles this behaved properly, but for bending angles as experienced by the lumbar spine in the pendulum tests, the rubber part would slip out. To prevent this some of the nodes of the cable were connected to nodes in the center of the rubber part. This setup prevented the rubber part from slipping out, but after reviewing the stresses in the rubber while bending it was determined that this solution is not representing the real component properly. The next approach was to create a tube of contact surfaces around the cable enclosed by a second tube of contact surfaces with a larger diameter connected to the rubber part. For bending only this worked well, but as soon as the neck experiences a small amount of torsion the tubes would collapse and therefore not move freely against each other. The final and working approach was to simulate the cable with an alternating string of beam elements and very short pieces of nodal rigid bodies. These keep the tubes from collapsing. Since nodal rigid bodies do not affect the time step of a simulation they could be chosen very small as to not significantly influence the behavior of the cable.

4.1.3.1 Lumbar Spine Optimization

The peak bending angle achieved with the optimized material parameters was for both the frontal simulation, Figure 4.22, and the lateral simulation, Figure 4.23, more than 30% larger than the test data. The frequency of the bending is also higher in both cases than the test.

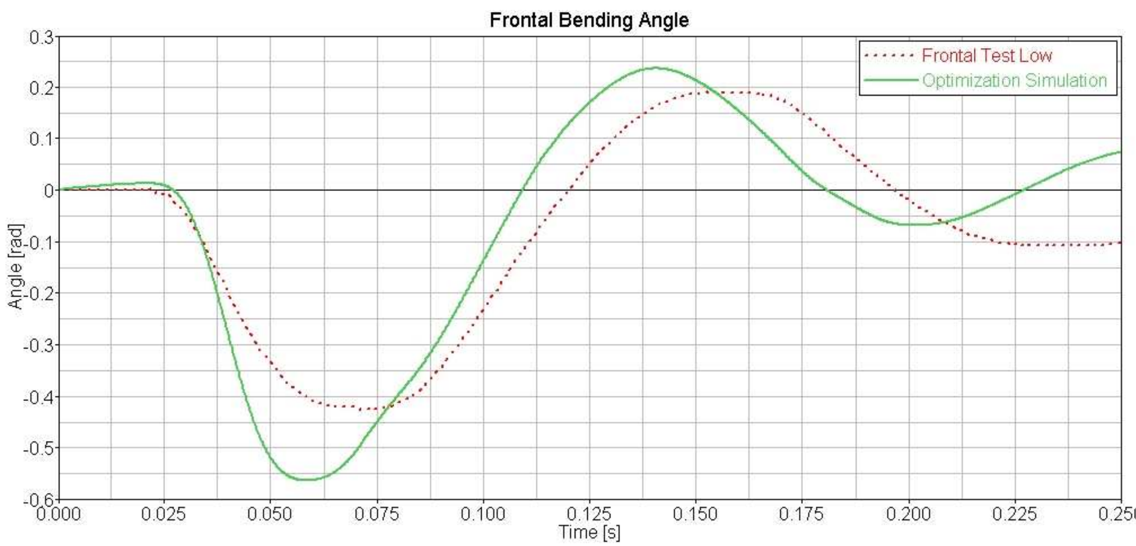

Figure 4.22: Optimization: Lumbar Spine Flexion Angle Frontal Low

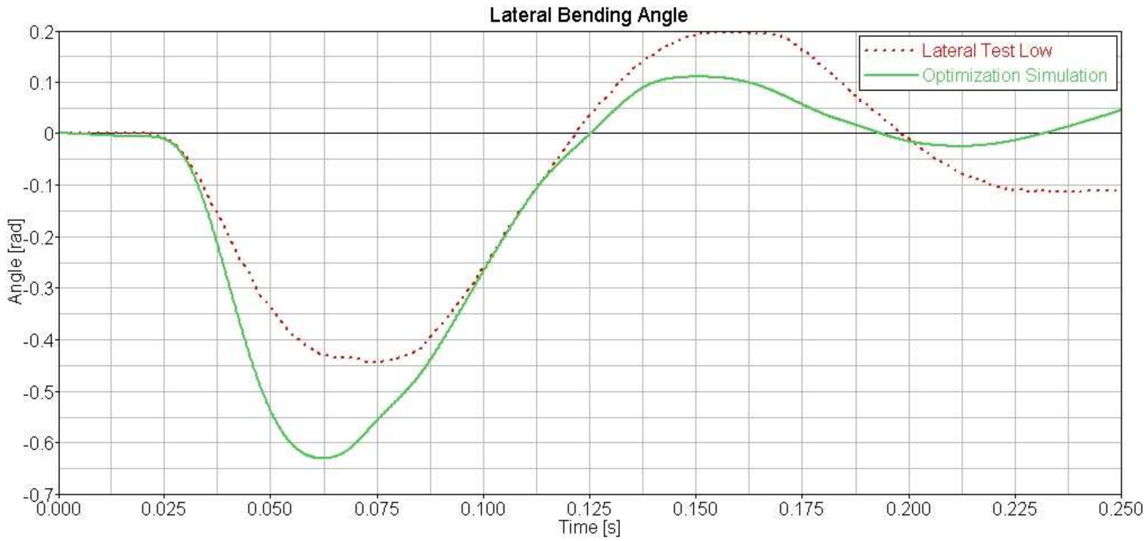

Figure 4.23 Optimization: Lumbar Spine Flexion Angle Lateral Low

The peak of moment of the lumbar spine load cell in the simulation only reaches about 55% of the moment in the test for the frontal case in Figure 4.24 and about 60% in the lateral case in Figure 4.25. Just as the bending angles above, the timing is off for the moments as well.

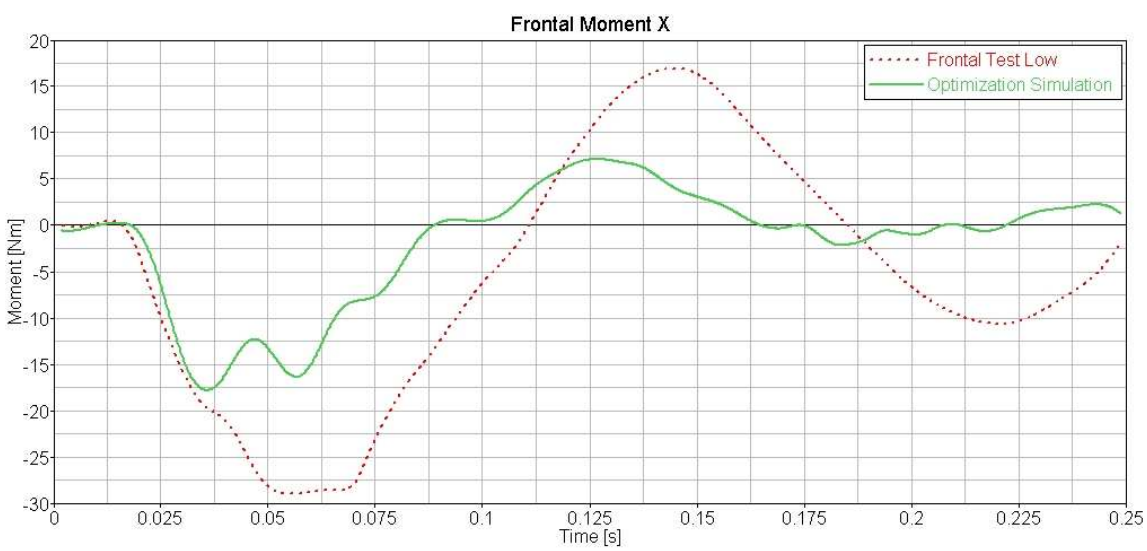

Figure 4.24: Optimization: Lumbar Spine Load Cell X Moment Frontal Low

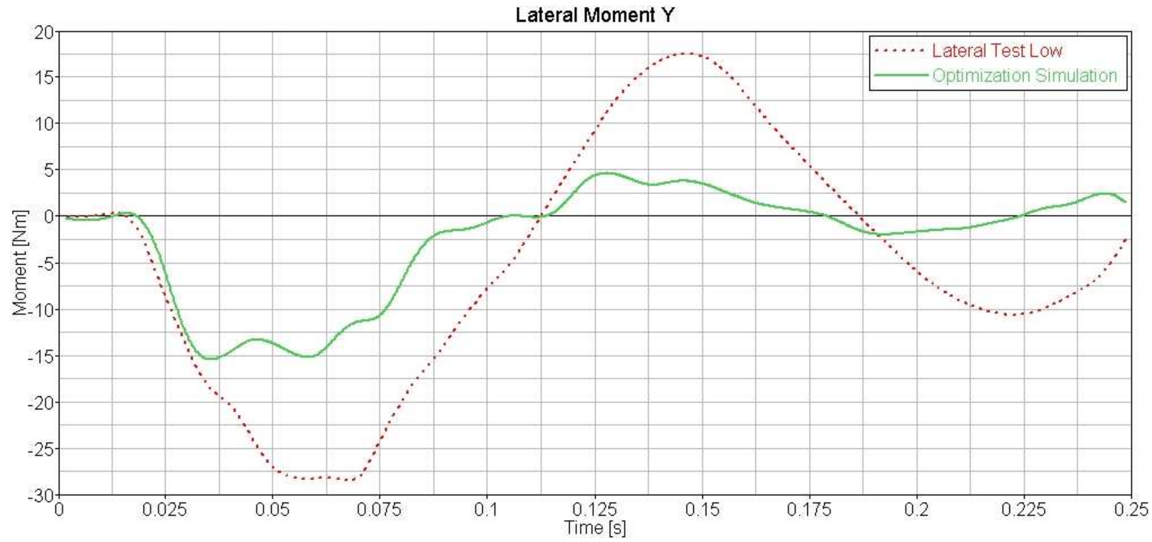

Figure 4.25 Optimization: Lumbar Spine Load Cell Y Moment Lateral Low

The forces in Y direction in the frontal simulation, Figure 4.26, are about 50% higher than the forces in the test, but the timing of the first peak is relatively good.

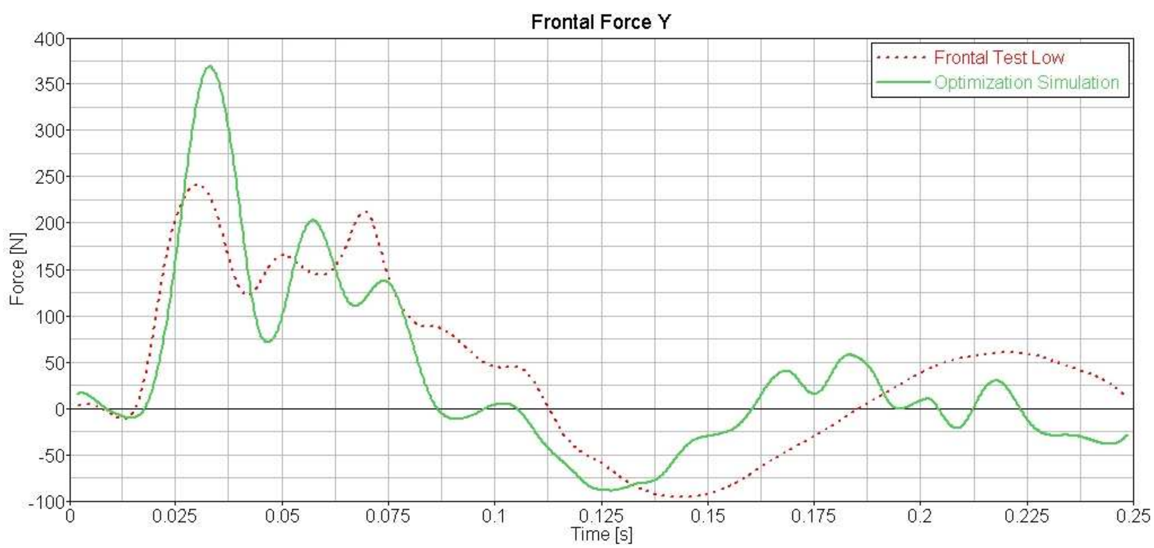

Figure 4.26: Optimization: Lumbar Spine Load Cell Y Force Frontal Low

In the lateral simulation timing of the peaks of the forces in X direction, pictured in Figure 4.27, match the test acceptable, but the value of the peak is about 50% higher in the simulation than in the test.

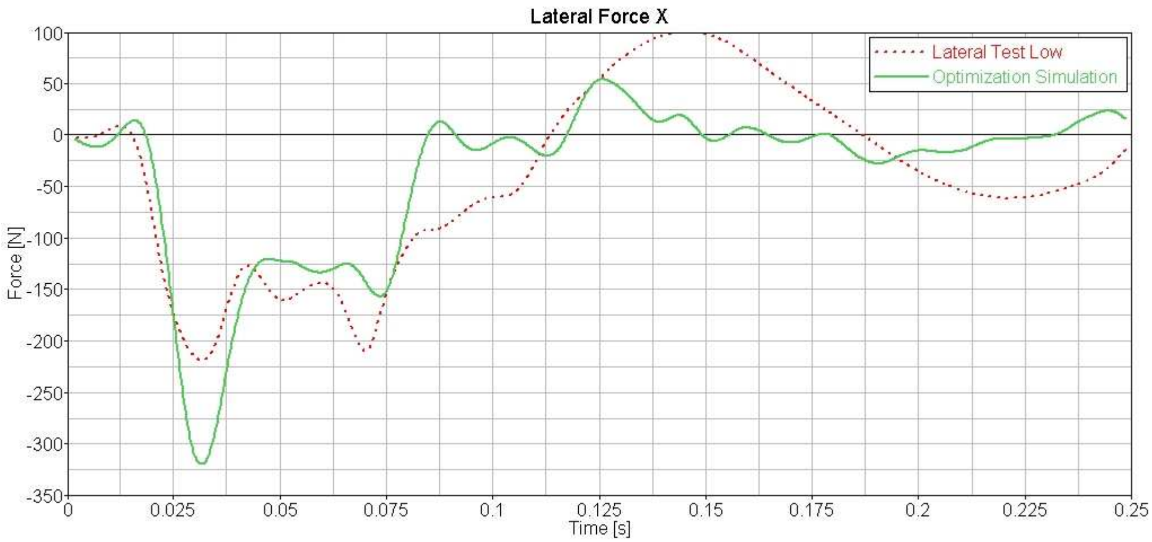

Figure 4.27 Optimization: Lumbar Spine Load Cell X Force Lateral Low

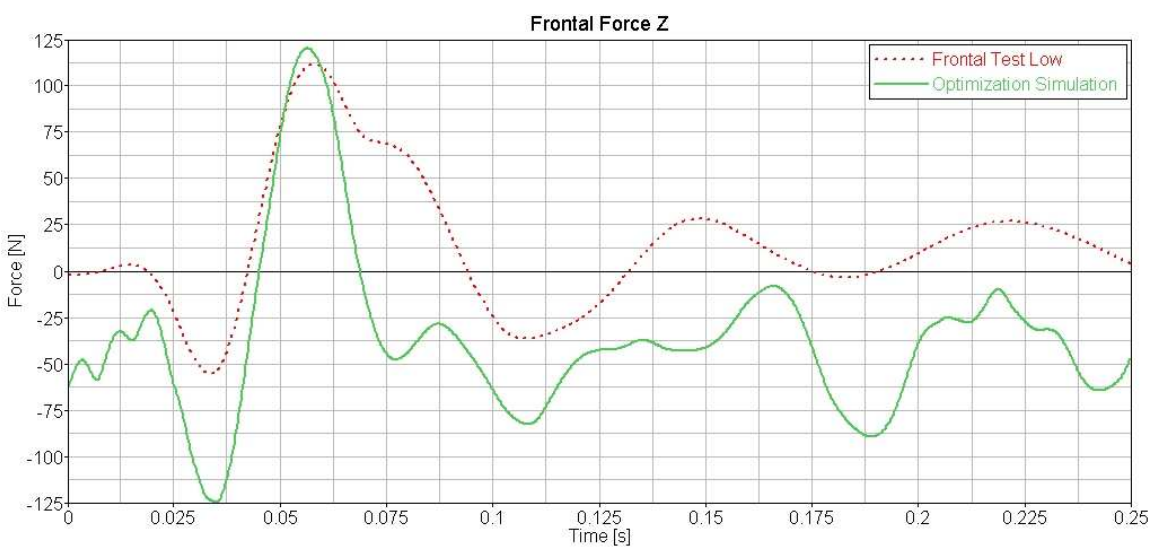

Figure 4.28 Optimization: Lumbar Spine Load Cell Z Force Frontal Low

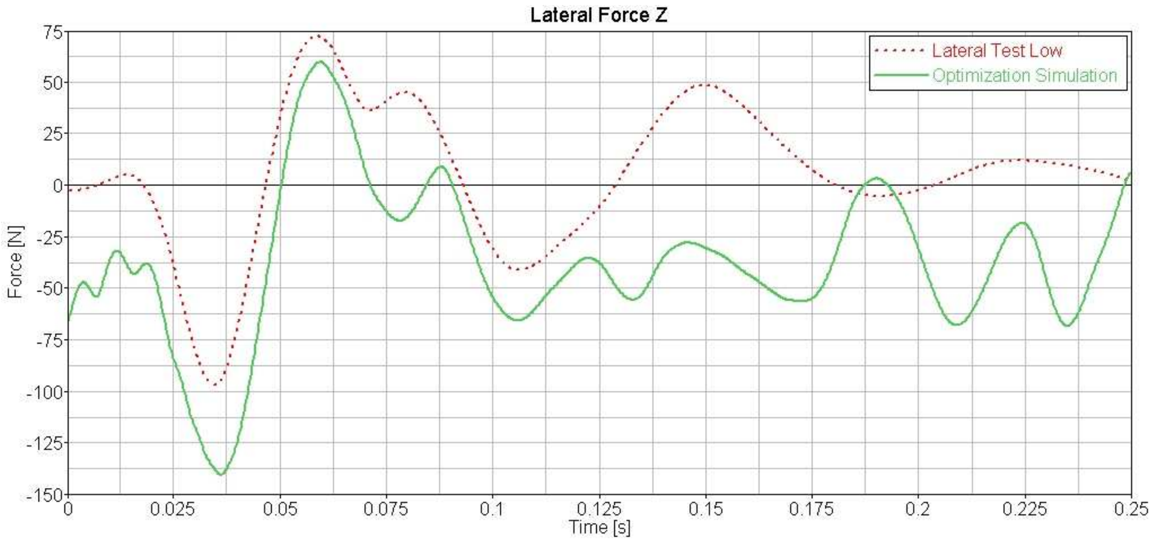

Figure 4.29 Optimization: Lumbar Spine Load Cell Z Force Lateral Low

4.1.3.2 Lumbar Spine Validation

For the validation of the lumbar spine, the frontal and the lateral pendulum test with the higher impact speed were chosen. As can be seen in Figure 4.30 and Figure 4.31 the peak bending angle is about 20% higher in the simulation than in the test. Also the simulated lumbar spine bends somewhat faster than the lumbar spine in the test.

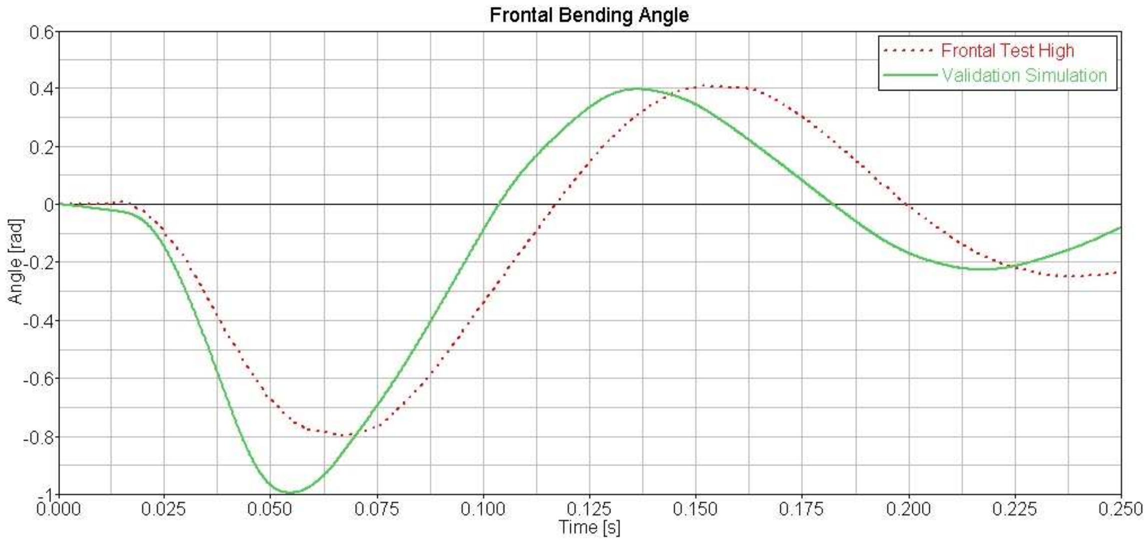

Figure 4.30 Validation: Lumbar Spine Flexion Angle Frontal High

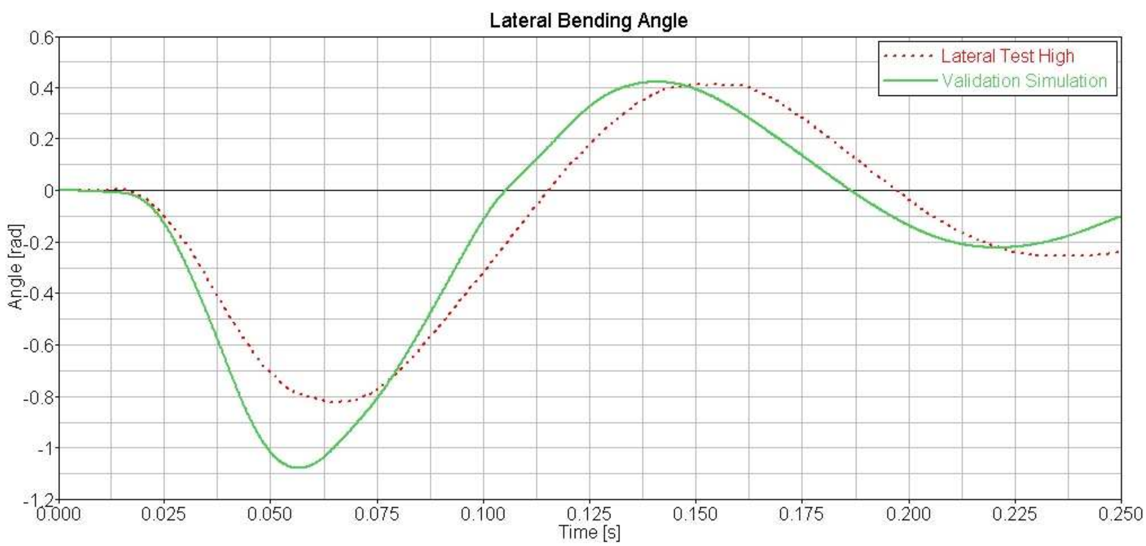

Figure 4.31 Validation: Lumbar Spine Flexion Angle Lateral High

As in the optimization, the moment measured at the load cell differs significantly between the test and the simulation (Figure 4.32, Figure 4.33).

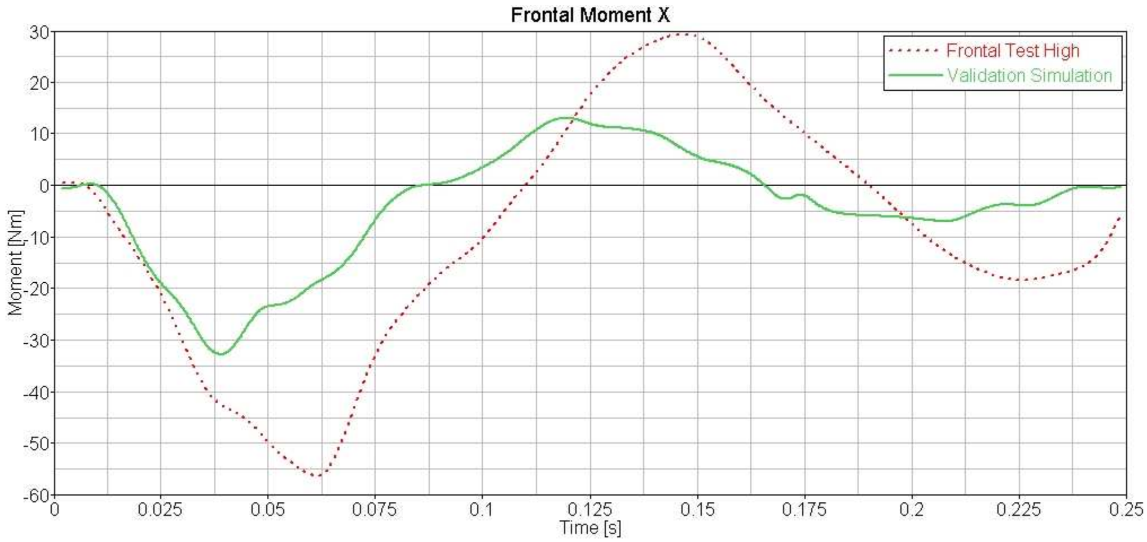

Figure 4.32: Validation: Lumbar Spine Load Cell X Moment Frontal High

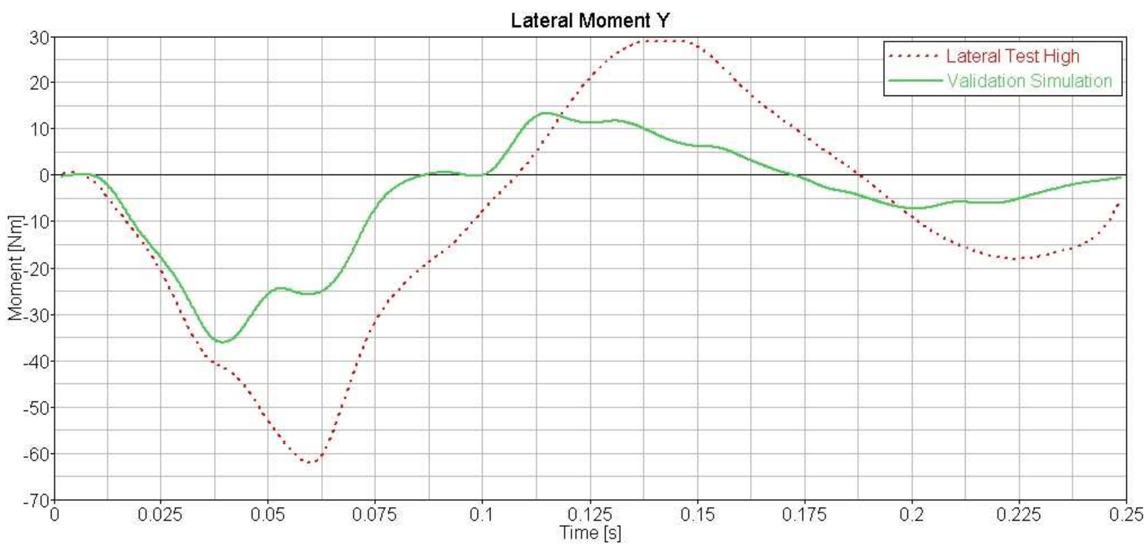

Figure 4.33 Validation: Lumbar Spine Load Cell Y Moment Lateral High

The timing and the shape of the curve of the force in Y direction for the frontal validation and for the force in X direction for the lateral validation match well. The peak force is higher in the simulation than the test for both directions, see Figure 4.34 and Figure 4.35.

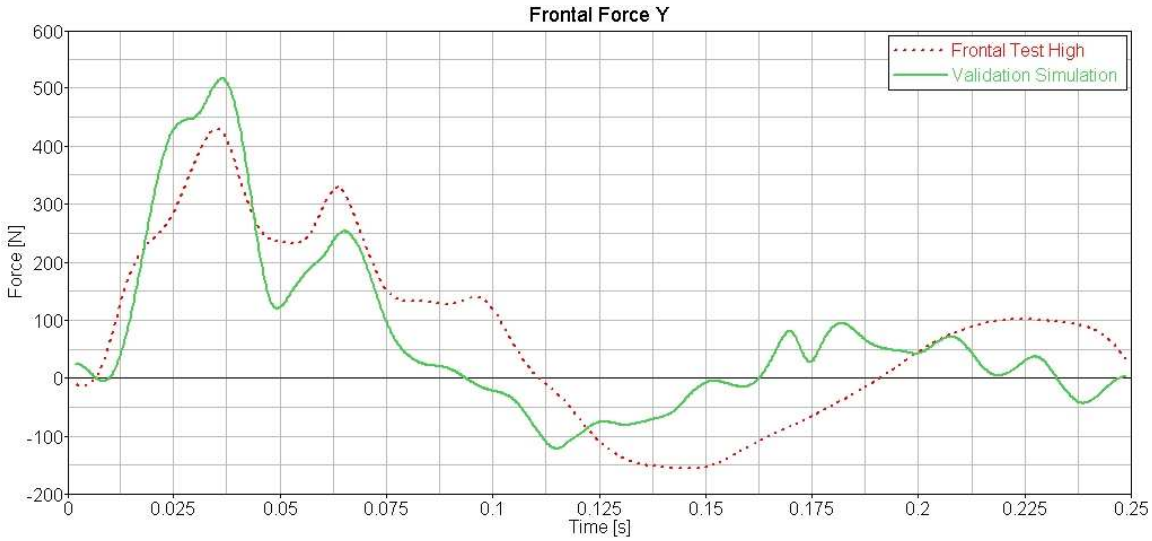

Figure 4.34 Validation: Lumbar Spine Load Cell Y Force Frontal High

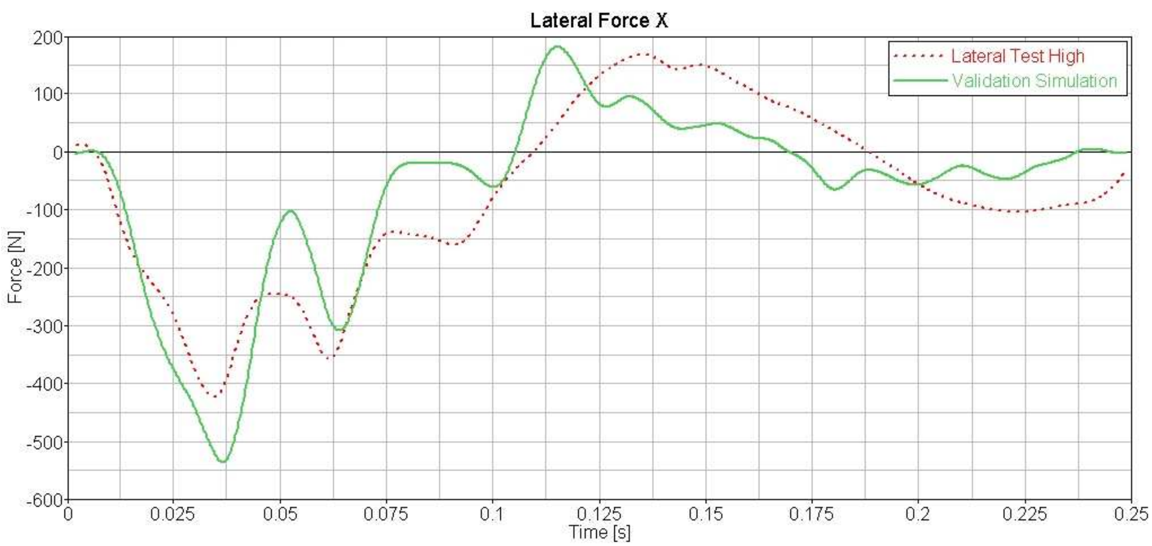

Figure 4.35 Validation: Lumbar Spine Load Cell X Force Lateral High

Figure 4.36 and Figure 4.37 show the forces in Z direction for the frontal and the lateral pendulum test. The peak forces are lower in test than in the simulation. The overall shape of the curves and the timing of the peak forces match reasonably well.

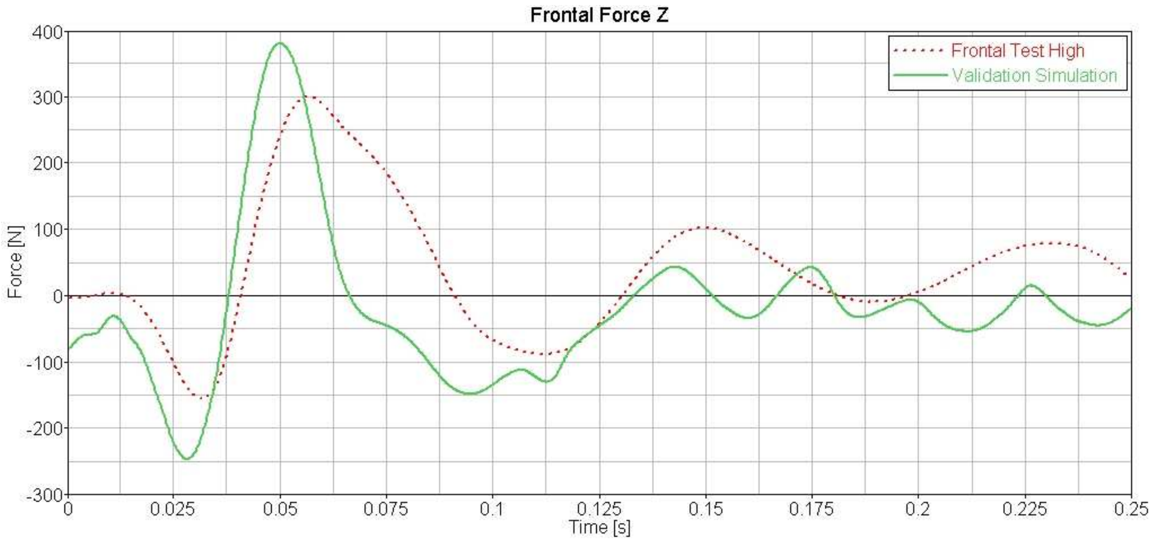

Figure 4.36 Validation: Lumbar Spine Load Cell Z Force Frontal High

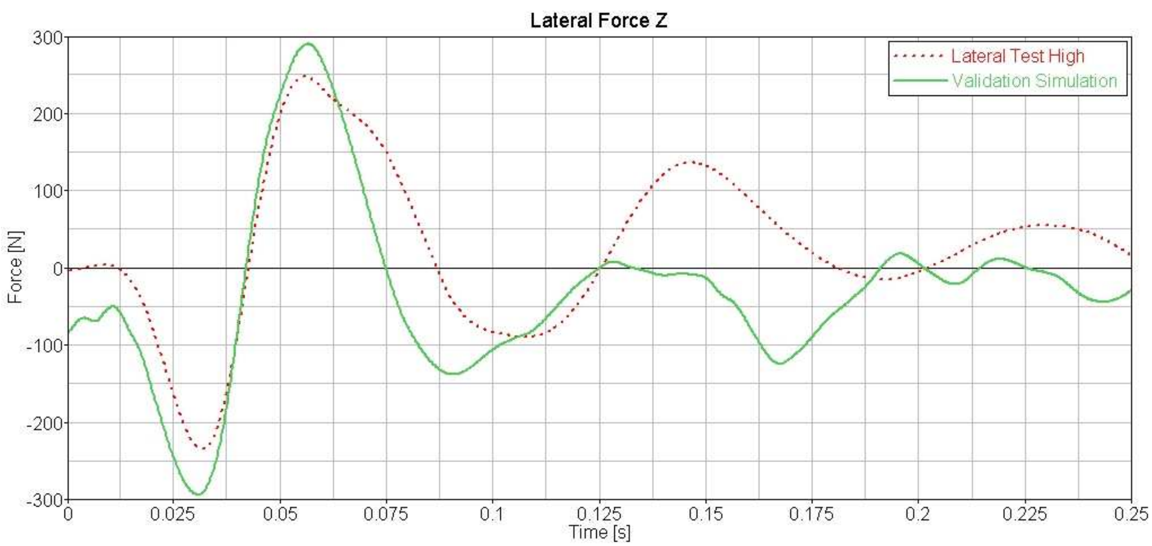

Figure 4.37 Validation: Lumbar Spine Load Cell Z Force Lateral High

The lumbar spine pendulum simulations only match the tests to an average combined rating of 63%, see Table 4.3. This is very low for component level tests. Maybe with a more complex material model and individual testing of the rubber part of the lumbar spine a better result could be achieved. Ideally the manufacturer would release the information of material used in the lumbar spine or material data about it.

Table 4.3: Objective Rating of Lumbar Spine Pendulum Tests Results

	crit 1: Peak Value	crit 2: Timing of Peak Value	crit 3: Overall Correlation	comb: Combined Objective Rating
Optimization Frontal Low Angle	0.731511	0.788572	0.654508	0.7194334
Optimization Lateral Low Angle	0.684996	0.846969	0.666727	0.7208842
Optimization Frontal Low Moment X	0.564517	0.639281	0.354233	0.5044267
Optimization Lateral Low Moment Y	0.532086	0.523527	0.367647	0.4690134
Optimization Frontal Low Force Y	0.632221	0.915141	0.551458	0.6615465
Optimization Lateral Low Force X	0.684214	0.993707	0.532961	0.674482
Optimization Frontal Low Force Z	0.857048	0.972408	0.256486	0.5625797
Optimization Lateral Low Force Z	0.679939	0.98989	0.29114	0.5509181
Validation Frontal Low Angle	0.765468	0.897261	0.659092	0.7538437
Validation Lateral Low Angle	0.738709	0.881024	0.722776	0.7695791
Validation Frontal Low Moment X	0.442613	0.637253	0.362207	0.4680083
Validation Lateral Low Moment Y	0.41497	0.658857	0.409484	0.4812362
Validation Frontal Low Force Y	0.827364	0.967032	0.566631	0.7300008
Validation Lateral Low Force X	0.77284	0.945365	0.588518	0.7268065
Validation Frontal Low Force Z	0.699667	0.880273	0.357695	0.5848333
Validation Lateral Low Force Z	0.824476	0.985873	0.45032	0.6667552

4.1.4 Ribcage Impact Test

The ribcage consist out of two materials. For both of which the material data is unknown. The optimization at the low and medium impact velocity and the validation at the high impact velocity are still relatively successful.

4.1.4.1 Ribcage Optimization

The data for the low impact velocity ribcage test in Figure 4.38 does not show an initial peak. The peak acceleration of the piston is the same for the optimization results and the test. The simulation shows the peak acceleration somewhat earlier.

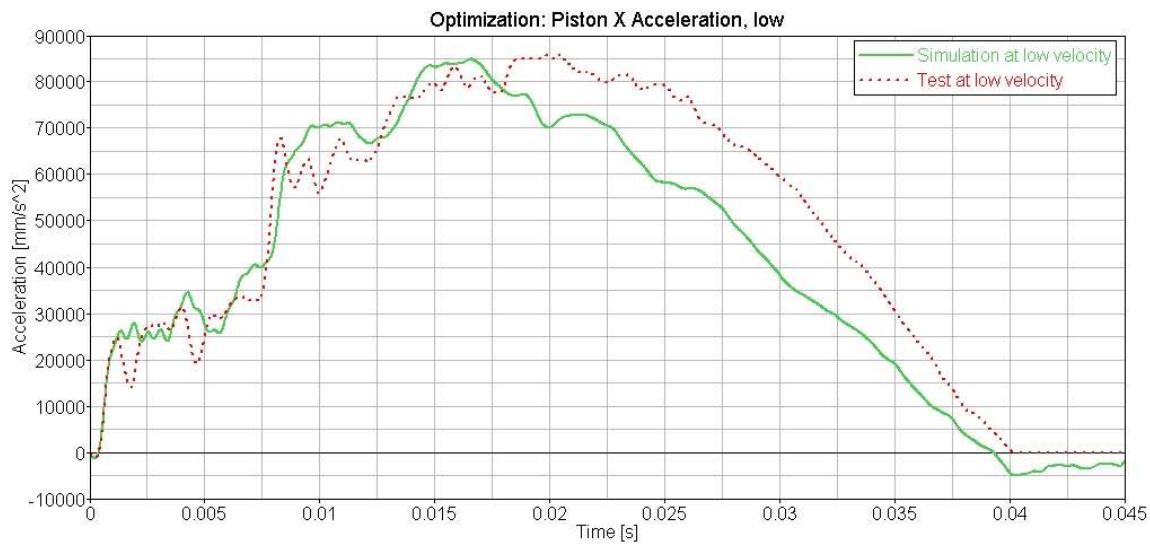

Figure 4.38: Optimization: Piston X Acceleration Low Velocity

A similar picture is presented for the optimization at the medium impact speed in Figure 4.39. The peak acceleration is approximately the same for the test and the simulation, but the peak in the simulation occurs earlier. In this case there is an initial spike and at this the simulation matches the test both in timing and peak very well.

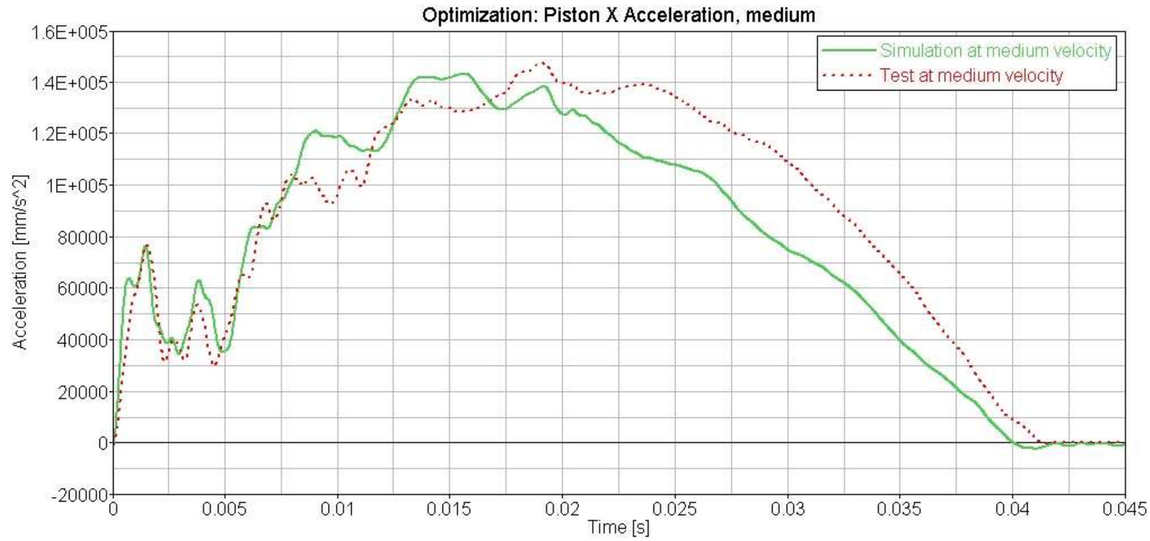

Figure 4.39: Optimization: Piston X Acceleration Medium Velocity

4.1.4.2 Ribcage Validation

For the validation the ribcage test with highest impact speed was chosen. The results of the validation simulation, shown in Figure 4.40, match the test relatively good. The initial spike and the value of peak acceleration of the test and the simulation are very close. The timing of the peak acceleration is a little earlier in the simulation.

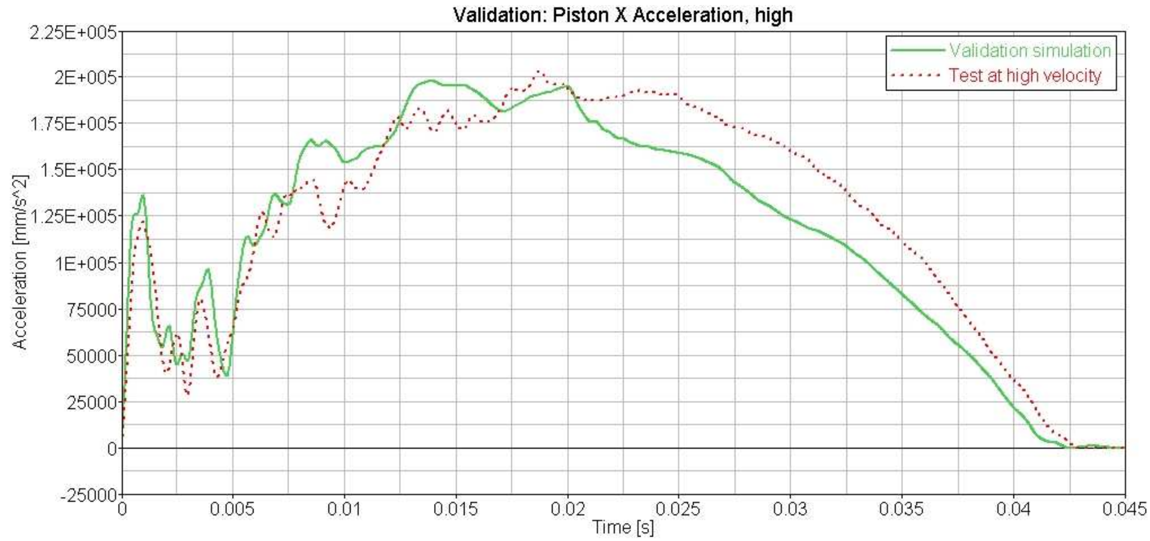

Figure 4.40: Validation: Piston X Acceleration High Velocity

Table 4.4 shows the objective ratings of the ribcage impact tests. The ribcage simulations match the tests with an average combined rating of 84%. Therefore the ribcage can be considered valid for frontal impact on a component level.

Table 4.4: Objective Rating of the Ribcage Impact Tests

	crit 1: Peak Value	crit 2: Timing of Peak Value	crit 3: Overall Correlation	comb: Combined Objective Rating
Optimization Low	0.947042	0.81255	0.810188	0.8429749
Optimization Medium	0.938831	0.817805	0.824629	0.8497872
Validation High	0.937984	0.740141	0.850458	0.823237

4.1.5 Abdomen Impact Test

For the abdomen simulations, the low and high impact speed tests were used for optimizing the material properties. The medium impact speed test was utilized for the validation of the abdomen.

4.1.5.1 Abdomen Optimization

The general shape and the peak acceleration of the test data was reasonably well approximated in the optimization for the low impact speed, Figure 4.41. However, the initial step that the test data shows could not be reproduced and the response of the simulated abdomen is somewhat slower than the tested Q3 abdomen.

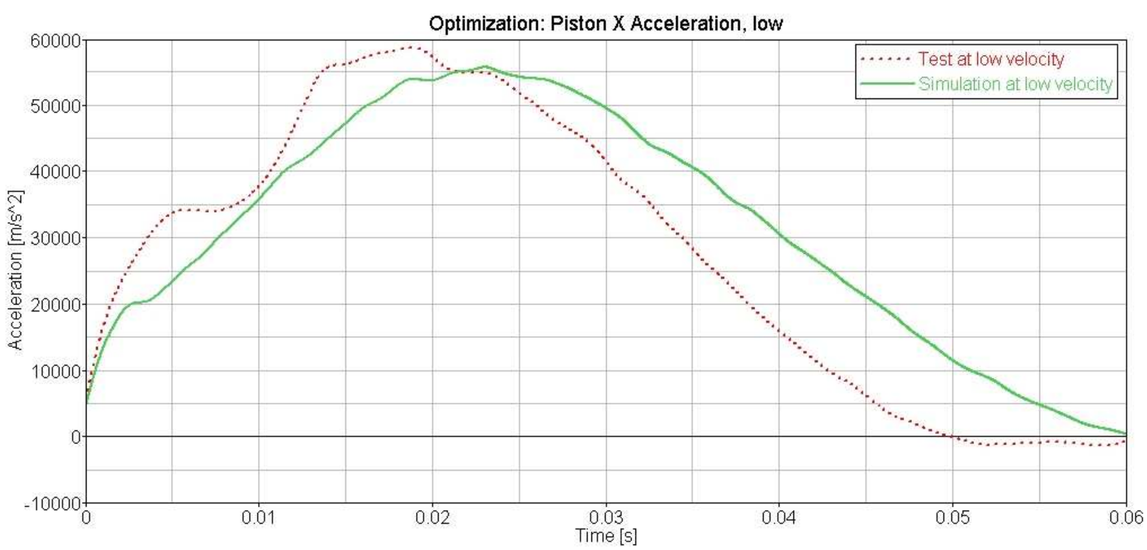

Figure 4.41: Optimization: Piston X Acceleration Low Velocity

In the optimization for the high impact speed, shown in Figure 4.42, the shape, peak and timing were closely matched to the test data. Only the initial step could not be matched as well.

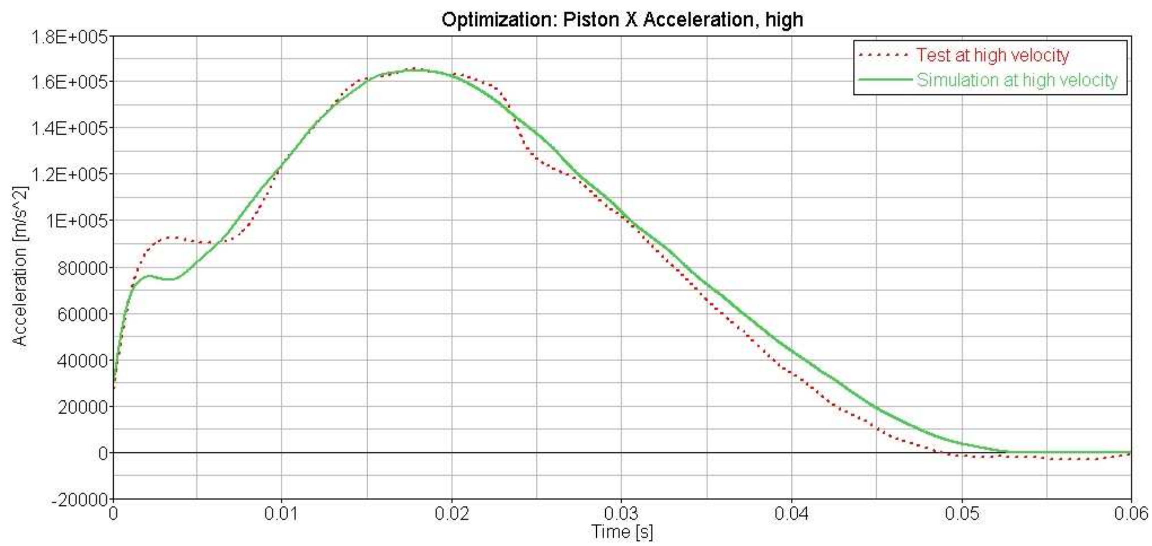

Figure 4.42: Optimization: Piston X Acceleration High Velocity

4.1.5.2 Abdomen Validation

The validation result of the abdomen (Figure 4.43) lies in between the two optimization results. The peak of the acceleration matches very well, but the overall timing is a little to slow in the simulation. Also the initial step is not as pronounced in the simulation as in the test data.

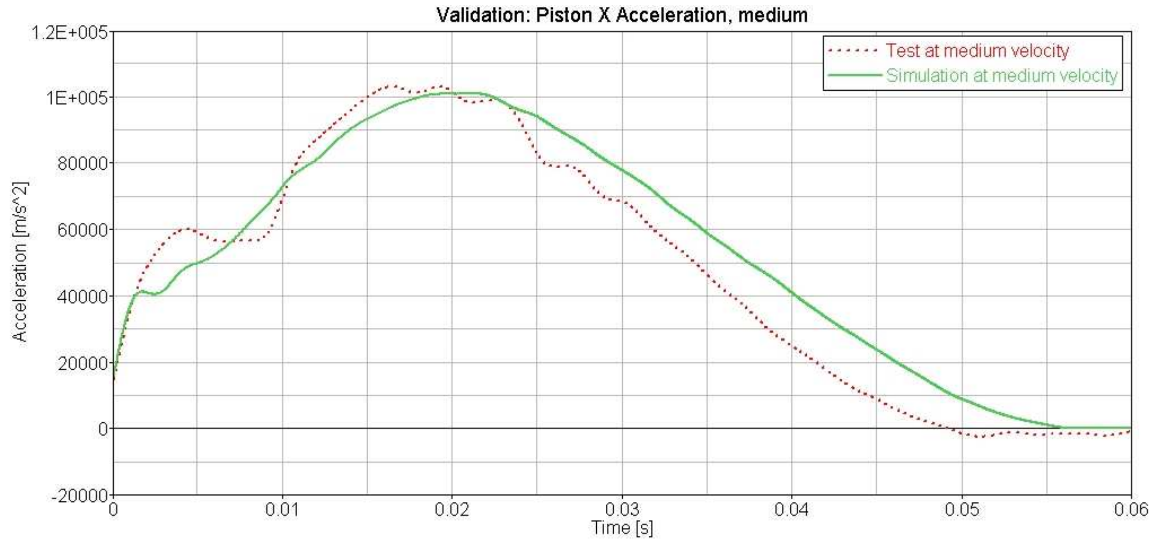

Figure 4.43: Validation: Piston X Acceleration Medium Velocity

The objective rating of the abdomen impact tests, shown in Table 4.5, indicate that the simulation matches the test to an average combined rating of 89%. The abdomen can therefore be considered validated.

Table 4.5: Objective Rating of the Abdomen Impact Tests

	crit 1: Peak Value	crit 2: Timing of Peak Value	crit 3: Overall Correlation	comb: Combined Objective Rating
Optimization Low	0.920635	0.815082	0.762852	0.8204333
Optimization High	0.994911	0.98991	0.935013	0.9619167
Validation Medium	0.977668	0.909453	0.853637	0.8998009

4.2 Complete Dummy

The tests that were run with the complete dummy were used for validation only. The setup of the tests is described in *Complete Dummy Tests Used for Validation.* In the following sections only the results for the main loading directions are presented. The signal to noise ratio of results from the minor directions is to small to make viable comparisons between tests and simulations.

4.2.1 Frontal Impact at Low Speed

The timing and the value of the peak resultant head acceleration of the simulation matches one of the tests perfectly for the frontal impact with the lower closing speed, Figure 4.44.

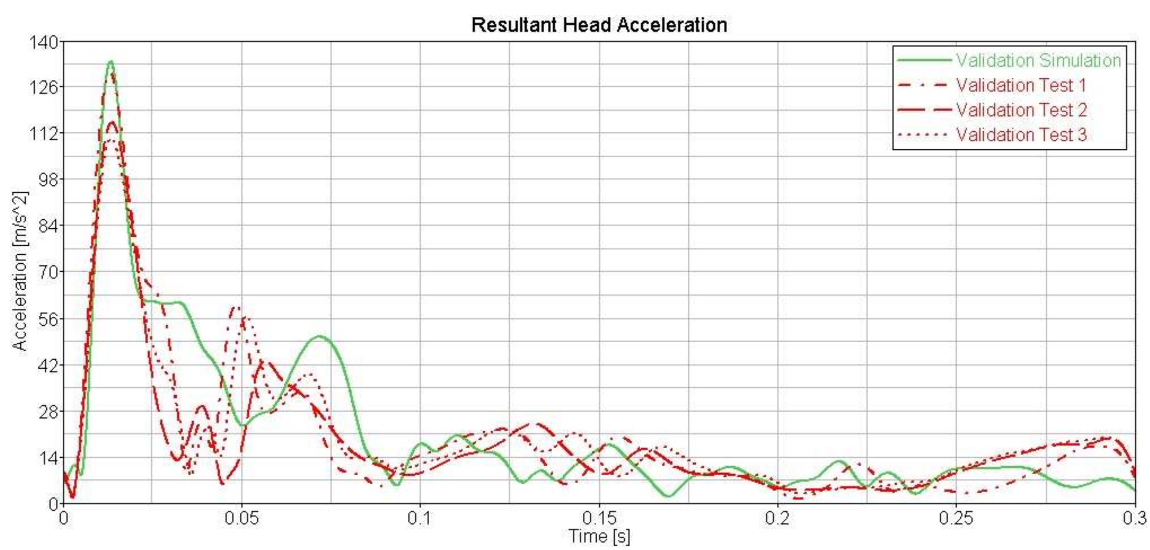

Figure 4.44: Resultant Head Acceleration

In the results for the upper neck, the forces in X direction, Figure 4.45, are to high for the first peak in the simulation. Also the rebound in the simulation is too high. However, the forces in Z direction, Figure 4.46, which are much higher, match very well. The moments around the Y axis of the upper neck load cell are much to low in the simulation, Figure 4.47. This is most probably mainly due to the nodding joint. The initial position of the nodding joint in the test is unknown. For the simulation the initial position was assumed to be in the center of its range of motion.

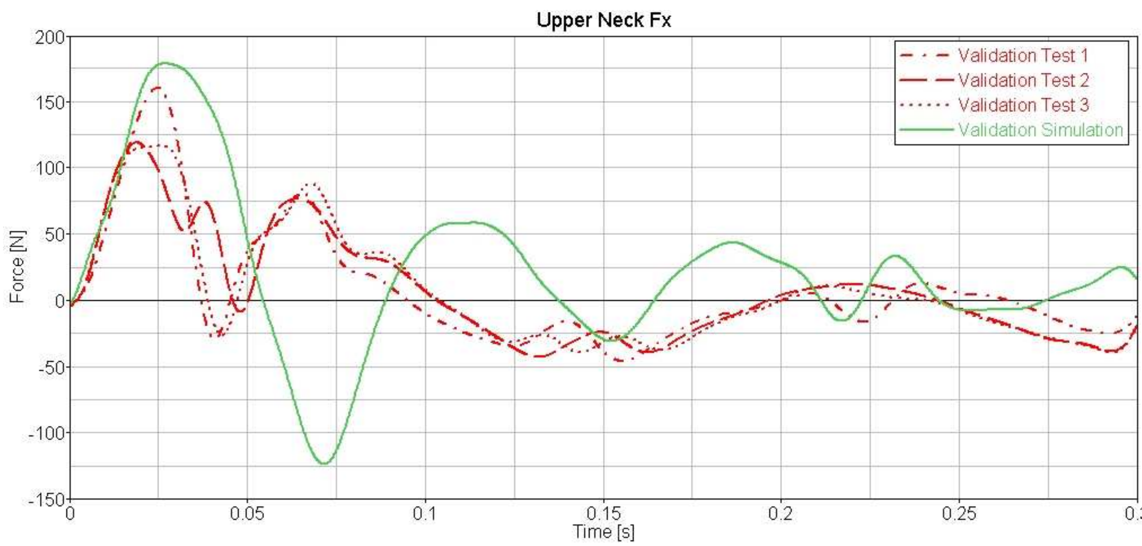

Figure 4.45: Upper Neck Force X

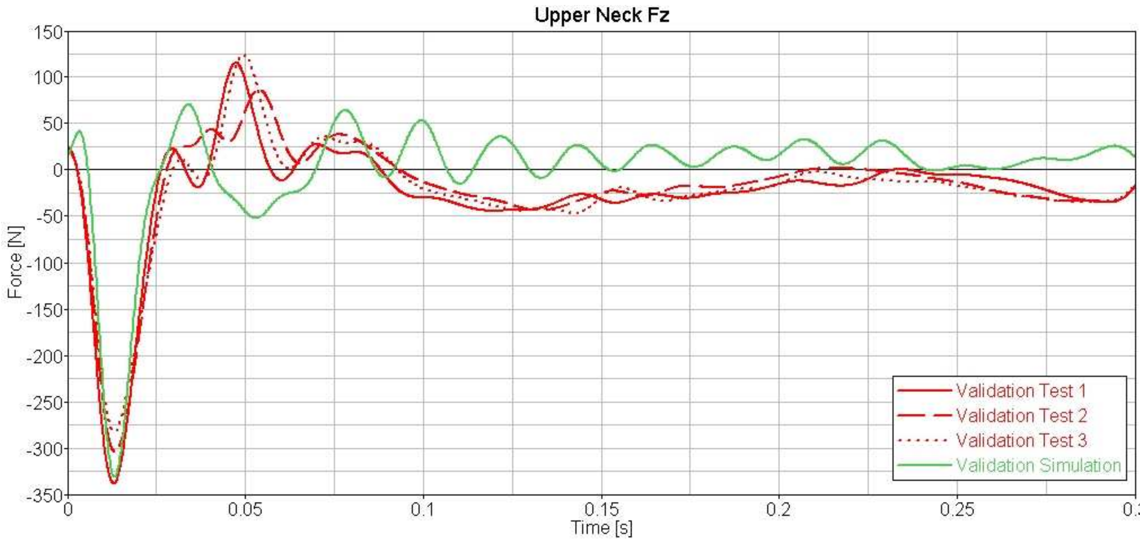

Figure 4.46: Upper Neck Force Z

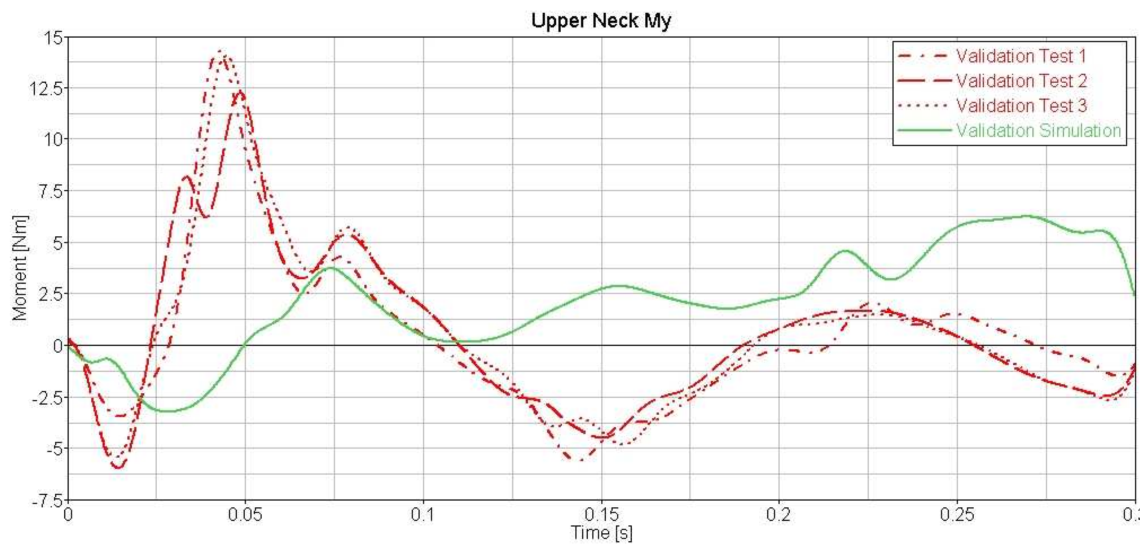

Figure 4.47: Upper Neck Moment Y

For the lower neck load cell, the forces in X direction, Figure 4.48, are off in timing and maximum force is about 20% to low in the simulation. The forces in Z direction, Figure 4.49, match well in timing and peak value between the simulation and the tests.

The value and timing of the peak moment around the Y axis, Figure 4.50, match, but in the overall shape the simulation oscillates to fast.

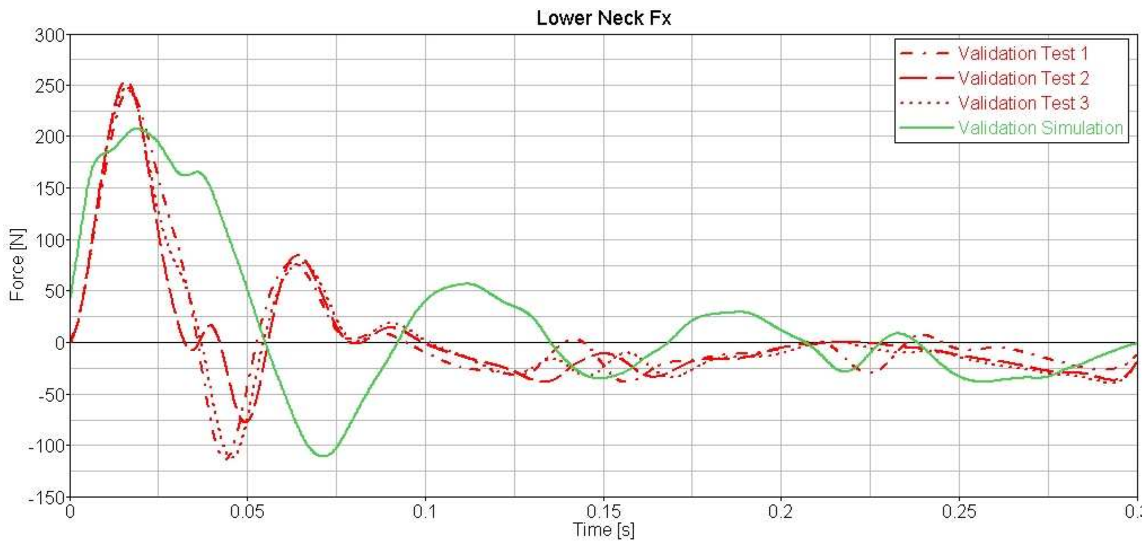

Figure 4.48: Lower Neck Force X

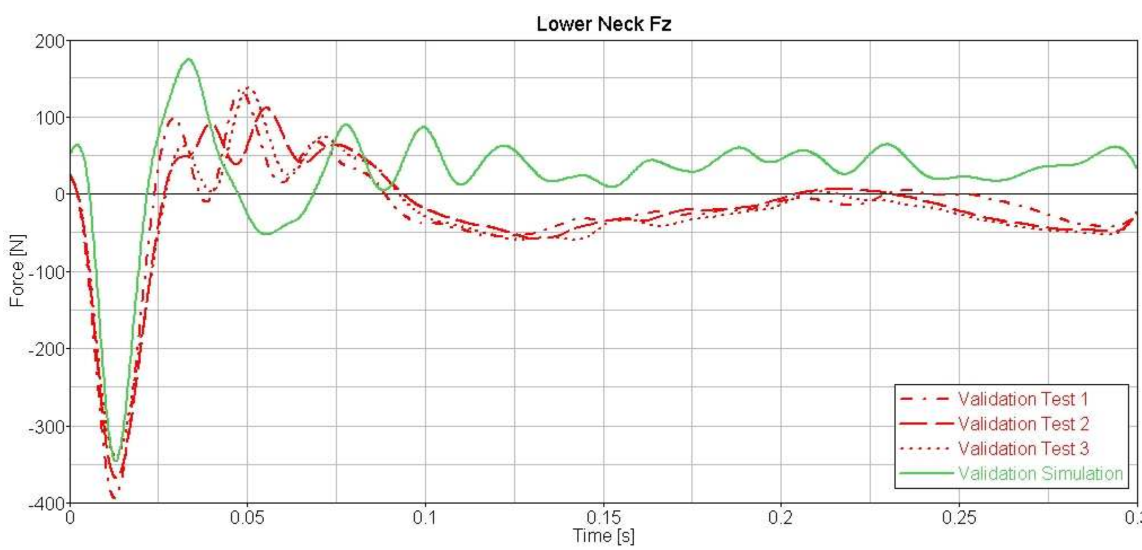

Figure 4.49: Lower Neck Force Z

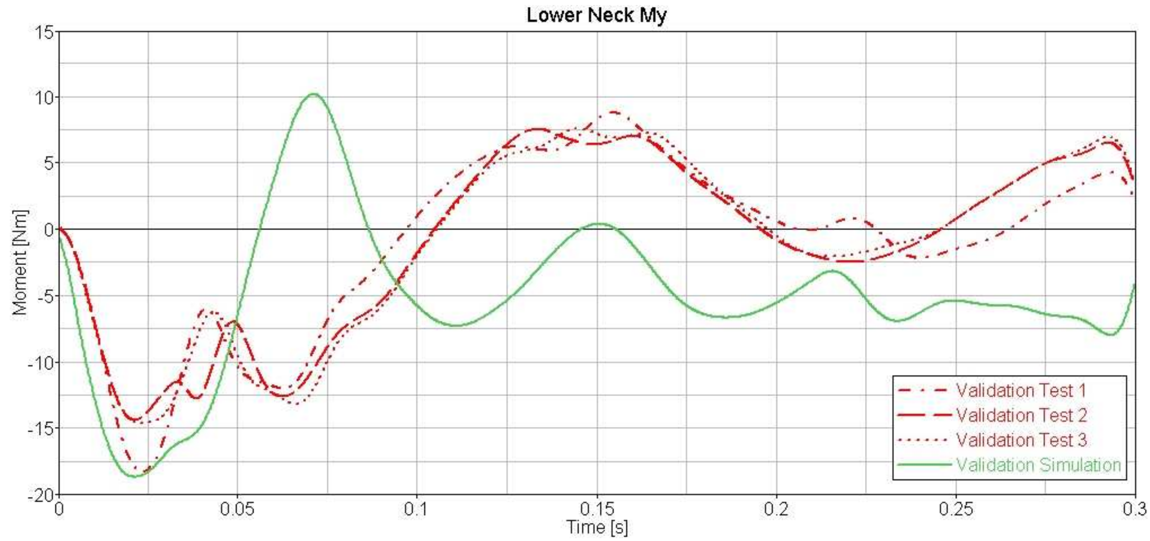

Figure 4.50: Lower Neck Moment Y

The peak chest acceleration is slightly higher in the simulation than in the tests, Figure 4.51. The timing matches well, but the simulation does not have the second peak in the acceleration. The chest deformation, Figure 4.52, in the simulation matches the tests well in timing and peak value.

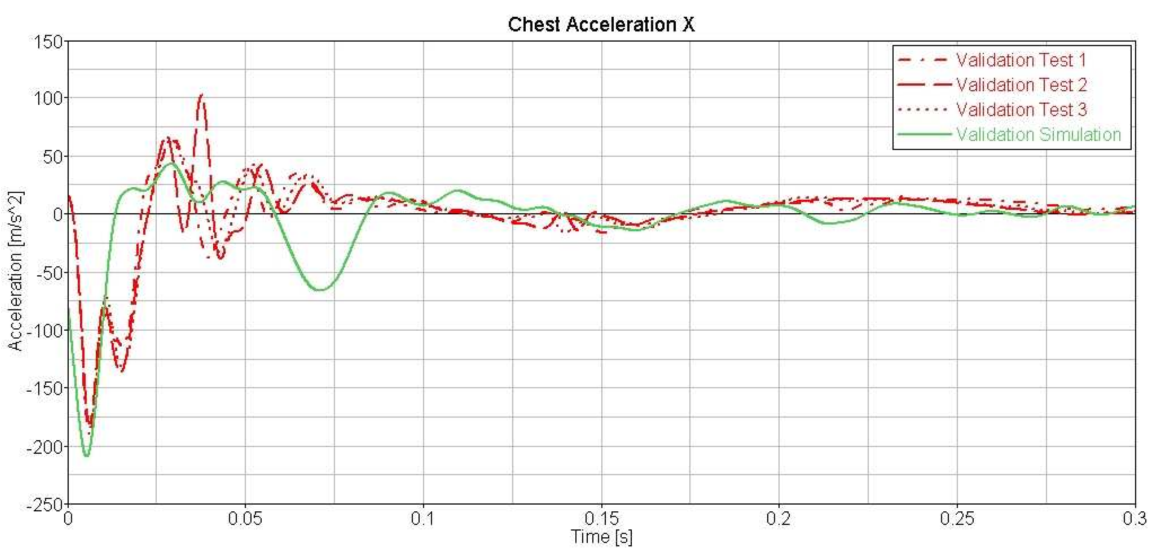

Figure 4.51: Chest Acceleration X

Figure 4.52: Chest Deformation

The peak force and its timing in X direction, Figure 4.53, and in Z direction, Figure 4.54, measured in the load cell that connects the lumbar spine to the pelvis, match well. The moment around the Y axis is too high in the simulation, Figure 4.55. The rebound is much to pronounced in the simulation.

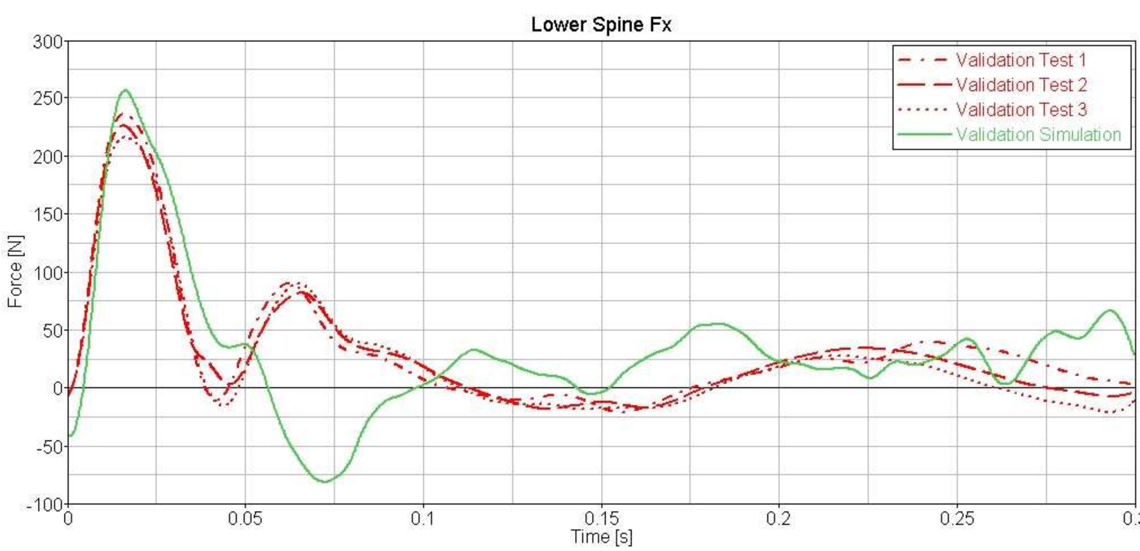

Figure 4.53: Lumbar Spine Force X

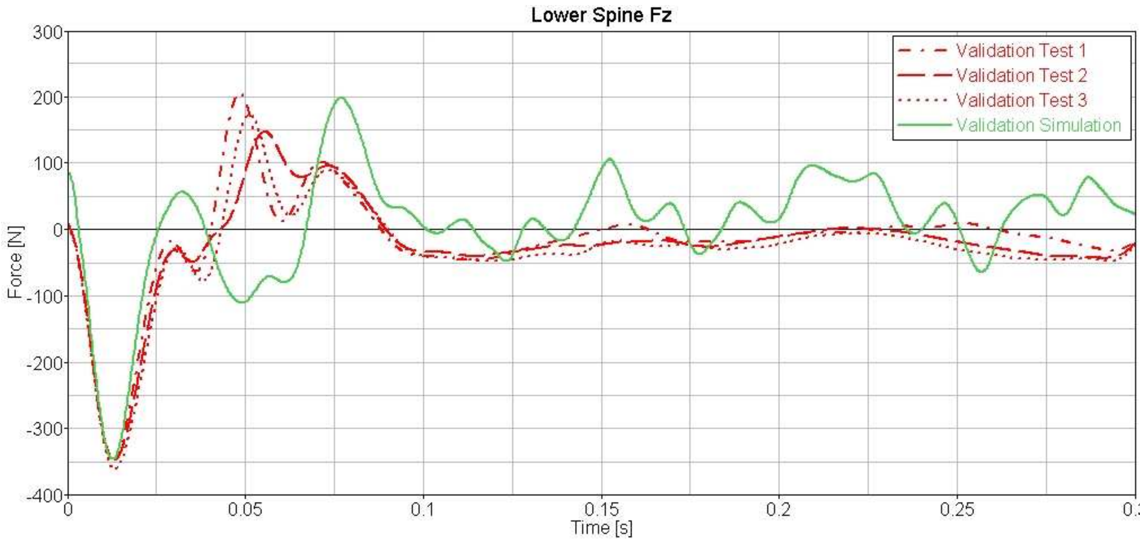

Figure 4.54: Lumbar Spine Force Z

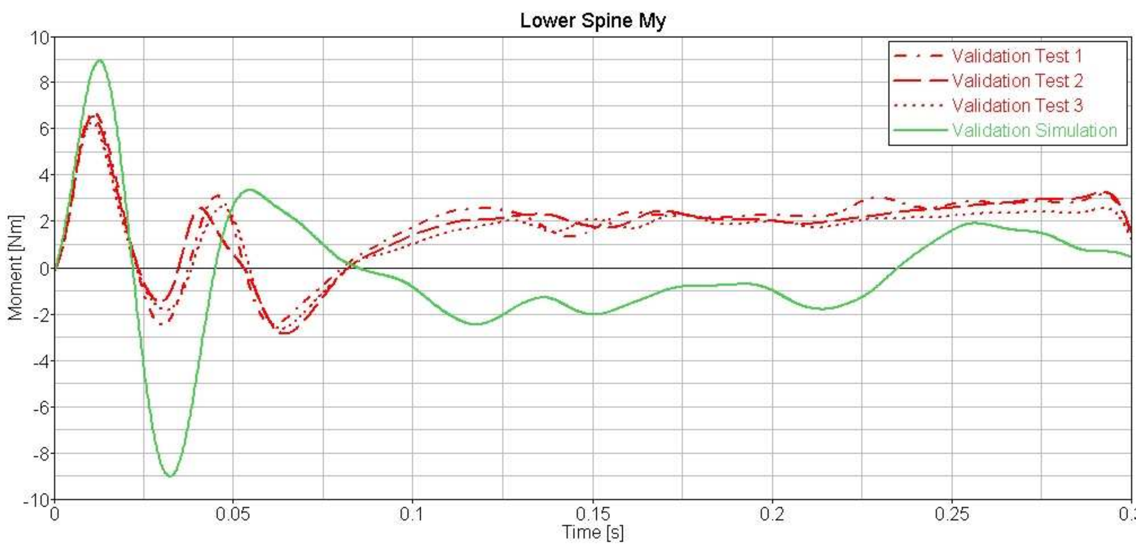

Figure 4.55: Lumbar Spine Moment Y

The pelvis acceleration in the simulation is very noisy, Figure 4.56. Its peak is higher than in the tests and it is a little delayed.

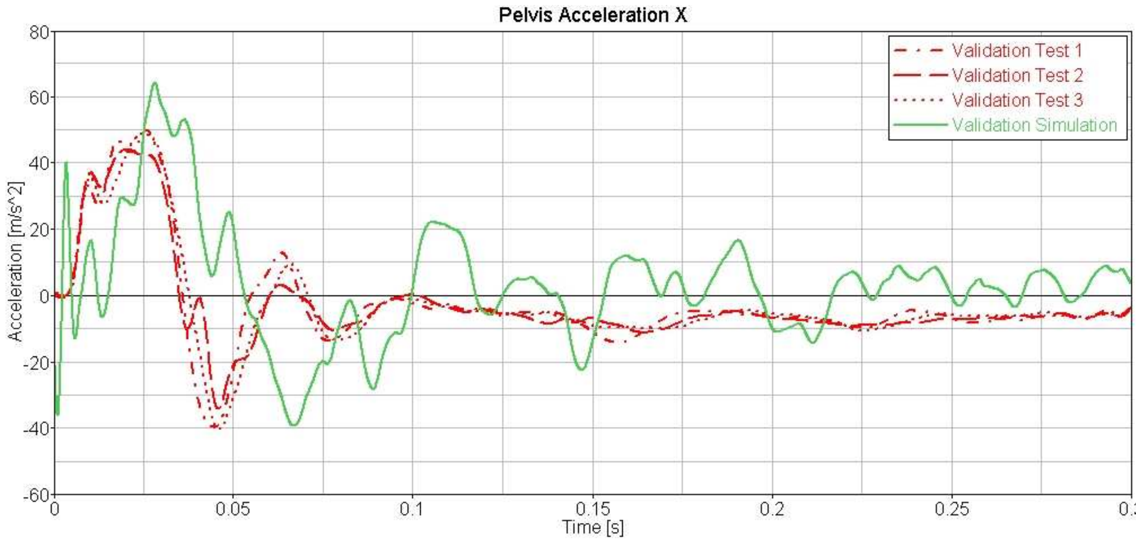

Figure 4.56: Pelvis Acceleration X

4.2.2 Frontal Impact at High Speed

The resultant head acceleration in the frontal validation simulation with the complete dummy is slightly higher than in the tests, see Figure 4.57. The timing of the peak matches perfectly, but the second peak is to high and to late.

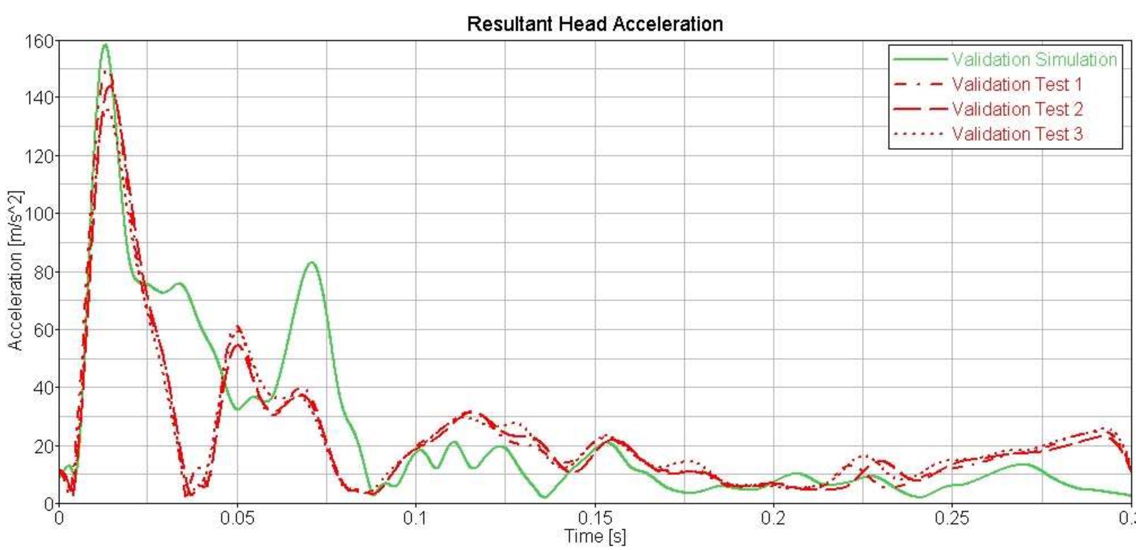

Figure 4.57: Resultant Head Acceleration

The force in X direction measured in the upper neck load cell, Figure 4.58, is to high in the simulation. The force of the rebound in the simulation is much too high. The timing and value of the peak force in Z direction, Figure 4.59, matches the tests very well. The moment around the Y axis in the upper neck load cell is much to low and late in the simulation, Figure 4.60. Similarly to the low speed frontal test, this is most probably mainly due to the nodding joint. The initial position of the nodding joint in the test is unknown. For the simulation the initial position was assumed to be in the center of its range of motion.

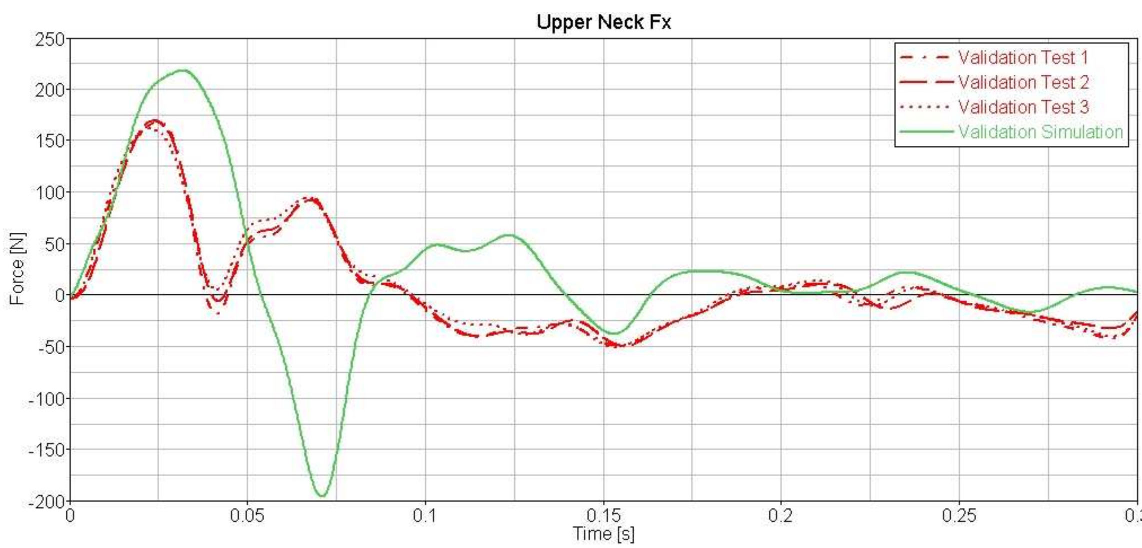

Figure 4.58: Upper Neck Force X

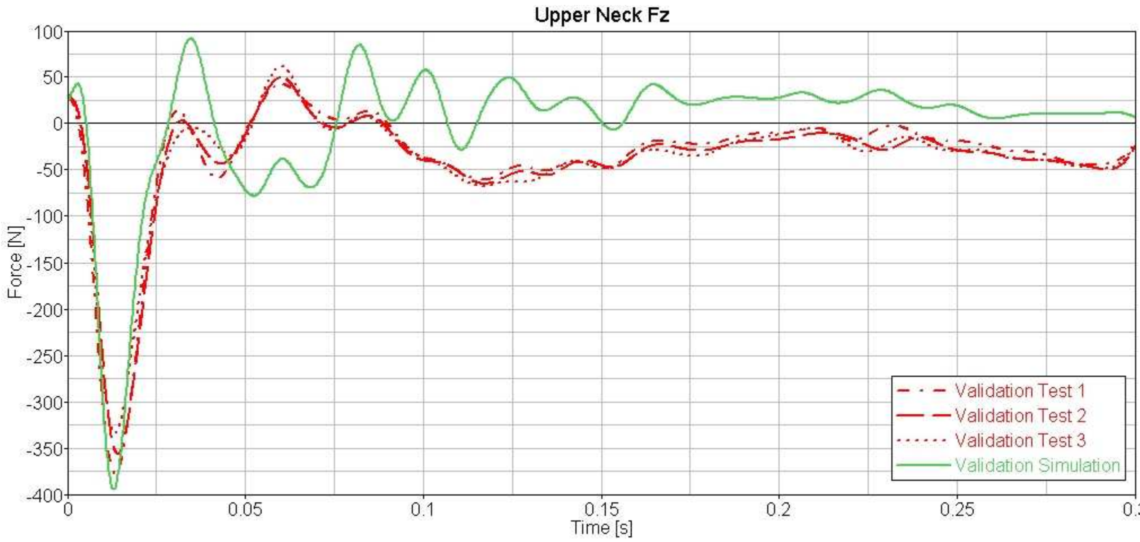

Figure 4.59: Upper Neck Force Z

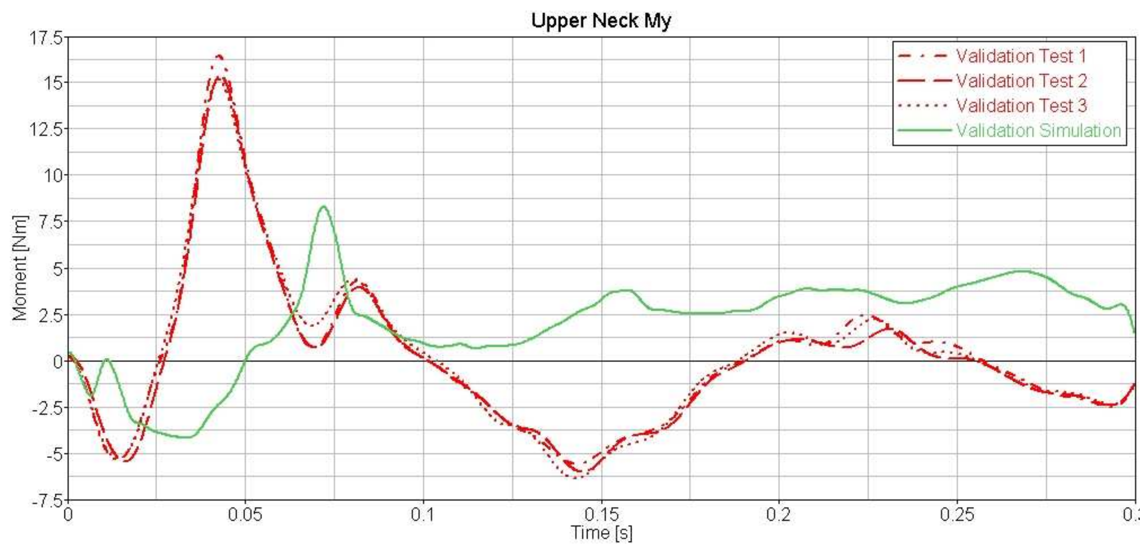

Figure 4.60: Upper Neck Moment Y

The force in X direction measured in the lower neck load cell, Figure 4.61, is higher in the test than in the simulation. The rebound of the force in the simulation is too strong and too late. The value and timing of the peak force in Z direction, Figure 4.62, matches well between the tests and the simulation. The peak moment around the Y axis in the simulation is a little to high and the rebound is to fast compared to the test results, Figure 4.63.

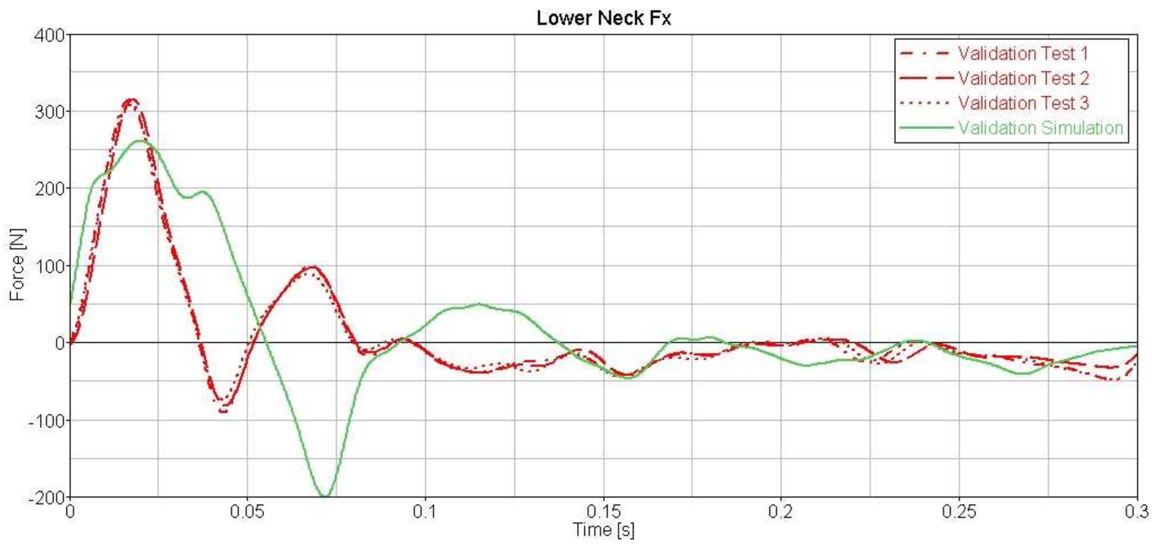

Figure 4.61: Lower Neck Force X

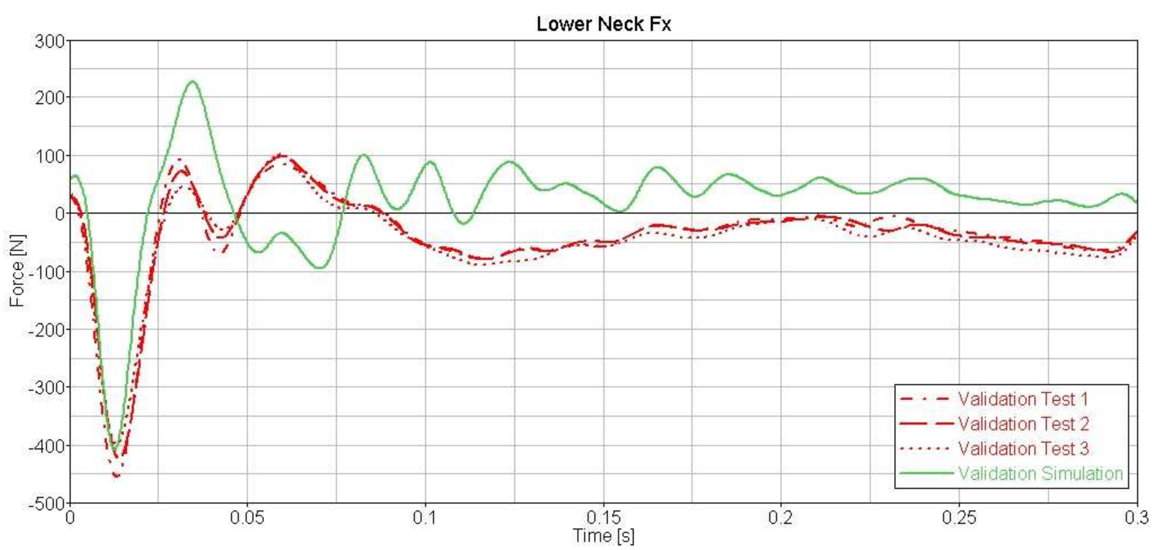

Figure 4.62: Lower Neck Force Z

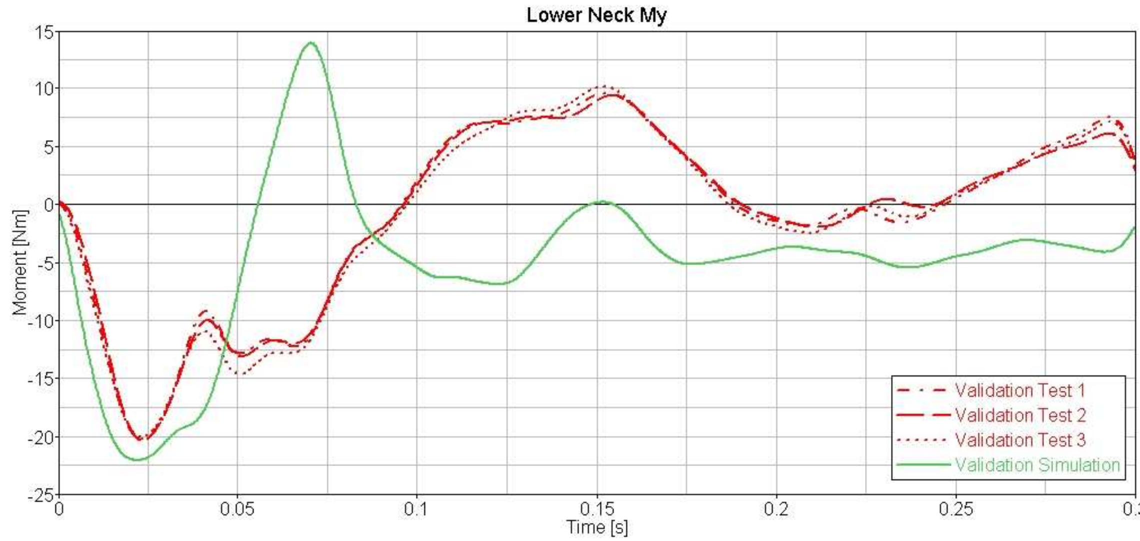

Figure 4.63: Lower Neck Moment Y

The maximum chest acceleration in the simulation is a little to high and to early compared to the test, Figure 4.64. The second peak of the chest acceleration in the test is not found in the simulation. Figure 4.65 shows the chest deformation, where test and simulation data match very well.

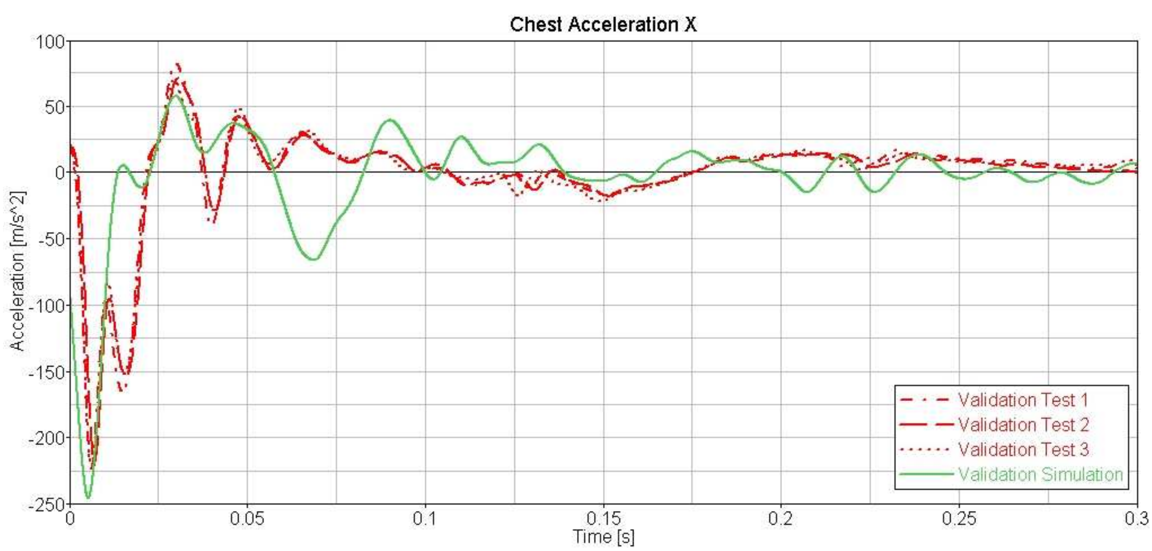

Figure 4.64: Chest Acceleration X

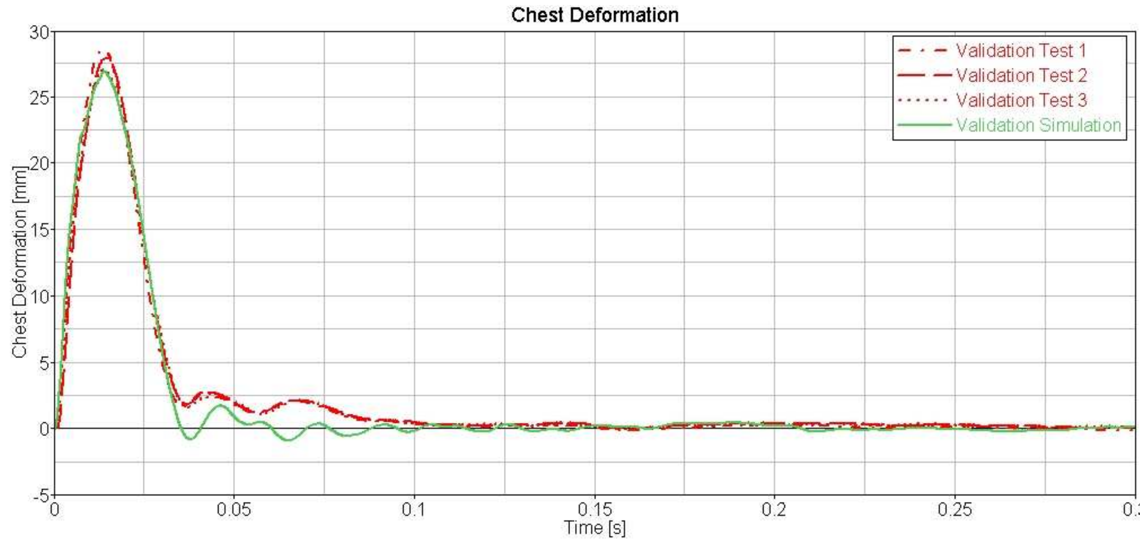

Figure 4.65: Chest Deformation

For the lumbar spine load cell, the peak force in X direction, Figure 4.66, in the simulation are about 20% higher than in the tests. The peak force in Z direction, Figure 4.67, is lower in the simulation than the tests. The moment around the Y axis of the load cell is significantly higher in the simulation than in the tests, Figure 4.68.

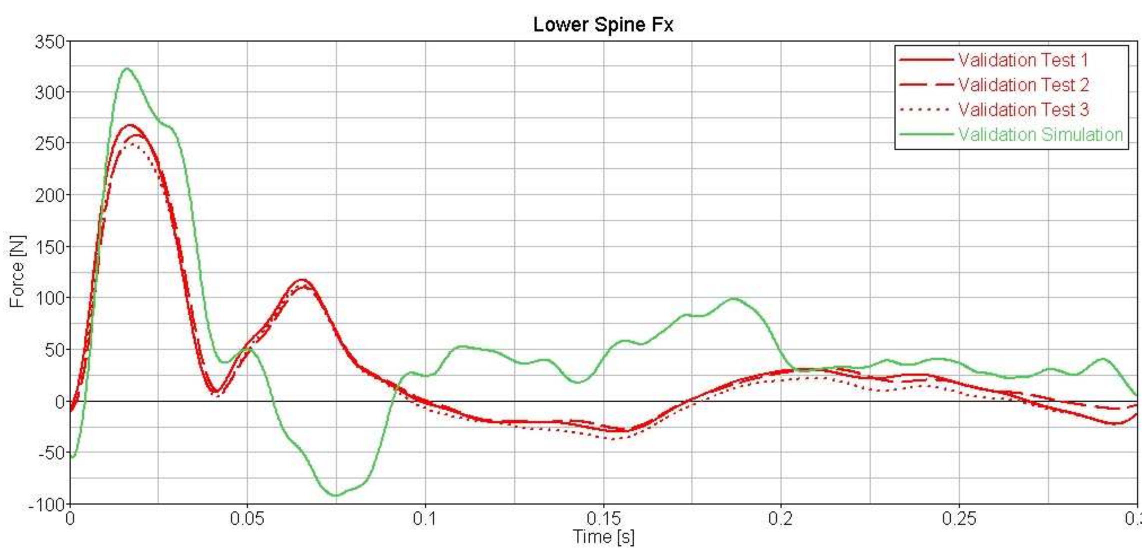

Figure 4.66: Lumbar Spine Force X

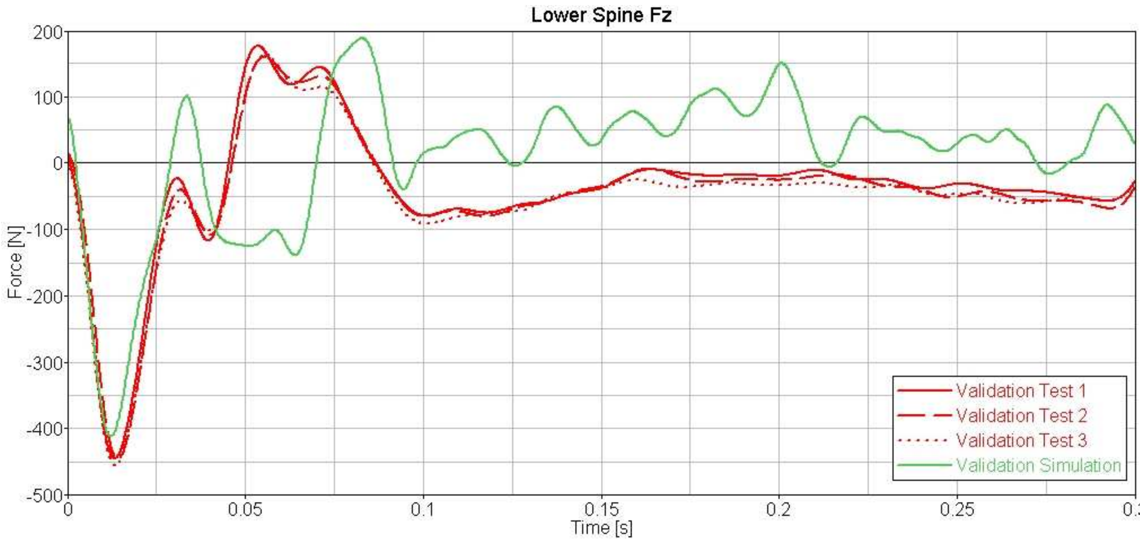

Figure 4.67: Lumbar Spine Force Z

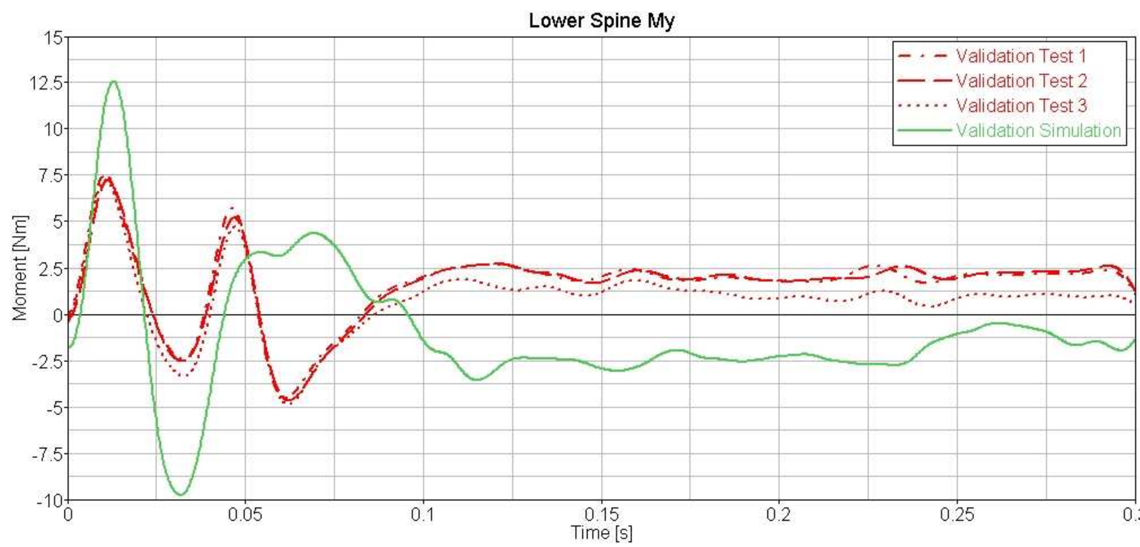

Figure 4.68: Lumbar Spine Moment Y

The pelvis acceleration in the simulation is very noisy and the peak acceleration is higher in the simulation than in the test, see Figure 4.69.

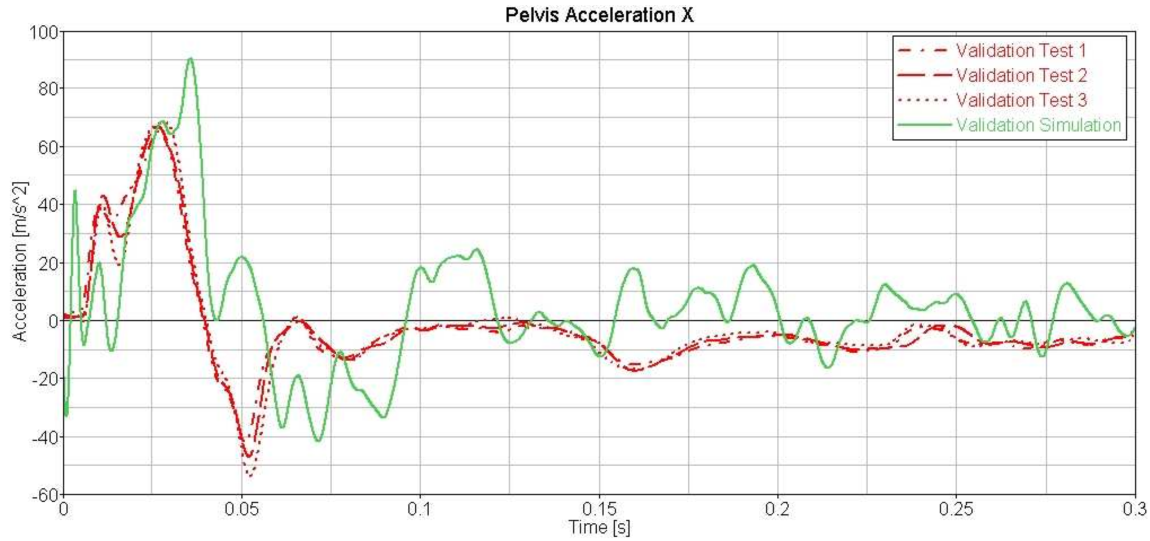

Figure 4.69: Pelvis Acceleration X

The objective ratings for the frontal impact tests of the complete dummy with low impact speed can be seen in Table 4.6. For the high impact speed the ratings are in Table 4.7. With equal weighing of the individual criteria the average combined rating for the low speed is 59% and for the high speed 61%. However, the criterion that lowers the ratings the most is criterion 3, the so called overall correlation. The overall correlation is lower the longer duration of the test data is considered for the rating. Further this criterion only considers a direct match. If a curve is simply time shifted, the overall correlation criterion can be very low. Looking at only a combined criterion of the peak value and the timing of the peak value yields to a combined rating of 805 for the low speed and 82% for the high speed. The Q3 finite element model can be considered validated for frontal impact.

Table 4.6: Objective Rating for the Frontal Impact Tests with Low Impact Speed

	crit 1: Peak Value	crit 2: Timing of Peak Value	crit 3: Overall Correlation	comb: Combined Objective Rating
Resultant Head Acceleration	0.974134	0.981997	0.652396	0.7984876
Upper Neck Force X	0.893747	0.922236	0.270097	0.5717885
Upper Neck Force Z	0.9793	0.985097	0.48565	0.702675
Upper Neck Moment Y	0.0761014	0.157756	0.0821418	0.1045621
Lower Neck Force X	0.84053	0.889511	0.381163	0.6255681
Lower Neck Force Z	0.876641	0.977302	0.393821	0.6426087
Lower Neck Moment Y	0.974246	0.9106	0.271964	0.5762501
Chest Acceleration X	0.890035	0.861458	0.347996	0.6099592
Chest Deformation	0.954728	0.924409	0.87339	0.9109426
Lower Spine Force X	0.921193	0.981761	0.513307	0.7151531
Lower Spine Force Z	0.994273	0.962346	0.389894	0.6470694
Lower Spine Moment Y	0.109985	0.34568	0.253938	0.2303962
Pelvis Acceleration X	0.721707	0.919391	0.237683	0.5291596

Table 4.7: Objective Rating for the Frontal Impact Tests with High Impact Speed

	crit 1: Peak Value	crit 2: Timing of Peak Value	crit 3: Overall Correlation	comb: Combined Objective Rating
Resultant Head Acceleration	0.942901	0.95472	0.590302	0.759748
Upper Neck Force X	0.737412	0.789323	0.266857	0.5342261
Upper Neck Force Z	0.953162	0.963474	0.491009	0.7041398
Upper Neck Moment Y	0.167086	0.59306	0.0791063	0.2455927
Lower Neck Force X	0.81291	0.845042	0.38318	0.6172548
Lower Neck Force Z	0.894124	0.948089	0.362286	0.6255744
Lower Neck Moment Y	0.917343	0.940154	0.335135	0.6116448
Chest Acceleration X	0.883276	0.862408	0.329992	0.5993893
Chest Deformation	0.940786	0.975839	0.883161	0.9230988
Lower Spine Force X	0.828139	0.959012	0.476098	0.6807877
Lower Spine Force Z	0.91808	0.918511	0.357197	0.6229293
Lower Spine Moment Y	0.573281	0.818207	0.207054	0.4696224
Pelvis Acceleration X	0.543791	0.751405	0.291812	0.4928983

4.2.3 Side Impact at Low Speed

In the side validation simulation of the complete dummy minus the arm on the impact side, the resultant head acceleration is around 15% higher and somewhat later than in the tests, Figure 4.70.

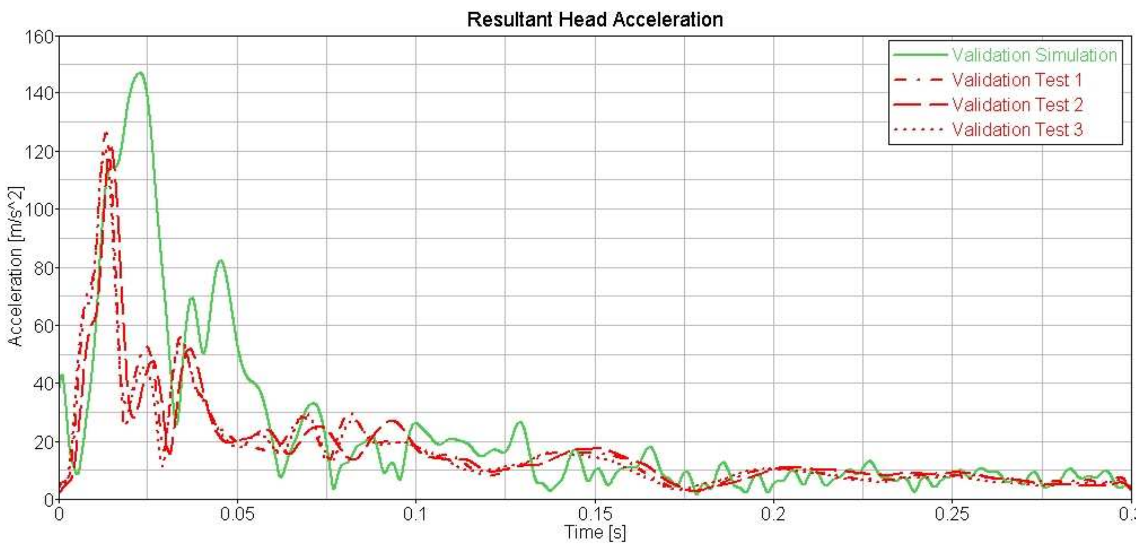

Figure 4.70: Resultant Head Acceleration

The forces in Y direction measured in the upper neck load cell are significantly higher in the simulation than the test, Figure 4.71. The timing and overall shape of the forces in Z direction match well between the simulation and the tests, Figure 4.72. The first peak of the moment around the X axis matches well between the simulation and the tests, but the second peak is to low and to late in the simulation, Figure 4.73.

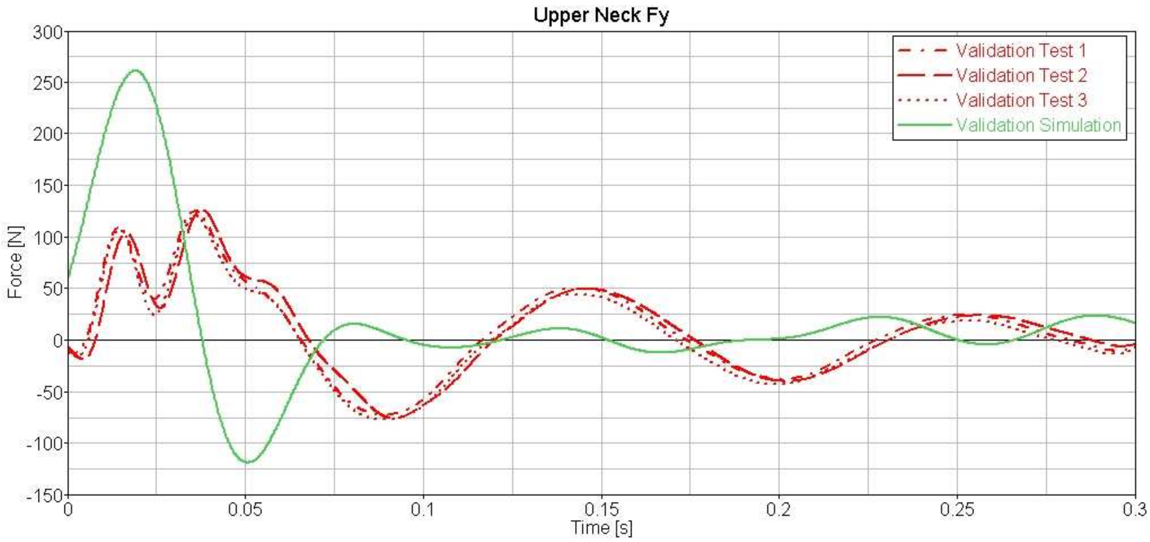

Figure 4.71: Upper Neck Force Y

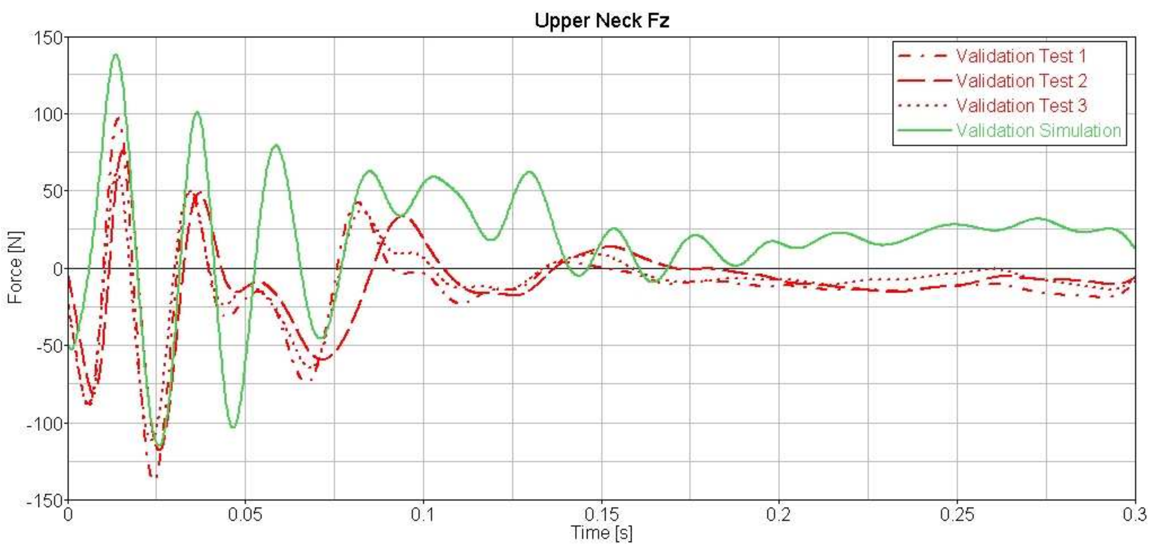

Figure 4.72: Upper Neck Force Z

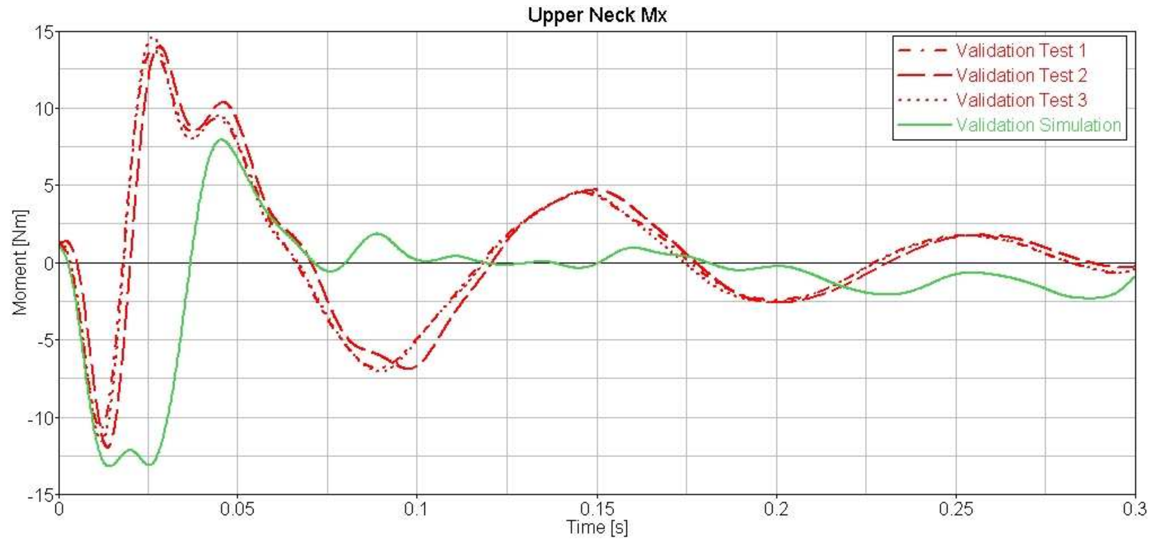

Figure 4.73: Upper Neck Moment X

In the simulation the duration of the peak force in Y direction in the lower neck load cell is too long and the rebound late and to strong compared to the tests, Figure 4.74. But the value of the first peak and the timing match very well. The force in Z direction, shown in Figure 4.75, matches well between tests and simulation. The moment around the Z axis, Figure 4.76, is not high enough in the simulation and dies down to quickly.

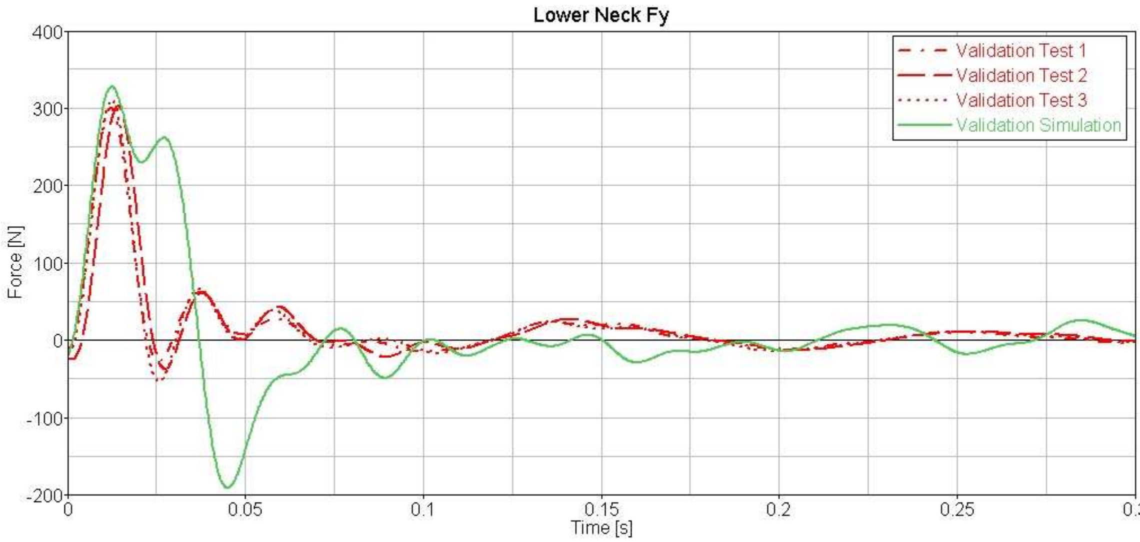

Figure 4.74: Lower Neck Force Y

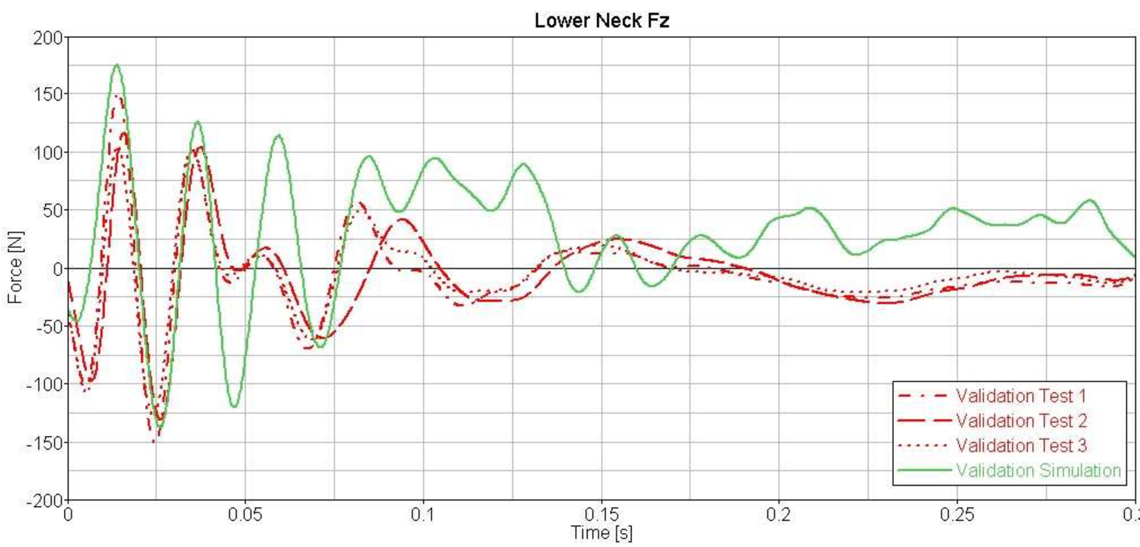

Figure 4.75: Lower Neck Force Z

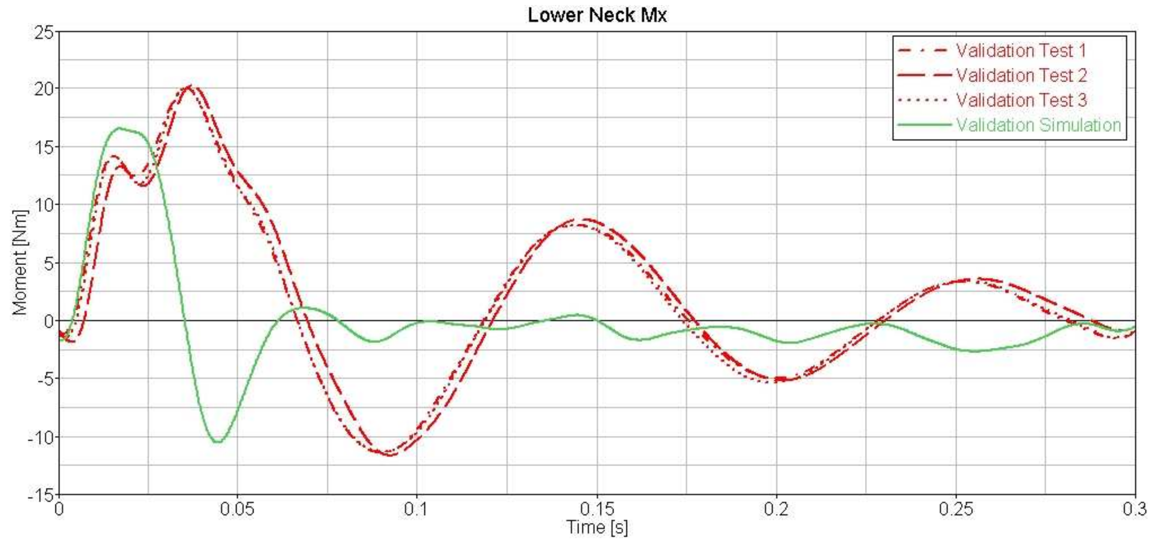

Figure 4.76: Lower Neck Moment X

The peak of the chest acceleration matches well between the tests and the simulation, Figure 4.77. However, the rebound is much too high in the simulation. The chest deflection was not measured in the lateral tests.

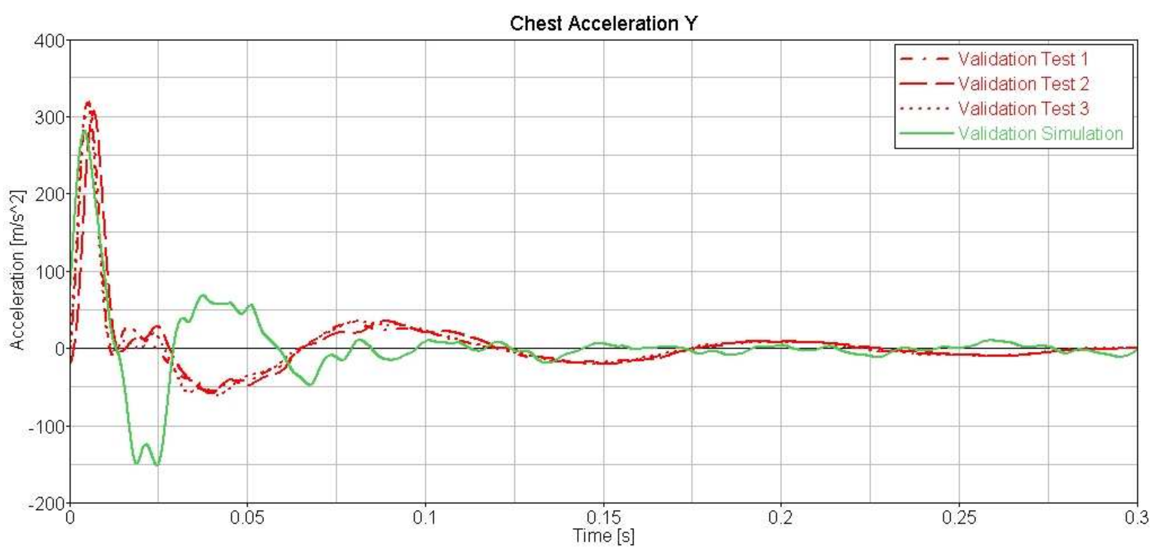

Figure 4.77: Chest Acceleration Y

The forces in Y direction measured in the lumbar spine load cell are much to low in the simulation, see Figure 4.78. The forces in Z direction are very noisy, particularly in the simulation, Figure 4.79. The peak moment around the X axis is about 20% to high in the simulation, but the timing matches very well, Figure 4.80.

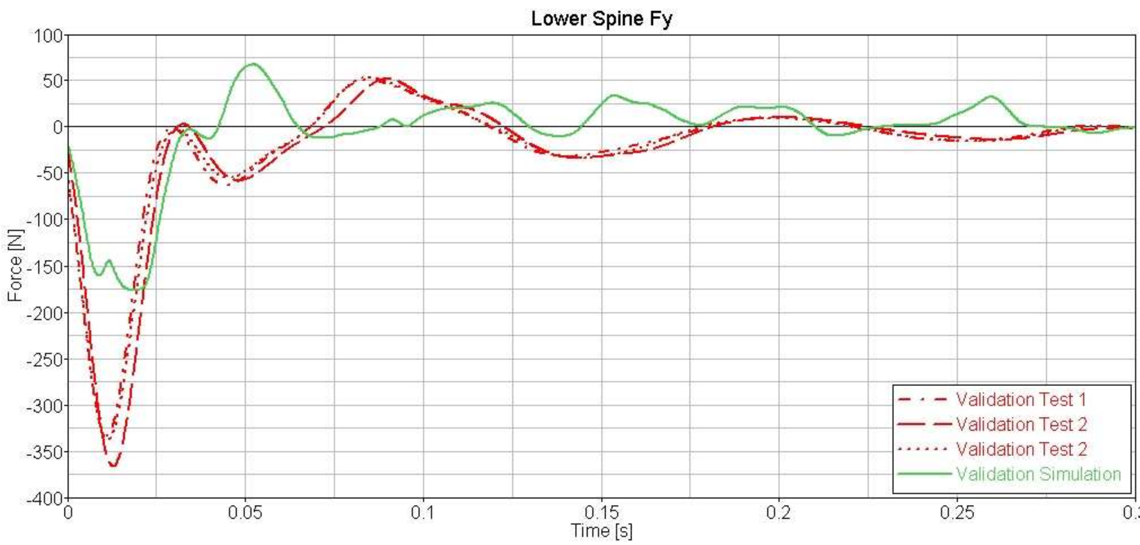

Figure 4.78: Lumbar Spine Force Y

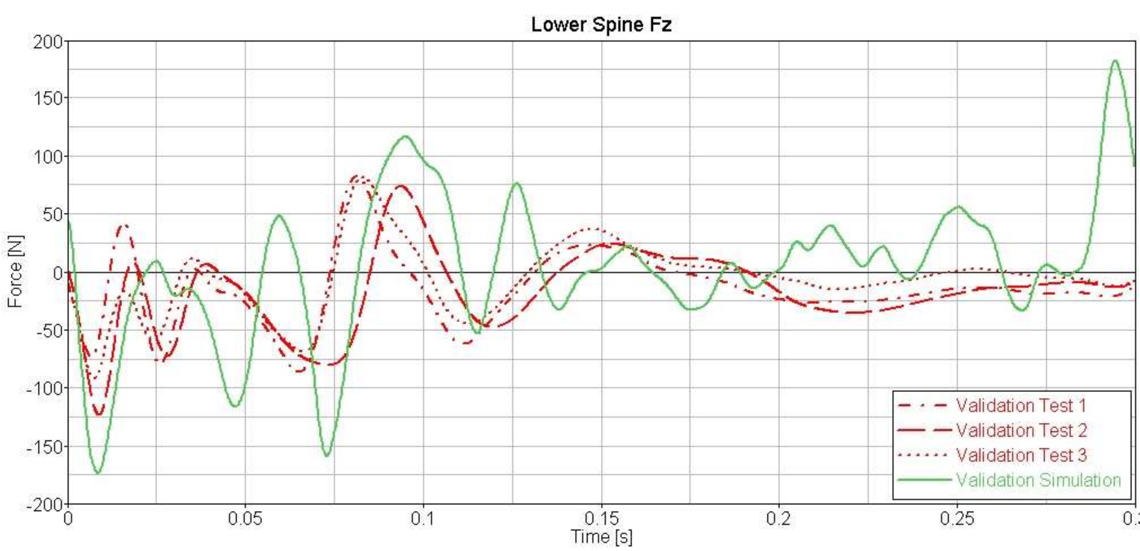

Figure 4.79: Lumbar Spine Force Z

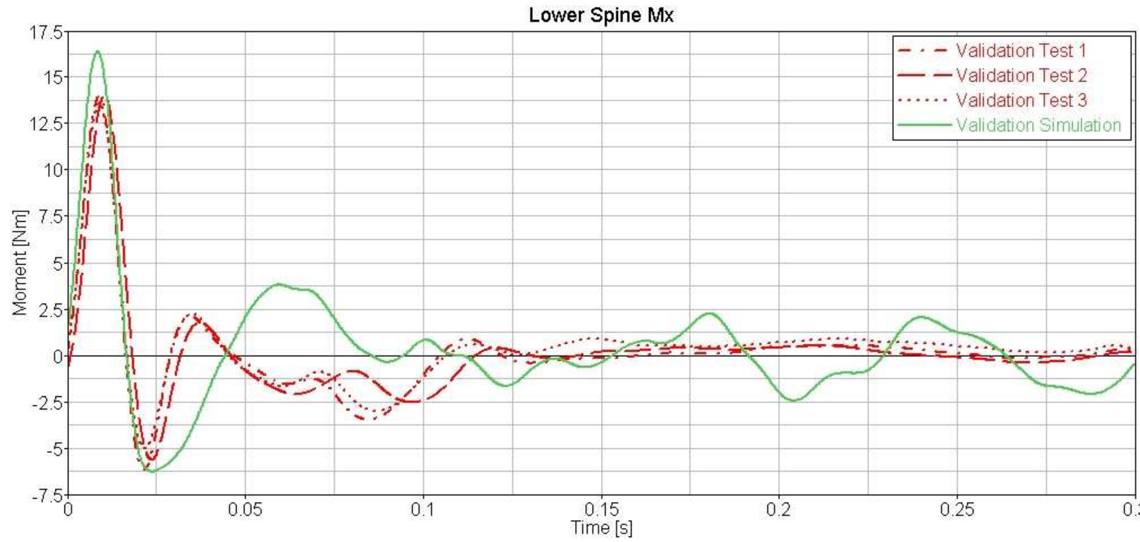

Figure 4.80: Lumbar Spine Moment X

The pelvis acceleration in Y direction is very noisy in the simulation. The peak acceleration is to early and about 25% too low, see Figure 4.81.

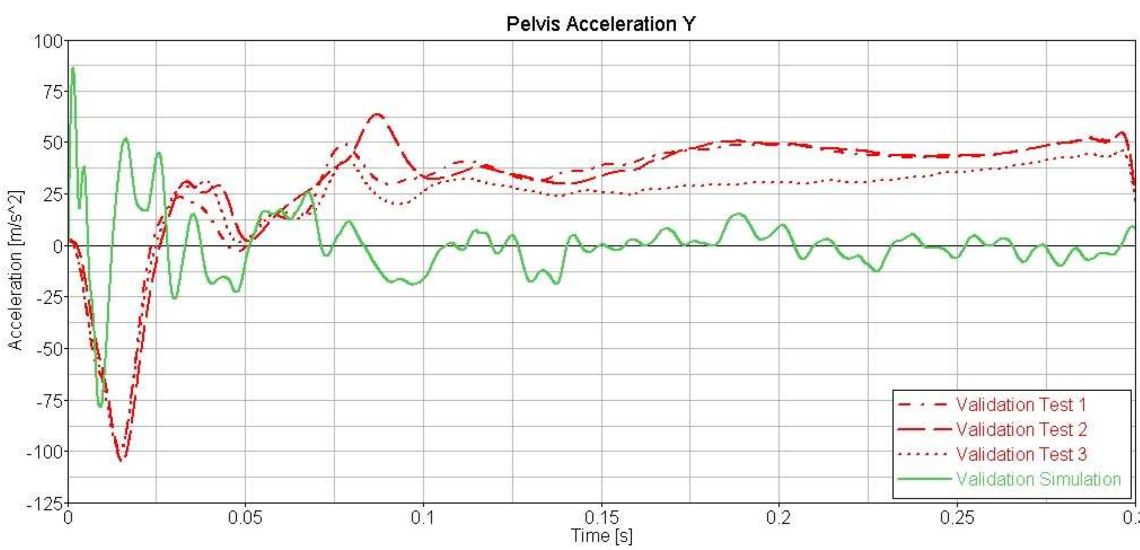

Figure 4.81: Pelvis Acceleration Y

4.2.4 Side Impact at High Speed

The resultant head acceleration measured in the lateral impact of the dummy with the higher impact speed is about 25%to high in the simulation and also later than the peak in the tests, see Figure 4.82.

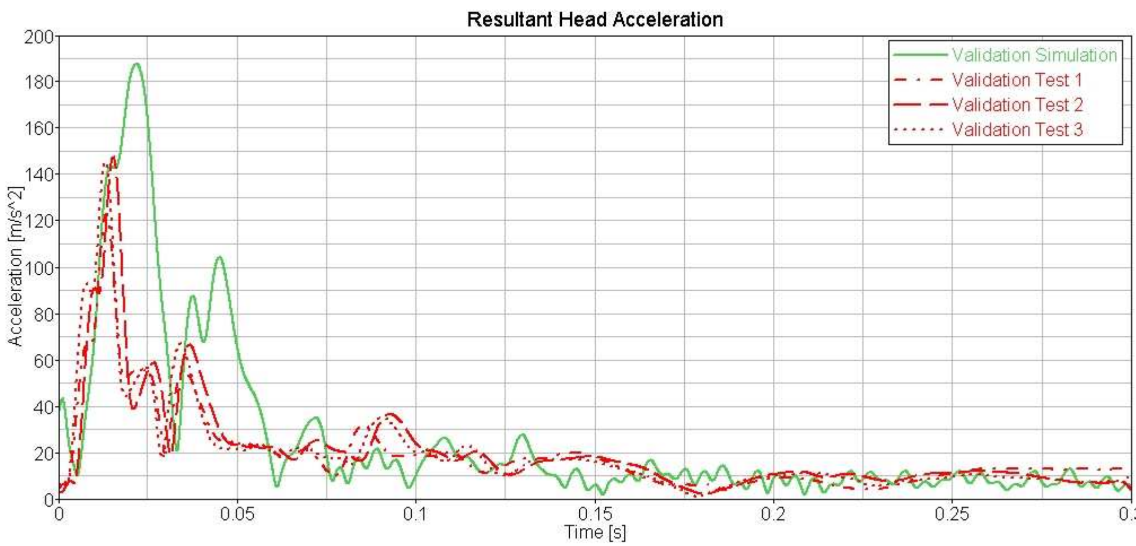

Figure 4.82: Resultant Head Acceleration

The force in Y direction at the upper neck load cell is significantly higher in the simulation than in the tests, Figure 4.83. Also in the Z direction the force in the simulation is higher than in the tests, but the timing matches well, Figure 4.84. The timing and peak value of the moment about the X axis matches well, Figure 4.85, but the duration of the peak is to long and the rebound is to late and not high enough.

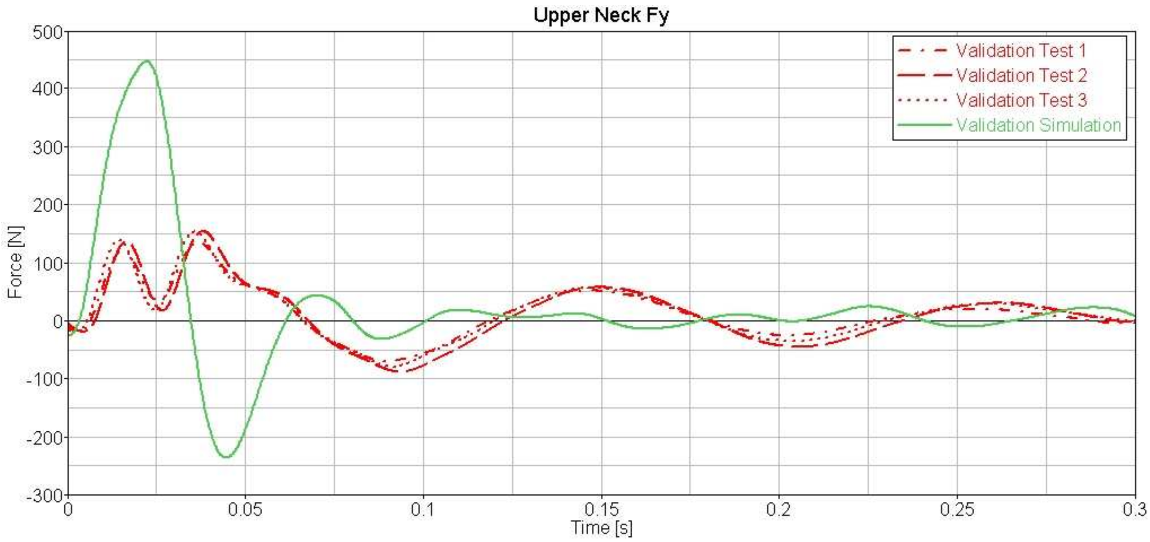

Figure 4.83: Upper Neck Force Y

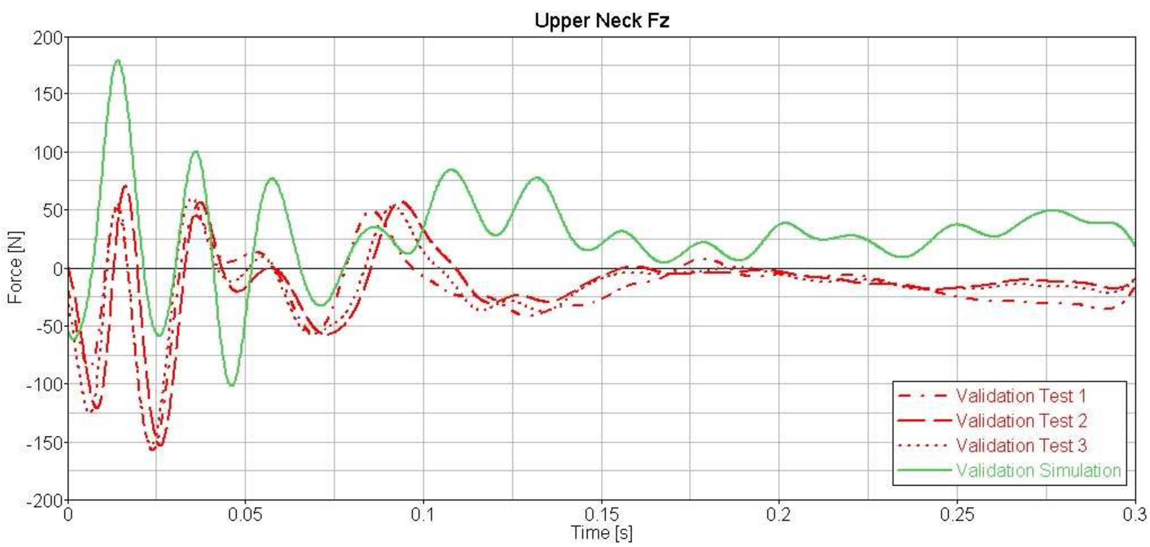

Figure 4.84: Upper Neck Force Z

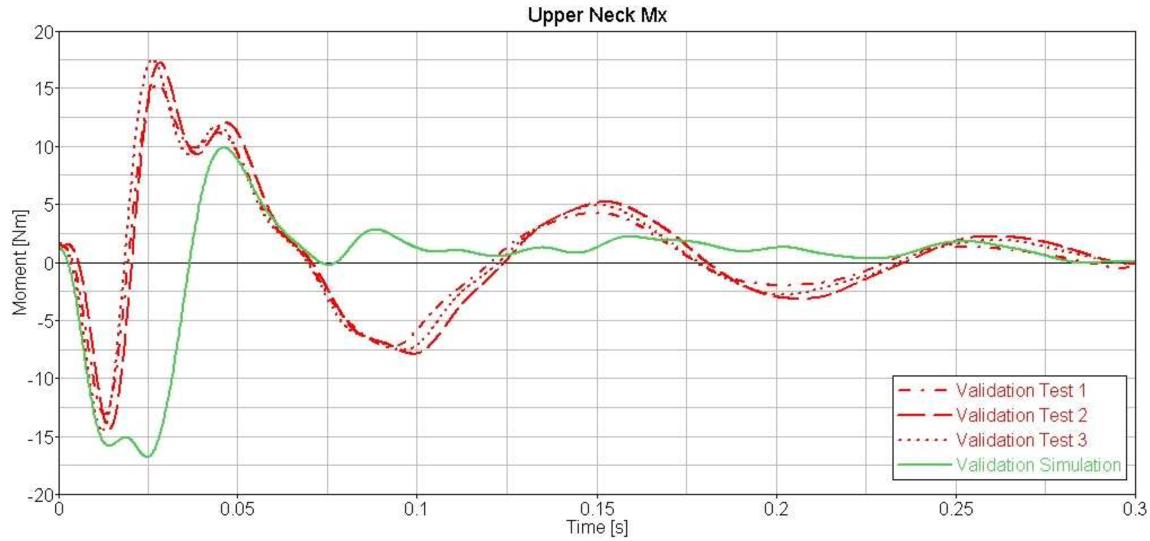

Figure 4.85: Upper Neck Moment X

The peak value and the timing of the force in Y direction at the lower neck load cell match well between the simulation and the tests. The duration of the peak and the rebound are too large in the simulation, Figure 4.86. The force in Z direction is too high in the simulation, but the timing matches the tests, Figure 4.87. The moment around the X axis is about 20% lower in the simulation than the tests and the timing of the peak is to early in the simulation, see Figure 4.88.

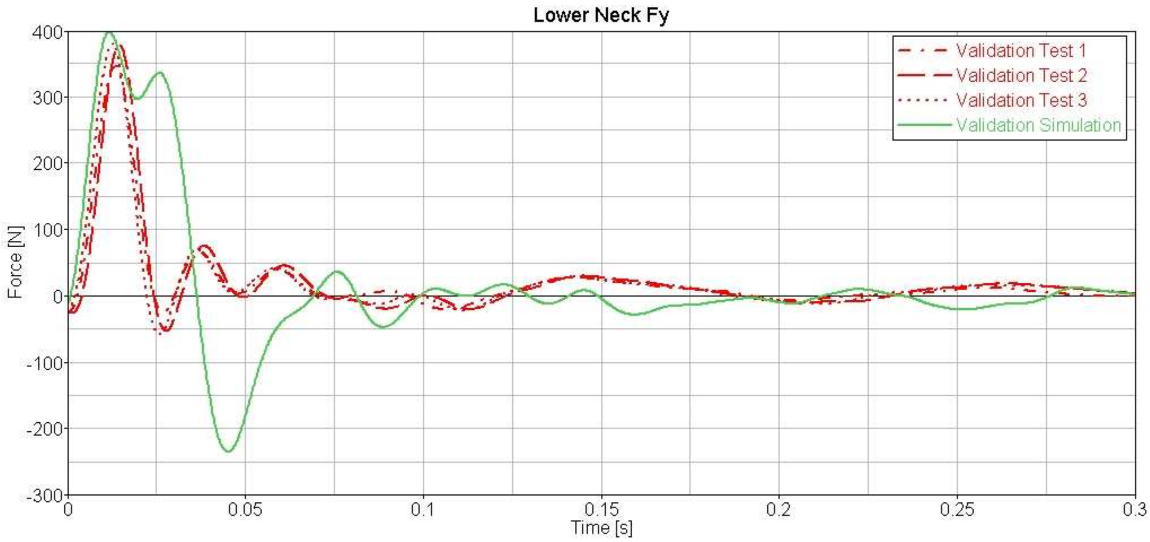

Figure 4.86: Lower Neck Force Y

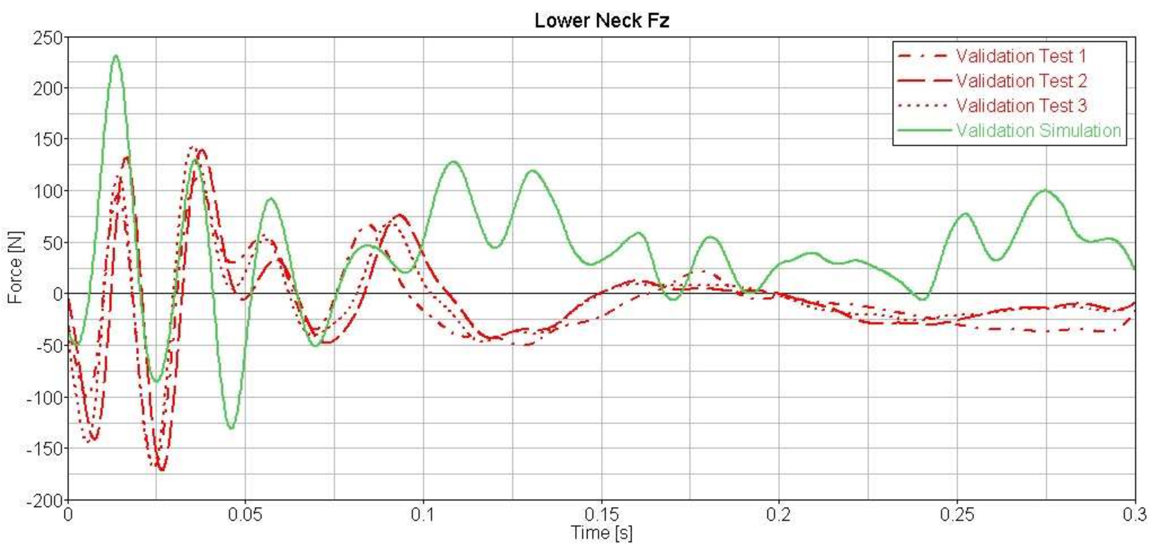

Figure 4.87: Lower Neck Force Z

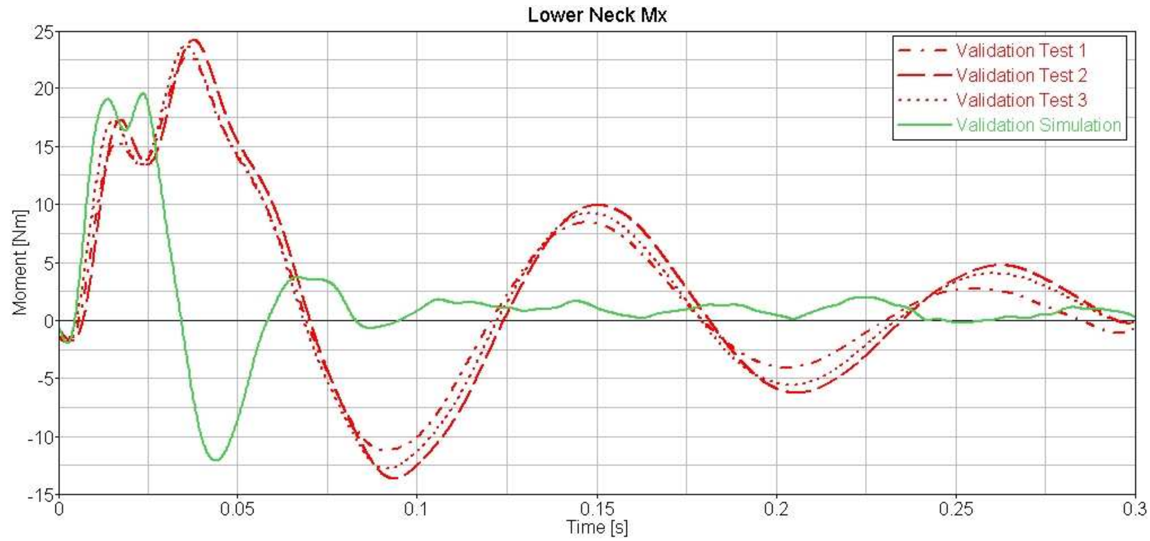

Figure 4.88: Lower Neck Moment X

The chest acceleration in the simulation is somewhat lower than the tests. The rebound of the acceleration is much stronger in the simulation, see Figure 4.89.

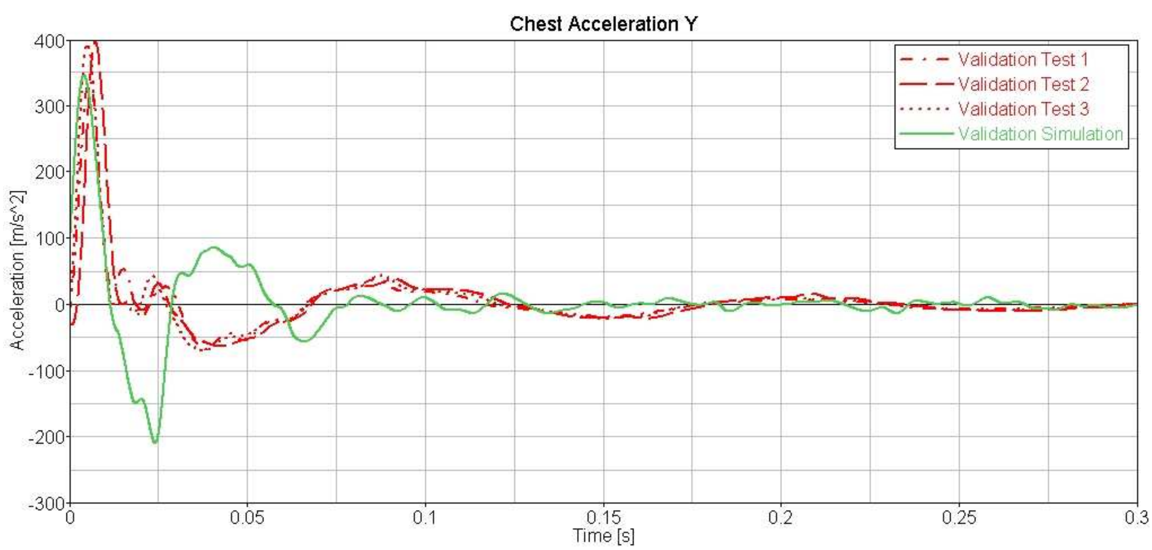

Figure 4.89: Chest Acceleration Y

The force in Y direction measured in the lumbar spine load cell is about 20% higher in the simulation, than the tests. The timing matches well, see Figure 4.90. The force in Z direction is very noisy in the simulation, but the first peak matches well in timing and value, see Figure 4.91. The moment about the X axis matches in timing and value of the peak as well as the rebound very well between the simulation and the tests, Figure 4.92.

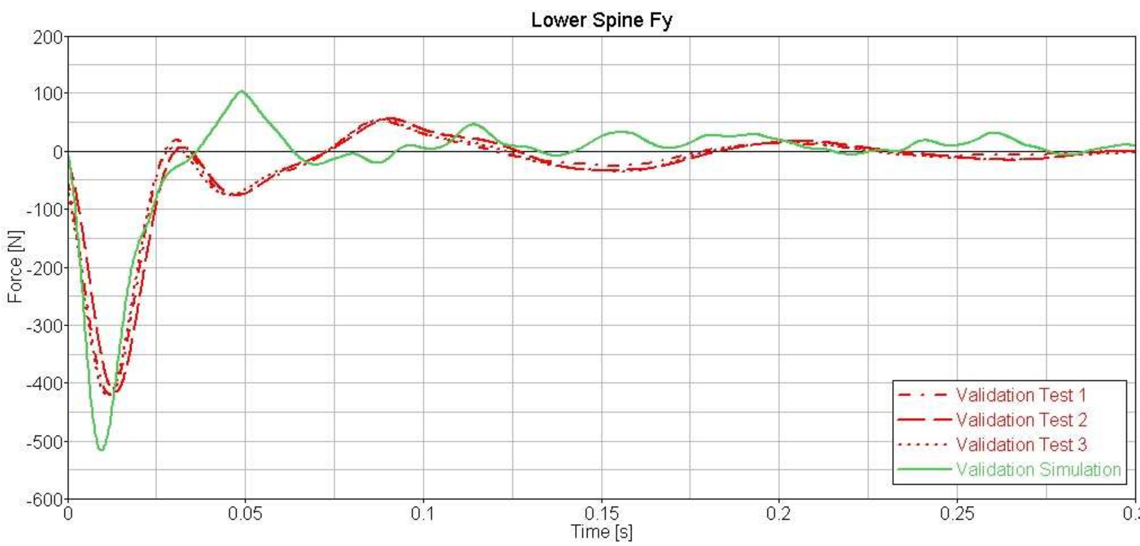

Figure 4.90: Lumbar Spine Force Y

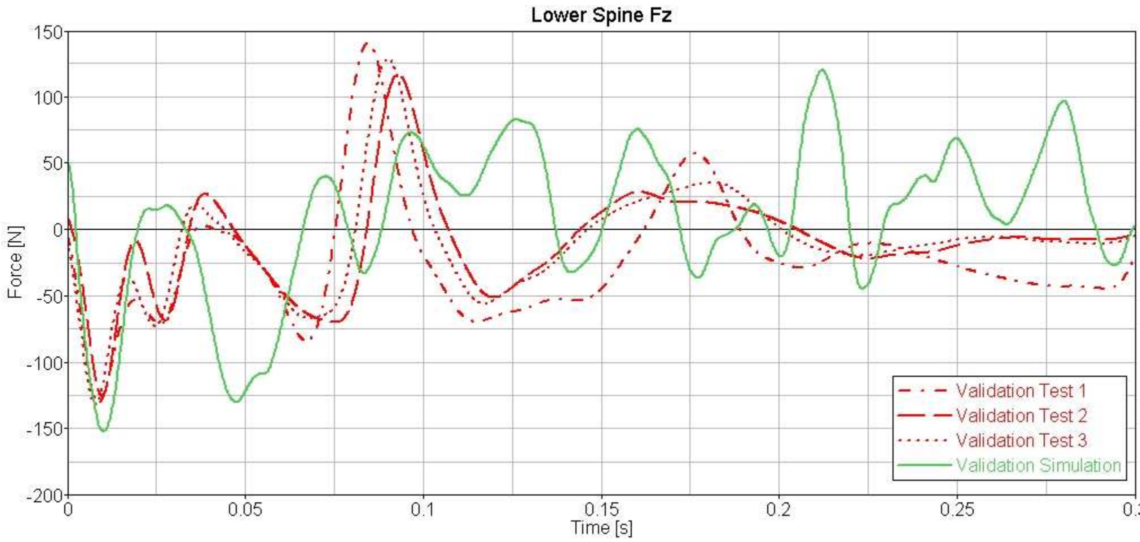

Figure 4.91: Lumbar Spine Force Z

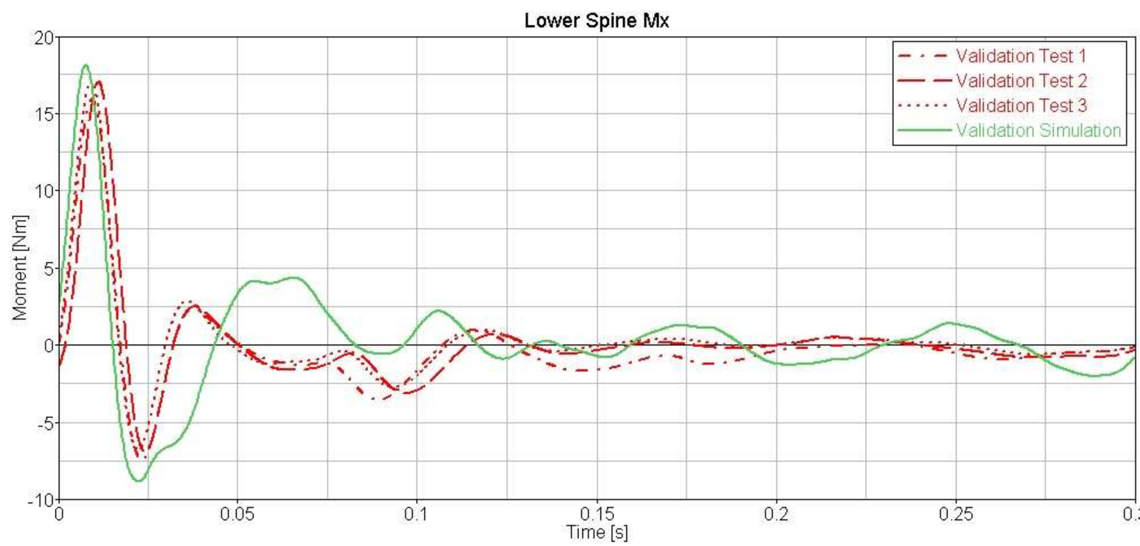

Figure 4.92: Lumbar Spine Moment X

The peak pelvis acceleration in the simulation is about 25% lower and earlier than in the tests, Figure 4.93.

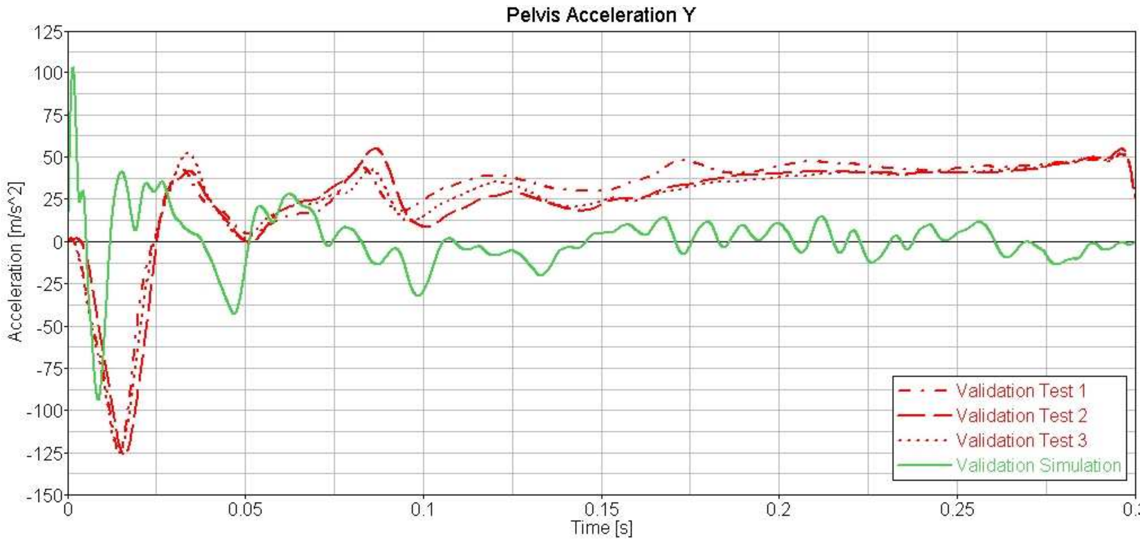

Figure 4.93: Pelvis Acceleration Y

Table 4.8 shows the objective ratings for the lateral impact tests of the complete dummy with low closing speed and Table 4.9 shows the ratings for the high closing speed. The average combined objective rating is 47% for the low speed and 49% for the high speed. Even when only considering the criteria for the peak value and for the timing of the peak, the average combined rating is only 63% for the low closing speed and 66% for the high closing speed. Therefore this finite element model of the Q3 dummy should in side impacts only be used to show tendencies, but not to find actual data points. The reasons for the poor correlation most probably lie in the performance of the rib cage in lateral impact and the shoulder clavicle complex. This complex is connected to the spine box and to the upper frontal center of the rib cage. Unfortunately no lateral component level impact test of the ribcage was available not a lateral or high speed test of the shoulder complex. With such tests available the performance of the finite element model of the Q3 in the side impact test simulations would most likely match the test data much better.

Table 4.8: Objective Rating for the Lateral Impact Tests with Low Impact Speed

	crit 1: Peak Value	crit 2: Timing of Peak Value	crit 3: Overall Correlation	comb: Combined Objective Rating
Resultant Head Acceleration	0.644459	0.589229	0.430144	0.5454386
Upper Neck Force Y	0.393163	0.53314	0.21268	0.3659437
Upper Neck Force Z	0.803771	0.563224	0.281398	0.5014461
Upper Neck Moment X	0.810535	0.508816	0.214947	0.454269
Lower Neck Force Y	0.945188	0.992055	0.281829	0.5841326
Lower Neck Force Z	0.864001	0.965462	0.249892	0.559413
Lower Neck Moment X	0.577018	0.476179	0.204994	0.3985194
Chest Acceleration Y	0.847678	0.807191	0.368078	0.6085485
Lower Spine Force Y	0.464886	0.602154	0.439011	0.4968973
Lower Spine Force Z	0.643954	0.0305703	0.259111	0.2661791
Lower Spine Moment X	0.850483	0.945041	0.43388	0.6604573
Pelvis Acceleration X	0.496443	0.121584	0.0822295	0.2110161

Table 4.9: Objective Rating for the Lateral Impact Tests with High Impact Speed

	crit 1: Peak Value	crit 2: Timing of Peak Value	crit 3: Overall Correlation	comb: Combined Objective Rating
Resultant Head Acceleration	0.599918	0.706616	0.44833	0.571639
Upper Neck Force Y	0.275043	0.586385	0.150913	0.3125921
Upper Neck Force Z	0.350499	0.549599	0.157541	0.3330543
Upper Neck Moment X	0.764274	0.880246	0.239207	0.5349861
Lower Neck Force Y	0.948591	0.937469	0.281415	0.5825005
Lower Neck Force Z	0.473954	0.514888	0.166304	0.3656744
Lower Neck Moment X	0.539129	0.648349	0.189641	0.4247487
Chest Acceleration Y	0.915875	0.73211	0.344689	0.5883875
Lower Spine Force Y	0.780439	0.816652	0.655969	0.7416844
Lower Spine Force Z	0.824138	0.970664	0.190058	0.5211841
Lower Spine Moment X	0.91446	0.838627	0.456793	0.6691263
Pelvis Acceleration X	0.412688	0.119688	0.0904415	0.1943571

4.3 Comparison with Hybrid III dummy in NCAP Test and MADYMO H3 and MADYMO Q3 in Sled Test Setup

In this section the results of the comparison of a test with the Hybrid III three-year-old, its MADYMO ellipsoid model, a MADYMO ellipsoid model of the Q3, and the finite element model of the Q3 are presented. The dummies were restrained in a child seat and the child seat was attached to the rear seat bench.

The test with the actual dummy is a New Car Assessment Program (NCAP) test. For the simulations the deceleration pulse of the rear right cross-member of the test was filtered, inverted and then applied to the sled in the simulation. More details about the simulation setup can be found in *3.3 Comparison with MADYMO Models.*

The first peak of the resultant head acceleration of the MADYMO Hybrid III is only about half the value of the test, see Figure 4.94. The second peak has the same value, as in the test, but is delayed.

The Q3 can not be directly compared to the test with the Hybrid III, but tendencies can be observed. The MADYMO Q3 matches the timing of the second peak of the test with the Hybrid III, but the value is almost double. The head acceleration of the finite element Q3 is on a relative high plateau compared to the two peaks from the other data.

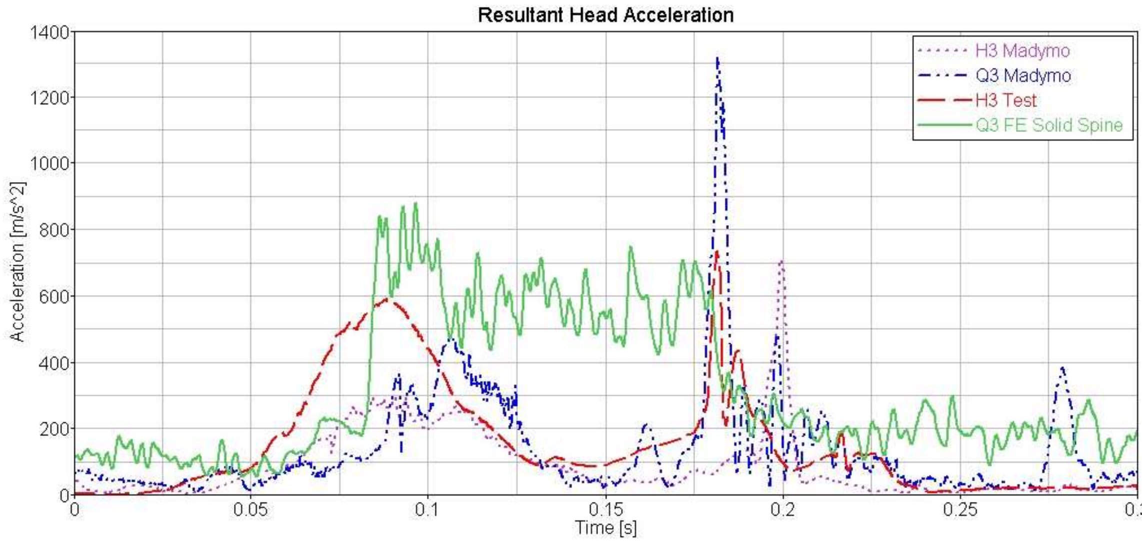

Figure 4.94: Resultant Head Acceleration

The neck injury criterion [62][63], calculated from the neck forces and neck moment can bee seen in Figure 4.95. The Hybrid III test results and the Hybrid III MADYMO simulation match relatively well in timing as well as in peak value. The Q3 MADYMO simulation shows the same timing, but more than double the peak value. The finite element model of the Q3 matches the first peak well in timing and value, but the second peak is too early.

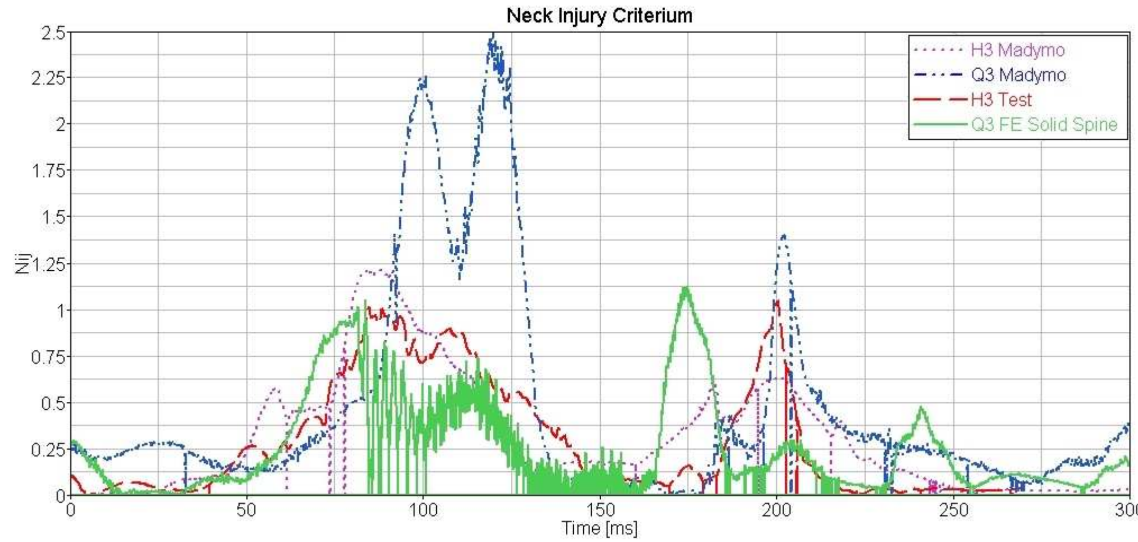

Figure 4.95: Neck Injury Criterion

The resultant chest acceleration in Figure 4.96 is much to low for the Hybrid III MADYMO simulation compared to the test results. The MADYMO Q3 is at a similar level as the MADYMO Hybrid III. The finite element model of the Q3 has a much higher chest acceleration than all the others.

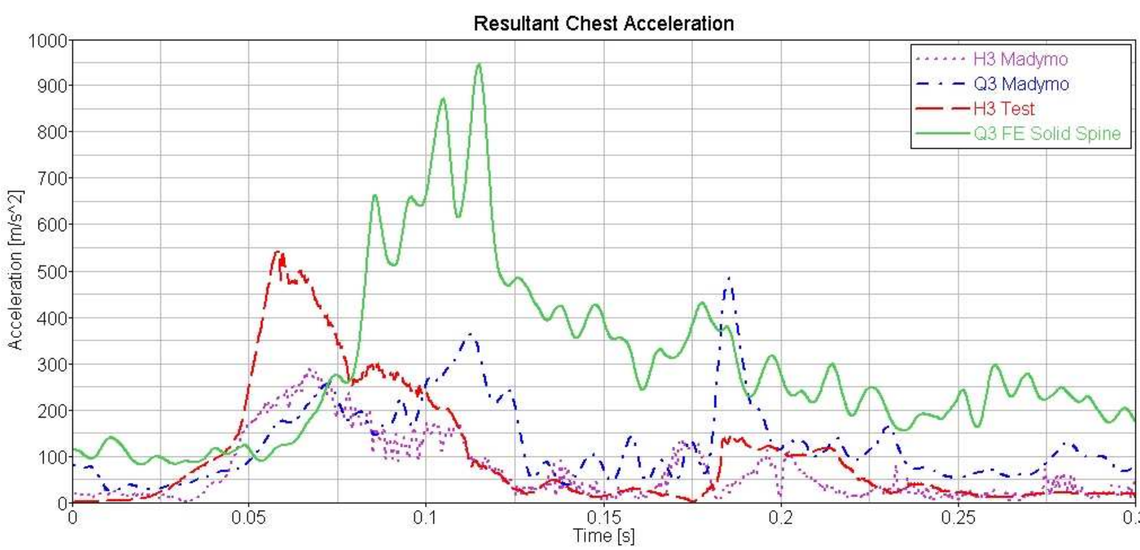

Figure 4.96: Resultant Chest Acceleration

Figure 4.97 shows the chest deflection. The absolute chest deflection is very similar for the test and all three simulations. However, for all three simulations there was a pre-simulation conducted to tension the harness of the child seat. This deflects the chest of the dummy. So it could be argued that the chest deflection has to be set to zero at the start time. This would mean that the MADYMO Q3 would have the lowest chest deflection, the finite element Q3 and the MADYMO Hybrid III would have about the same level of chest deflection and the test with the Hybrid III would have the highest chest deflection.

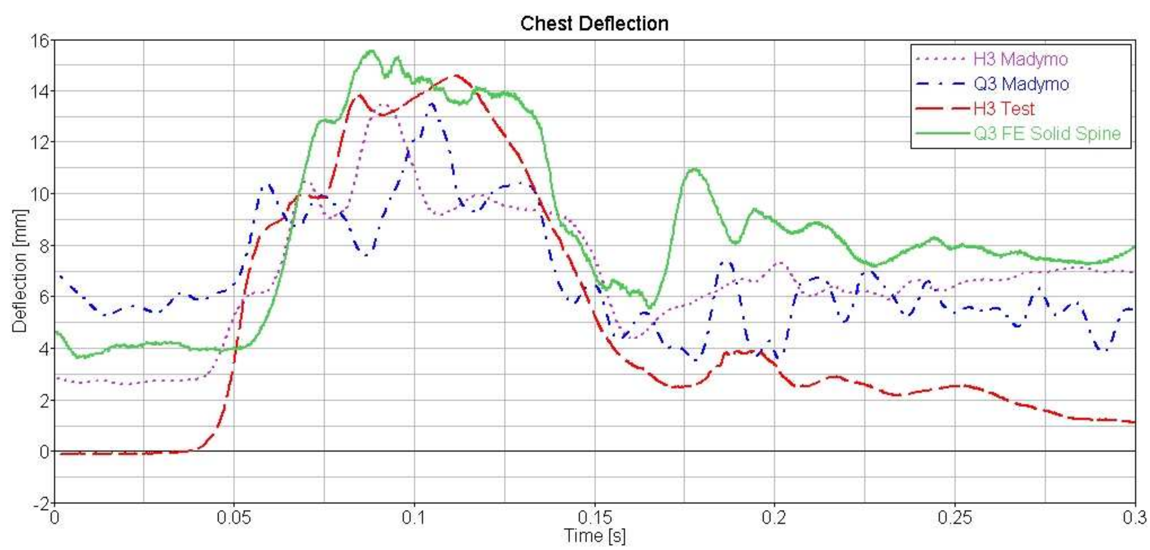

Figure 4.97: Chest Deflection

The comparison of a test with the Hybrid III, the MADYMO model of the Hybrid III, the MADYMO model of the Q3, and the finite element model of the Q3 developed in this research shows that in a simulation with many different parts, like in this case the seat bench of the vehicle, the child seat, and the dummy it is difficult to completely match the results of a test or a different model, even a match between the outcome of two different models of the same dummy is hard to achieve. However, the outcome in the test and presented simulations are approximately in the same region. Since the Hybrid III and the Q3 are different dummies nothing else can be expected. The differences between the MADYMO Q3 and finite element Q3 model are significant. In this case it is difficult to know which of the models represents reality better.

4.4 Comparison of Q3 with Solid and with Flexible Spine in a Sled Test Setup

The following section describes the results of the comparison between the finite element model of the Q3 with the original spine and a finite element version where the material of the upper part of the rigid spine box has been replaced by the material of the neck. The setup for this comparison is the dummy in a child seat that is fixed to a simulated rear seat bench as used for the comparison to the MADYMO dummies. The setup is shown in Figure 3.29 and the acceleration of the sled is shown in Figure 3.30. More details about the methodology can be found in Chapter *3.3* and *3.4* .

As can be seen in Figure 4.98 the peak of the resultant head acceleration is earlier in the version with the flexible spine, but the value of the peak remains the same. However, the resultant head acceleration in the simulation with the flexible spine comes down to a lower level faster which results in a lower head injury criterion number.

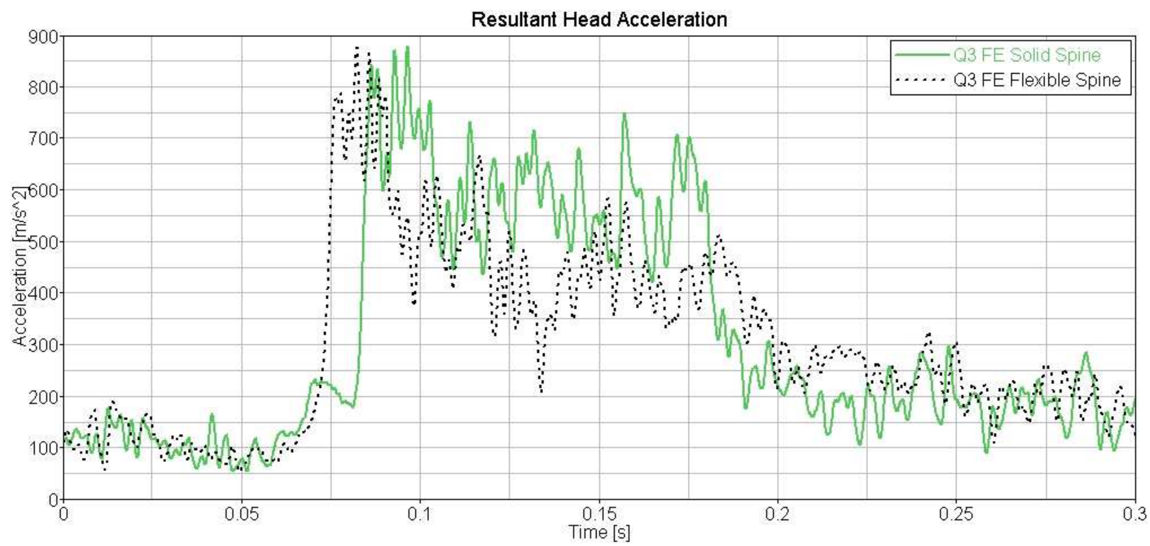

Figure 4.98: Resultant Head Acceleration

A similar picture for the neck injury criterion in Figure 4.99, both have about the same value at the first peak, but the general shape is lower in the version with the flexible spine. Also, the second peak is about 15% higher for the model with the solid spine.

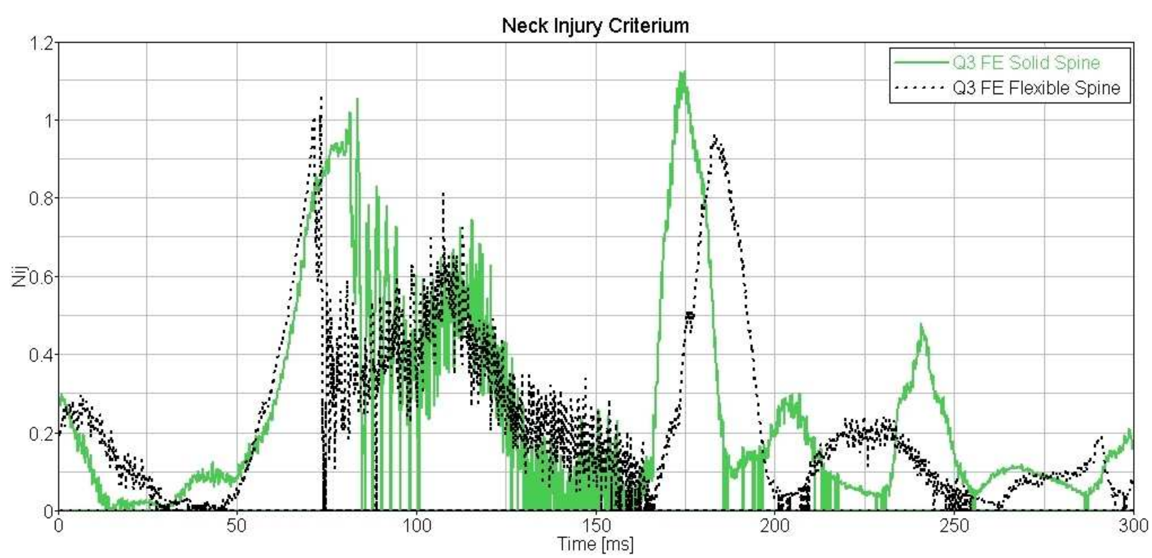

Figure 4.99: Neck Injury Criterion

The changes in the spine of the dummy resulted in a much higher resultant chest acceleration, see Figure 4.100. The resultant chest acceleration for both cases was extremely noisy. Converting part of the rigid spine to a flexible material reduced the size and therefore the mass of the rigid part that the accelerometer is attached to. This can lead to drastically more noise in a finite element simulation.

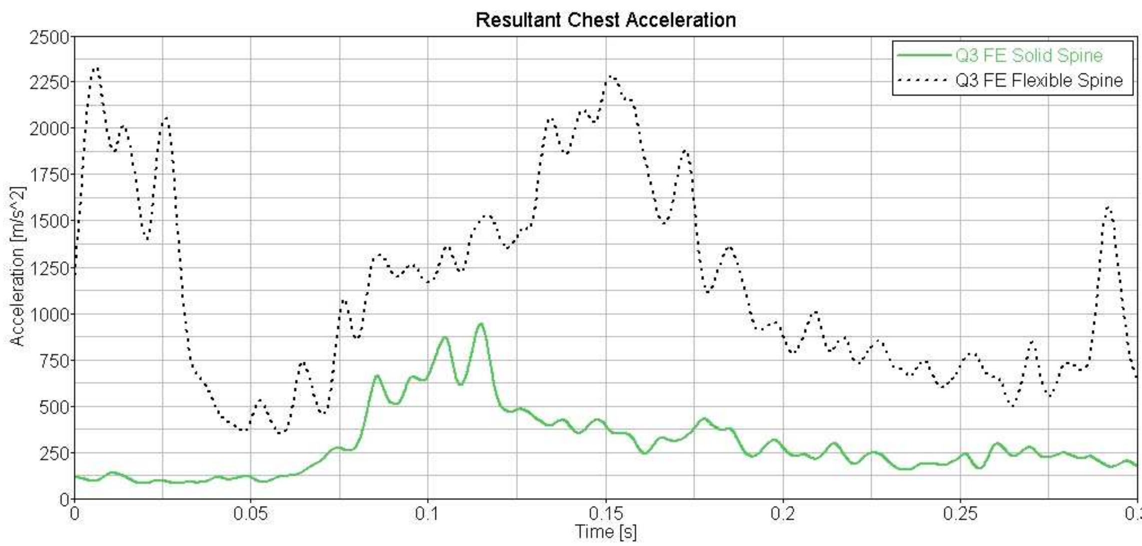

Figure 4.100: Resultant Chest Acceleration

The chest deformation was reduced by converting the solid spine of the dummy to a partially flexible, see Figure 4.101.

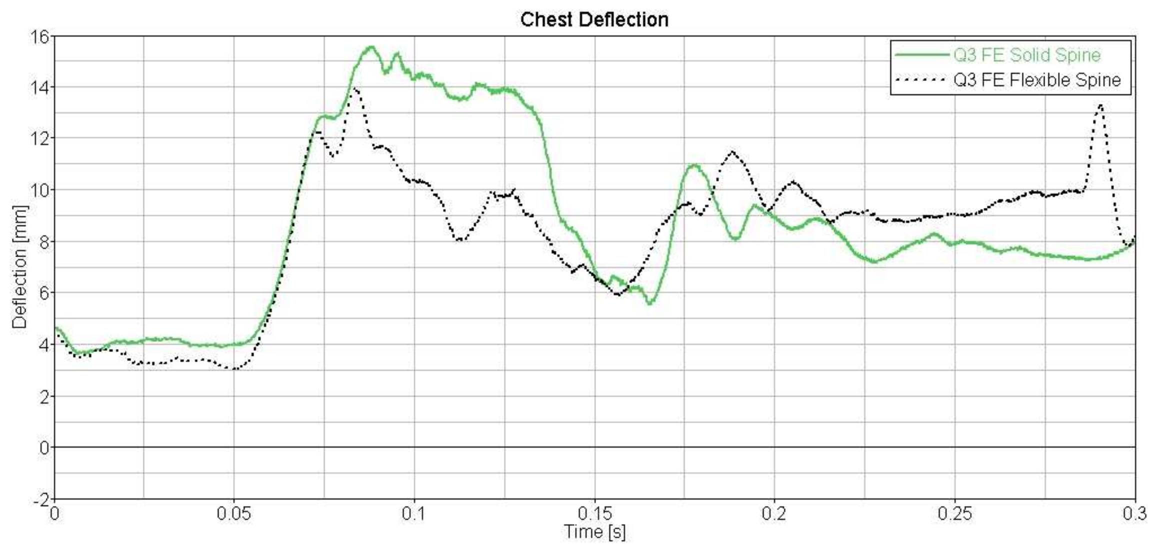

Figure 4.101: Chest Deflection

A visual comparison of the two simulations can be found in the appendix of this report, Figure A.6.1. It shows that the model with flexible spine experiences a larger head extension and neck bending than the model with the solid spine box. This seems to be similar to the neck and spine bending the human model in the research by Zhang et al. [70] experiences.

In summary, the relatively small change of the upper part of the neck resulted in a rather significant change in the measured outcome of the dummy. Therefore it is critical to develop a child dummy as biofidelic as possible to represent children in a realistic manner. With the lack of child cadaver tests, maybe a way to achieve this would be to reconstruct a number of crashes in great detail and then modify a dummy so that the injuries are represented well. If the developed finite element human model [48] is considered valid, this can be used to improve the finite element model of the Q3 in terms of biofidelity, which in turn could lead to modifications and improvements in the real Q3 dummy,

CHAPTER 5 - CONCLUSIONS

The finite element model of the Q3 anthropomorphic test device presented in this research can be a valuable tool in future child safety research. Even though the optimization and validation of some of the parts of the dummy have some deficiencies, namely, the poor correlation of some of the variables, the model can be considered validated, especially for frontal impact.

The complete dummy tests used for the validation of the model presented in this document have a higher severity than a typical sled test. Therefore, a large discrepancy between the test and the simulation can be expected especially in the measurements that are taken further away from the impact point, which in this case is the chest. Additional tests of the dummy could help to further optimize the material properties, thereby improving the model and its validation results. Public disclosure of the material properties or tests of material samples, which are currently proprietary, could improve the material models and accelerate modeling efforts. With the availability of additional material data, more detailed material models can be used within LS-DYNA. This could lead to better validation results.

The optimization at the component level, which was utilized to find previously unknown material properties, as presented in this research has proven to yield to good results. The properties of the materials of the dummy were found with the presented method. The use of this method can be expanded to other problems where the material properties are unknown. For best results the tests used for optimization should be a simple setup with possibly only one unknown material and should stress the materials in a similar fashion as it is later used in the model.

The sled test simulations with the original finite element model of the Q3 and the model with the modified more flexible spine show a reduction in head acceleration and in the neck injury criterion with the flexible spine. This is consistent with previous research [58][70] and is more realistic. Current production child dummies are over-predicting neck injuries in children as can be concluded by comparing test results to actual injuries sustained in the field [3][35][50][51]. It is important to use the most humanlike dummies possible to represent humans in crash testing.

The presented research shows a way to make the Q3 child dummy more biofidelic in terms of head and neck response. The finite element model can be a valuable tool to improve the design of the Q3 dummy. Further research and physical tests of the proposed design changes of the spine are necessary before such changes can be implemented in the dummy.

The rating criterion used in this research rates the accuracy of the model relatively objectively. This particular rating criterion has its strengths in combining three individual criteria, namely, the comparison of the peak, the timing of the peak and the overall shape, and in being easy to implement. The weaknesses of the criterion are the drastic change sensitivity depending on the timing of the peak of main event and the fact that the shape function not only compares the pure shape of two functions, but also already includes the timing and the peak of the functions.

Since the presented finite model of the Q3 dummy was created, the actual Q3 dummy has undergone several design changes, especially for side impact conditions. A special side impact version of the dummy was developed, the Q3-S. This was necessary since the shoulder region proofed to be not durable enough and resulted in non-repeatable tests. During the research a later version of the dummy was digitized and meshed, but no tests or material data of that newer version of the dummy were available for validation.

As a result of the continuous development of the Q3 the number of tests that could be used for this research was very limited and no additional test data for the version of the dummy presented in this research can be expected in the future.

The finite element model of the Q3 dummy will be made publicly available on the website of the National Crash Analysis Center of The George Washington University.

CHAPTER 6 - REFERENCES

[1] Advisory Group for Aerospace Research and Development (AGARD), 1996, *"Anthropomorphic Dummies for Crash and Escape System Testing*", AGARD-AR-330, Neuilly-Sur-Seine, France

[2] Alt, W., 2002, "*Nichtlineare Optimierung - Eine Einführung in Theorie, Verfahren und Anwendungen"*, Vieweg, Braunschweig/Wiesbaden, Germany

[3] Arbogast, K., Chen, I., Durbin, R., Winston, F., 2004, *"Injury risks for children in child restraint systems in side impact crashes"*

[4] Arbogast, K., Ghati, Y., Menon, R., Tylko, S., Tamborra, N., Morgan, R,. 2005, *"Field Investigation of Child restraints in Side Impact Crashes",* Traffic Injury Prevention, Volume 6, Number 4, Taylor and Francis Ltd, pp. 351-360(10)

[5] Arora, J., 2004, "*Introduction to Optimum Design*", second edition, Elsevier Academic Press, London, UK, Chap. 11

[6] Automation Creations, Inc., "*MatWeb Material Property Data"*, http://www.matweb.com/index.asp?ckck=1

[7] Bathe K.J., 1996, "*Finite Element Procedures",* Prentice-Hall, Englewood Cliffs, NJ, USA

[8] Behr, M.; Arnoux, P.; Serre, T.; Bidal, S.; Kang, H.; Thollon, L.; Cavallero, C.; Kayvantash, K.; Brunet, C., 2003, *"A Human Model for Road Safety: From Geometrical Acquisition to Model Validation with Radioss"*, Computer Methods in Biomechanics and Biomedical Engineering, Taylor and Francis Ltd, London, UK, Volume 6, pp. 263-273

[9] Brady, G., 1996, *"Materials Handbook"*, McGraw-Hill Book Company, New York, NY, USA

[10] Brun Cassan, F., Page, M., Princemaille, Y., Kallieris, D., Tarriafre, C., 1993, "*Comparative Study of Restrained Child Dummies and Cadavers in Experimental Crashes",* Child Occupant Protection, SAE 933105

[11] Burdi, A., Huelke, D., Snyder, R., Lowrey, G., 1969, *"Infants and Children in the Adult World of Automobile Safety Design: Pediatric and Anatomical Considerations for Design of Child Restraints"*, Journal Biomechanics, Vol. 2, Elsevier, Orlando, FL, USA, pp. 267-280

[12] Carley, K., Kamneva, N., Reminga, J., 2003, *"Response Surface Methodology"*, Center for Computational Analysis of Social and Organizational Systems Technical Report, Carnegie Mellon University, Pittsburgh, PA, USA

[13] Cook R.D., Malkus D.S., Plesha M.E., 1989 "*Concepts and applications of finite element analysis*", third edition, John Wiley & Sons, New York, NY, USA

[14] Currey, J. D., Butler, G., 1975, "*The Mechanical Properties of Bone Tissue in Children"*, J Bone Joint Surgery, Vol 57A, no. 6, pp. 810-814.

[15] Dalenoort, A., Griotto, G., Mooi, H., Baldauf, H., Weissenbach, G., 2005, *"A Stochastic Virtual Testing Approach in Vehicle Passive Safety Design: Effect of*

Scatter on Injury Response", SAE World Congress, Detroit, MI, USA, SAE 2005-01-1763

[16] Dejeammes, M., Tarriafre, C., Thomas, C., Kallieris, D., 1984, "*Exploration of Biomechanical Data Toward a Better Evaluation of Tolerance for Children Involved in Automotive Accidents"*, Twenty-Eighth Stapp Car Crash Conference Proceedings, SAE 840530

[17] Denton ATD, Inc., *"History of Anthropomorphic Test Devices"*, www.tno-automotive.cn/knowledge/MADYMO_UM/2004International/P1.pdf

[18] DeSantis Klinich, K., Saul, R., Auguste, G., Backaitis, S., Kleinberger, M., 1996, *"Techniques for Developing Child Dummy Protection Reference Values",* Child Injury Protection Team, National Highway Traffic Safety Agency, Washington, DC, USA

[19] Domschke, W., Drexl, A., 2007, "*Einführung in Operations Research"*, seventh edition, Springer, Berlin, Germany, Chap. 2

[20] Du Bois, P., *"Crashworthiness Engineering"*, course notes

[21] Dupis, R., Meyer, F., Willinger, R., 2006, "*Three-year-old child neck finite element modelization"*, European Journal of Orthopaedic Surgery & Traumatology, Springer, Paris, France, Vol. 16

[22] Eichelberger, M. R., 1992, *"Pediatric Trauma: Prevention, Acute Care, Rehabilitation"*, B C Decker Inc., Hamilton, Ontario, Canada

[23] First Technology Safety Systems, 2006, "*Q3 Child Dummy*", http://www.ftss.com/pcat/products.cfm?obr=NS&bm=3&pcat=q3, accessed Nov. 2007

[24] Fuchs, S., Barthel, M.J., Flannery, A.M., Christoffel, K.K., 1989, *"Cervical Spine Fractures Sustained by Young Children in Forward-Facing Car Seats",* Pediatrics, 84(2), pp. 348-354

[25] Hallquist, J., 1998, "*LS-DYNA Theoretical Manual"*, Livermore Software Technology Corporation, Livermore, CA, USA, Chap. 21

[26] Happee, R., Janssen, A., Fraterman, E., Monster, J., 2003, "*Application of MADYMO Occupant Models in LS-DYNA/MADYMO Coupling",* 4th European LS-DYNA Users Conference, Ulm, Germany

[27] Happee, R., van Haaster, R., Michaelsen, L., Hoffmann, R., 1998, *"Optimization of vehicle passive safety for occupants with varying anthropometry",* ESV Conference, Windsor, Canada, June 1998

[28] Herrmann, L., Peterson, F., 1968, *"A Numerical procedure for Viscoelastic Stress Analysis"*, Bulletin of the 7th Meeting of the ICRPG Mechanical Behavior Working Group, CPIA Publication No. 177, Orlando, FL, USA

[29] Hilker, C., Yoganandan, N., Pintar, F., 2002, *"Experimental Determination of Adult and Pediatric Neck Scale Factors"*, Stapp Car Crash Journal, Vol. 46, pp. 417-429

[30] Hirsch, C., Evans, F., G., 1965, "*Studies on Some Physical Properties of Infant Compact Bone",* Acta Orthop. Scandinav., Vol. 35, pp.300-313

[31] Hovenga, P., Spit, H., Uijldert, M., Dalenoort, M., 2005, "Improved prediction of Hybrid-III injury values using advanced multibody techniques and objective rating", SAE 2005-01-1307

[32] Hubbard, R. P., 1971, "*Flexure of Layered Cranial Bone*", Journal Biomechanics, Vol 4, pp. 251-263

[33] Jacob, C., Charras, F., Troseille, X., Hamon, J., Pajon, M., Lecoz, J., 2000, "*Mathematical Models Integral Rating*", International Journal of Crashworthiness, Volume 5, Issue 4

[34] Kallieris, D., Barz, J., Schmidt, G., Heess, G., Mattern, R., 1976, "*Comparison Between Child Cadavers and Child Dummy by Using Child Restraint Systems in Simulated Collisions*", 20th Stapp Car Crash Conference Proceedings, SAE 760815

[35] Klinich, K., Burton, R., 1993, "*Injury Patterns of Older Children in Automotive Accidents*", Child Occupant Protection, SAE 933082

[36] Knothe, K., Wessels, H., 1999, *"Finite Elemente: Eine Einführung für Ingenieure"*, Springer Verlag, Berlin, Germany, Chap. 3

[37] Lewis, P.E., Ward, J. P., 1991, *"The Finite Element Method: Principles and Applications"*, Addison Wesley Publishing Company, Boston, MA, USA

[38] Maltese, M., Eppinger, R., 2002, *"Development of improved Injury Criteria for the Assessment of Child Restraint Systems",* National Transportation Biomechanics Research Center, National Highway Traffic Safety Agency, Docket # NHTSA-02-11707

[39] Matsusita, T., Sato, T., Hirabazashi, K., Fujimura, S., Asazuma, t., Takatori, T., 1994, *"X-Ray Study of the Human Neck Motion Due to Head Inertia Loading"*, 38th Stapp Car Crash Conference, SAE 942208

[40] McKay, M., Beckman, R., Conover, W., 2000, *"A Comparison of Three Methods for Selecting Values of Input Variables in the Analysis of Output from a Computer Code"*, Technometrics, American Statistical Association, Vol. 42, No. 1, pp. 55-61

[41] Mertz, H., Irwin, A., *"Biomechanical Bases for the CRABI and Hybrid III Child Dummies",* 41st Stapp Car Crash Conference Proceedings, SAE 973317

[42] Mertz, H., Irwin, A., Melvin, J., Stalnaker, R., Beebe, M., 1989, "*Size weight and biomechanical impact response requirements for adult size small female and large male dummies*", SAE-890756

[43] Mertz, H., Irwin, A., Prasad, P., 2003, *"Biomechanical and Scaling Bases for Frontal and Side Impact Injury Assessment Reference Values",* Stapp Car Crash Journal, Vol. 47, pp. 155-188

[44] Mertz, H., Patrick, L., 1971, *"Strenght and response of the Human Neck"*, 15th Stapp Car Crash Conference Proceedings, SAE 7108855

[45] Mertz, H., Prasad, P., Irwin, A., 1997, *"Injury Risk Curves for Children and Adults in Frontal and Rear Collisions",* 41st Stapp Car Crash Conference Proceedings, SAE 973318

[46] Mertz, H.J., 1985, "*Anthropomorphic models. The biomechanics of trauma*", Appelton-Century-Crofts, Norwalk, CT, USA

[47] Mertz, H.J., 1993, "*Anthropomorphic Test Devices. Accidental injury: biomechanics and prevention*", Springer, New York, NY, USA

[48] Mizuno, K., Iwata, K., Deguchi, T., Ikami, T., 2006, *"Development of a Three-Year-Old Child FE Model",* Traffic Injury Prevention, Vol. 6, pp. 361-371

[49] Nocedal, J., Wright, S.J., 1999, "*Numerical Optimization*", Springer, New York, NY, USA

[50] Paine, M., Griffiths, M., Brown, J., Case, M., Johnstone, O., 2003, "*Protecting Children in Car Crashes: The Australian Experience*", 18th Enhanced Safety of Vehicles Conference Proceedings, Nagoya, Japan

[51] Park, C.-K., 2004, "*Examine the Performance on Child Restraint Systems(CRS) in New Car Assessment Program(NCAP) Tests*", CE 262 Term Project, The George Washington University, Washington, DC

[52] Pipkorn, B., Eriksson, M., 2003 *"A Method to Evaluate the Validity of Mathematical Models*", 4th European MADYMO User Conference, Brussels, Belgium

[53] Press, W., Teukolsky, S., Vetterling, W., Flannery, B., 2007, "*Numerical Recipes*", third edition, Cambridge University Press, New York, USA, Chap. 10

[54] Ratingen, M. van, Twisk, D., Schrooten, M., Beusenberg, M., Barnes, A., Platten, G., 1997, *"Biomechanically based design and performance targets for a 3-year old child crash dummy for frontal and side impact",* Child Occupant Protection Symposium 1997, SAE 973316

[55] Schneider, L., Bowman, B., Snyder, R., Peck, L., 1976, *"A Prediction of Response of the Head and Neck of the US Adult Military Population to Dynamic Impact Acceleration from Selected Dynamic Test Subjects"*, University of Michigan Highway Safety Research Institute, Ann Arbor, MI, USA, Report UMHSRI-76-10

[56] Schwarz, H.R., 1993, *"Methode der Finiten Elemente"*, Teuber Verlag, Stuttgart, Germany

[57] Seemann, M., Muzzy, W., Lustick, L., 1986, *"Comparison of Human and Hybrid III Head and Neck Dynamic Response"*, 30th Stapp Car Crash Conference Proceedings, SAE 861892

[58] Sherwood, C., Shaw, C., van Rooij, L., Kent, R., Gupta, P., Crandall, J., Orzechowski, K., Eichelberger, M., Kallieris, D., 2002, *"Prediction of Cervical Spine Injury Risk for the 6-year-old Child in Frontal Crashes"*, Traffic Injury Prevention, Taylor and Francis Ltd., London, UK, Vol. 4, pp. 206-213

[59] Thunnissen, J., Happee, R., Eummelen, P., Beusenberg, M., 1994, *"Scaling of adult to Child Responses applied to the thorax"*, IRCOBI Conference, Lyon, September 21-23

[60] Thunnissen, J., Wismans, J., Ewing, C., Thomas, D., 1995, "*Human Volunteer Head-Neck Response in Frontal Flexion: a New Analysis*", 39th Stapp Car Crash Conference Proceedings, SAE 952721

[61] TNO, 1999, *"TNO Q3 Dummy User Documentation"*, TNO Automotive, Delft, The Netherlands

[62] TNO, 2003, "*MADYMO Database manual version 6.1*", TNO Automotive, Delft, The Netherlands

[63] TNO, 2003, "*MADYMO Theory manual version 6.1*", TNO Automotive, Delft, The Netherlands

[64] Twisk, D., Spit, H., Bebee, M., Depinet, P., 2007, *"Effect of Dummy Repeatability on Numerical Model Accuracy"*, SAE 2007-01-1173

[65] Waterman, N., Ashby, M., 1996, *"The Materials Selector"*, Chapman & Hall, London, UK, second edition, Vol. 3

[66] Wismans, J., Maltha, J., Melvin, J., Stalnaker, R., 1979, "*Child Restraint Evaluation by Experimental and Mathematical Simulation"*, 23rd Stapp Car Crash Conference Proceedings, SAE 791017

[67] Wismans, J., Philippens, M., van Oorschot, E., Kallieris, D., Mattern, R., 1987, *"Comparison of Human Volunteer and Cadaver Head-Neck Response in Frontal Flexion",* 31st Stapp Car Crash Conference Proceedings, SAE 872194

[68] Wismans, J., van Oorschot, E.,, Woltring, H., 1986, *"Omni-Directional Human Head-Neck Response"*, 30th Stapp Car Crash Conference Proceedings, SAE 861893

[69] Yamada, H., 1970, *"Strength of Biological Materials",* Williams & Wilkins Co., Philadelphia, PA, USA

[70] Zhang, W., Kapoor, T., Tot, M., Altenhof, M., Howard, A., Mizuno, K., 2007, *"A Comparison of the Kinematics of a Child Finite Element Model and the Hybrid III 3-Year-Old Dummies in Frontal Crashes"*, SAE World Congress 2007, Detroit, MI, USA, SAE 2007-01-0977

[71] Zobrist, G., Leonard, J., 2000, "*Simulation Systems*", Overseas Publishers Association, Amsterdam, The Netherlands, Chap. 3

APPENDIX

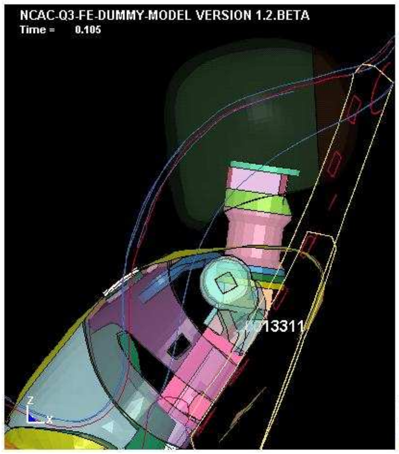
NCAC-Q3-FE-DUMMY-MODEL VERSION 1.2.BETA
Time = 0.105

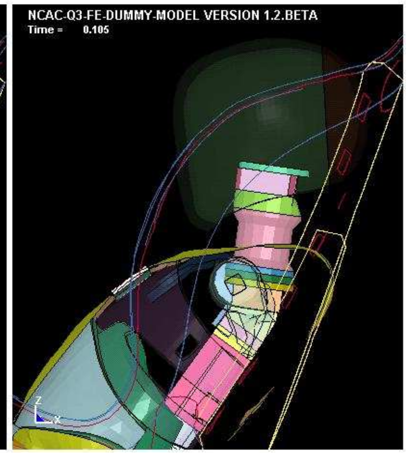
NCAC-Q3-FE-DUMMY-MODEL VERSION 1.2.BETA
Time = 0.105

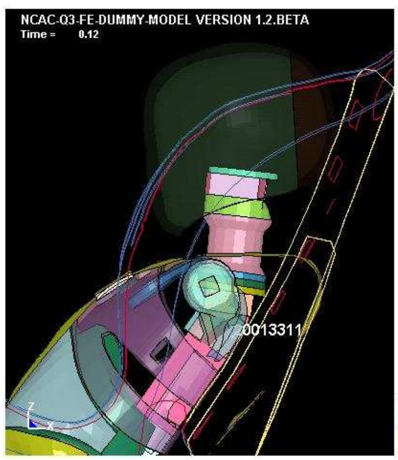
NCAC-Q3-FE-DUMMY-MODEL VERSION 1.2.BETA
Time = 0.12

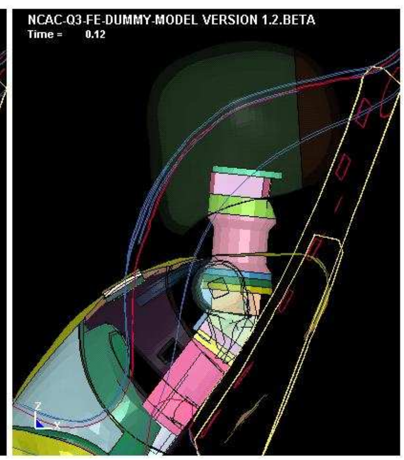
NCAC-Q3-FE-DUMMY-MODEL VERSION 1.2.BETA
Time = 0.12

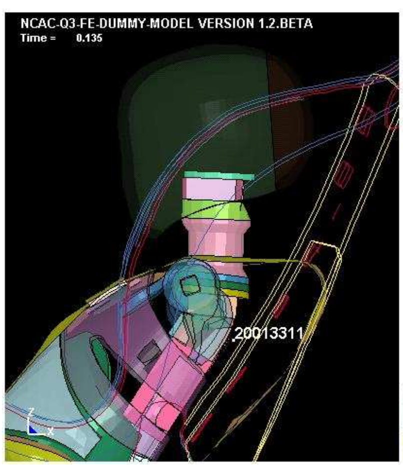
NCAC-Q3-FE-DUMMY-MODEL VERSION 1.2.BETA
Time = 0.135
20013311


NCAC-Q3-FE-DUMMY-MODEL VERSION 1.2.BETA
Time = 0.135

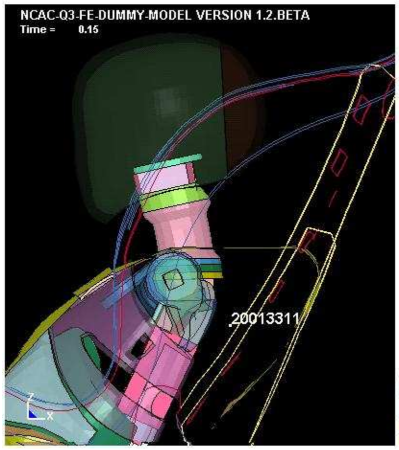
NCAC-Q3-FE-DUMMY-MODEL VERSION 1.2.BETA
Time = 0.15
20013311
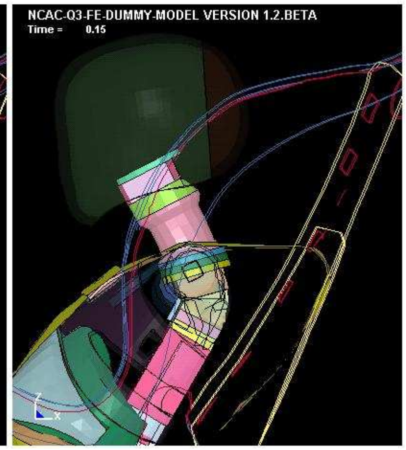
NCAC-Q3-FE-DUMMY-MODEL VERSION 1.2.BETA
Time = 0.15
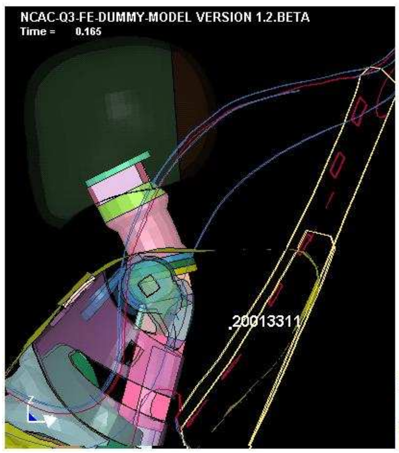
NCAC-Q3-FE-DUMMY-MODEL VERSION 1.2.BETA
Time = 0.165
20013311

NCAC-Q3-FE-DUMMY-MODEL VERSION 1.2.BETA
Time = 0.165
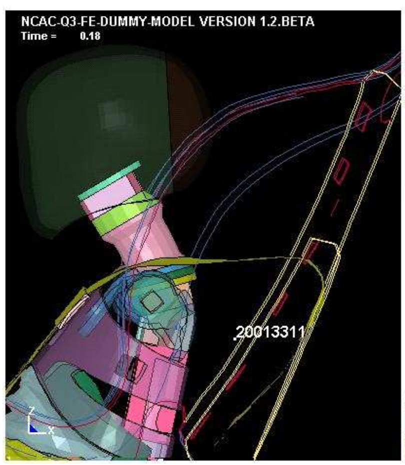
NCAC-Q3-FE-DUMMY-MODEL VERSION 1.2.BETA
Time = 0.18
20013311

NCAC-Q3-FE-DUMMY-MODEL VERSION 1.2.BETA
Time = 0.18

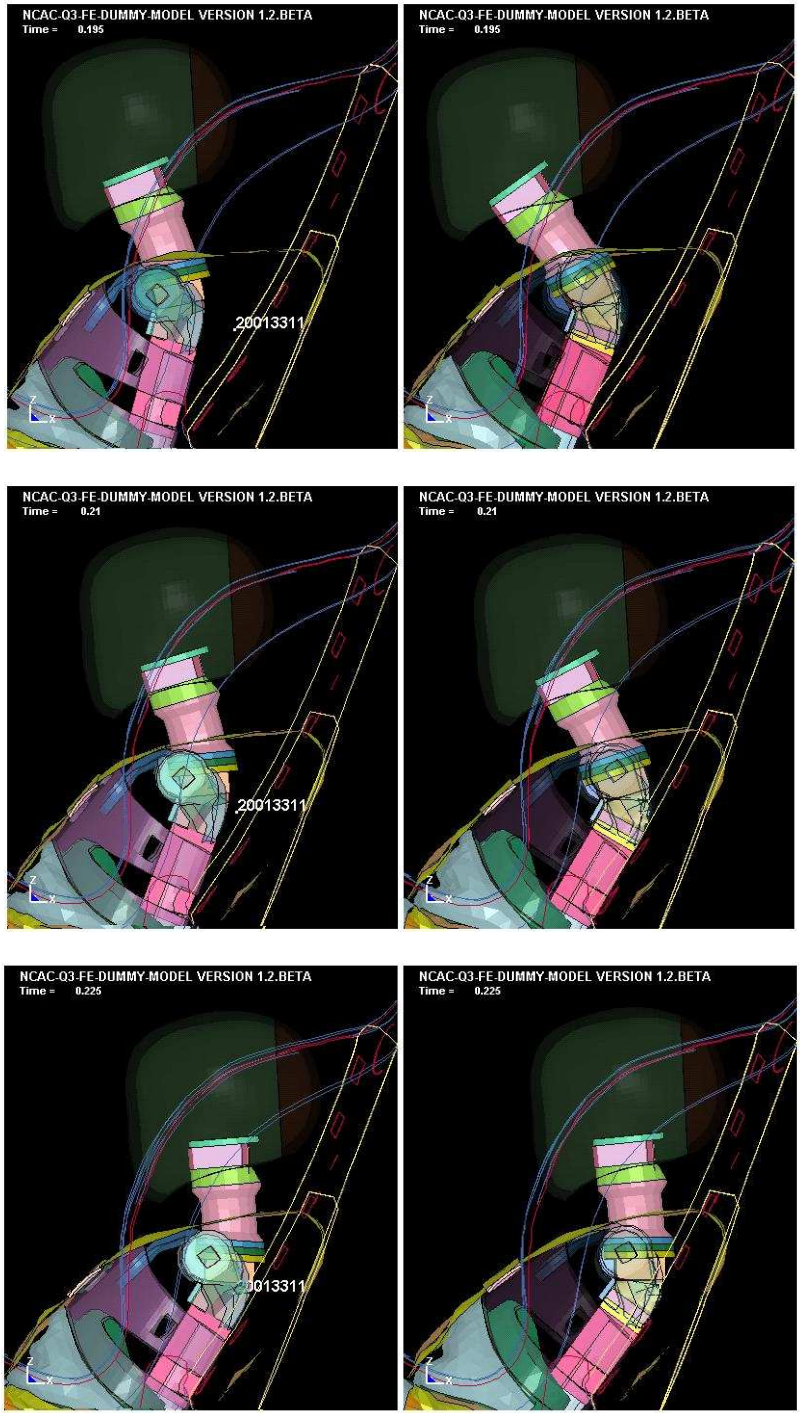
NCAC-Q3-FE-DUMMY-MODEL VERSION 1.2.BETA
Time = 0.195
20013311
NCAC-Q3-FE-DUMMY-MODEL VERSION 1.2.BETA
Time = 0.195
NCAC-Q3-FE-DUMMY-MODEL VERSION 1.2.BETA
Time = 0.21
20013311
NCAC-Q3-FE-DUMMY-MODEL VERSION 1.2.BETA
Time = 0.21
NCAC-Q3-FE-DUMMY-MODEL VERSION 1.2.BETA
Time = 0.225
0013311
NCAC-Q3-FE-DUMMY-MODEL VERSION 1.2.BETA
Time = 0.225

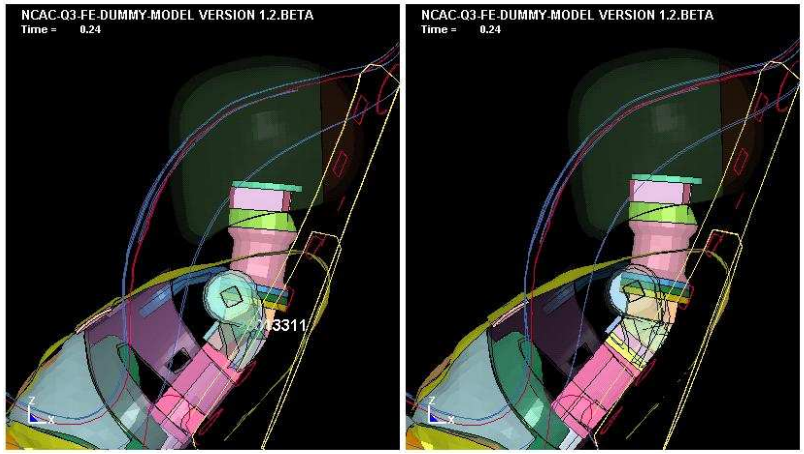

Figure A.6.1: Comparison Between Original Q3 (left) and Q3 with Modified Spine (right)